

AD-A175 234

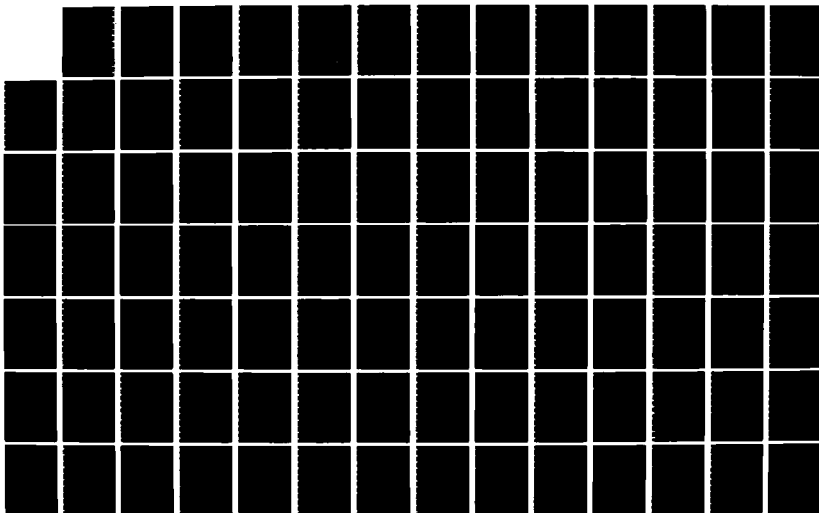
A RESEARCH PROGRAM FOR THE NEUTRAL/ION CHEMISTRY OF
METALS IN THE STRATOS. (U) ATMOSPHERIC AND
ENVIRONMENTAL RESEARCH INC CAMBRIDGE MA M K KO ET AL.

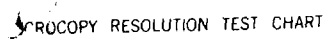
1/2

UNCLASSIFIED

30 JUL 86 AFGL-TR-86-0169 F19628-83-C-0123 F/G 4/1

NL





PHOTOCOPY RESOLUTION TEST CHART

AFGL-TR-86-0169

12

A RESEARCH PROGRAM FOR THE NEUTRAL/ION
CHEMISTRY OF METALS IN THE STRATOSPHERE
AND MESOSPHERE

Malcolm K. W. Ko
Nien Dak Sze
José M. Rodriguez

Atmospheric and Environmental Research, Inc.
840 Memorial Drive
Cambridge, Massachusetts 02139

30 July 1986

Final Report

July 1, 1983 to Sept. 30, 1986

AD-A175 234

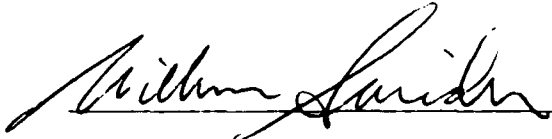
DTIC FILE COPY

APPROVED FOR PUBLIC RELEASE; DISTRIBUTION UNLIMITED

AIR FORCE GEOPHYSICS LABORATORY
AIR FORCE SYSTEMS COMMAND
UNITED STATES AIR FORCE
HANSCOM AFB, MASSACHUSETTS 01731

DTIC
ELECTE
DEC 18 1986
B

This technical report has been reviewed and is approved for publication.

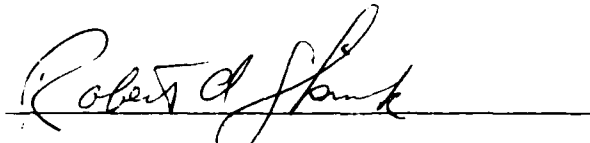


WILLIAM SWIDER
Contract Manager



JOHN E. RASMUSSEN, Chief
Ionospheric Interactions Branch

FOR THE COMMANDER



ROBERT A. SKRIVANEK, Director
Ionospheric Physics Division

This report has been reviewed by the ESD Public Affairs Office (PA) and is releasable to the National Technical Information Service (NTIS).

Qualified requestors may obtain additional copies from the Defense Technical Information Center. All others should apply to the National Technical Information Service.

If your address has changed, or if you wish to be removed from the mailing list, or if the addressee is no longer employed by your organization, please notify AFGL/DAA, Hanscom AFB, MA 01731. This will assist us in maintaining a current mailing list.

Do not return copies of this report unless contractual obligations or notices on a specific document requires that it be returned.

REPORT DOCUMENTATION PAGE

1a REPORT SECURITY CLASSIFICATION Unclassified			1b RESTRICTIVE MARKINGS		
2a SECURITY CLASSIFICATION AUTHORITY			3 DISTRIBUTION / AVAILABILITY OF REPORT Approved for public release; Distribution unlimited.		
2b DECLASSIFICATION / DOWNGRADING SCHEDULE					
4. PERFORMING ORGANIZATION REPORT NUMBER(S)			5 MONITORING ORGANIZATION REPORT NUMBER(S) AFGL-TR-86-0169		
6a. NAME OF PERFORMING ORGANIZATION Atmospheric & Environmental Research, Inc		6b OFFICE SYMBOL (If applicable)	7a NAME OF MONITORING ORGANIZATION Air Force Geophysics Laboratory		
6c. ADDRESS (City, State, and ZIP Code) 840 Memorial Drive Cambridge, MA 02139			7b ADDRESS (City, State, and ZIP Code) Hanscom AFB Massachusetts 01731		
8a. NAME OF FUNDING / SPONSORING ORGANIZATION		8b OFFICE SYMBOL (If applicable)	9 PROCUREMENT INSTRUMENT IDENTIFICATION NUMBER F19628-83-C-0123		
8c. ADDRESS (City, State, and ZIP Code)			10 SOURCE OF FUNDING NUMBERS		
			PROGRAM ELEMENT NO 61102F	PROJECT NO 2310	TASK NO G3
			WORK UNIT ACCESSION NO BA		
11 TITLE (Include Security Classification) A Research Program for the Neutral/Ion Chemistry of Metals in the Stratosphere and Mesosphere					
12 PERSONAL AUTHOR(S) Malcolm K.W. Ko, Nien Dak Sze, Jose M. Rodriguez					
13a. TYPE OF REPORT Final Report		13b TIME COVERED FROM 7/1/83 TO 9/30/86		14 DATE OF REPORT (Year, Month, Day) 1986 July 30	
15 PAGE COUNT 130					
16 SUPPLEMENTARY NOTATION					
17 COSATI CODES			18 SUBJECT TERMS (Continue on reverse if necessary and identify by block number)		
FIELD	GROUP	SUB-GROUP	Ionosphere		
			Sodium		
			Mesosphere		
			Metals		
19 ABSTRACT (Continue on reverse if necessary and identify by block number)					
<p><u>Abstract:</u> A one-dimensional model has been developed to calculate densities and diurnal behavior of background trace gases as well as metal neutral and ionic species between 60 and 120 km. Particular attention has been given to the modeling of sodium species, given the availability of both observational and kinetic data. Key results follow.</p> <p>a) We found that an estimated input of 2×10^4 Na atoms $\text{cm}^{-2} \text{sec}^{-1}$ (1.2×10^2 tons/year) from ablation of meteors will produce a layer of neutral sodium atom around 90 km with concentrations of $3 - 5 \times 10^3 \text{ cm}^{-3}$, in agreement with observations. The observed diurnal variation of the Na column density (less than 14% of the mean) requires a rate of less than (Cont'd on reverse side)</p>					
20 DISTRIBUTION / AVAILABILITY OF ABSTRACT <input type="checkbox"/> UNCLASSIFIED/UNLIMITED <input checked="" type="checkbox"/> SAME AS RPT <input type="checkbox"/> DTIC USERS			21 ABSTRACT SECURITY CLASSIFICATION Unclassified		
22a NAME OF RESPONSIBLE INDIVIDUAL William Swider			22b TELEPHONE (Include Area Code)		22c OFFICE SYMBOL AFGL/LID

Cont of Block 19:

$10^{-13} \text{ cm}^3 \text{ sec}^{-1}$ for the reaction of NaO_2 with O , and at most $1 - 2 \times 10^{-10} \text{ cm}^3 \text{ sec}^{-1}$ for the reaction of NaO with H_2O . Most of the sodium is converted to NaO_2 , NaOH , and NaCl below 90 km.

- b) Recent measurements of the rates for reactions of NaO_2 and NaOH with HCl , and of the photoabsorption cross sections of NaCl allow for realistic estimates of the impact of sodium chemistry on chlorine partitioning in the upper stratosphere. Incorporation of Na chemistry in current photochemical models could increase the calculated ClO concentrations near 50 km by up to a factor of two with a corresponding decrease in calculated O_3 abundances at that altitude of as much as 15%.
- c) The model calculates densities of Na^+ of order $2-3 \times 10^2 \text{ cm}^{-3}$ at 100 km with a diurnal variation of factors of 400 and 3 at 90 and 100 km, respectively. The topside scale height of the neutral sodium layer is determined by the abundance of Na^+ above 90 km. The observed scale height ($\sim 3 \text{ km}$) can be successfully simulated by either assuming a slow rate ($\sim 7 \times 10^{-32} \text{ cm}^6 \text{ sec}^{-1}$) for the clustering reaction of Na^+ with N_2 , or by adopting a downward ion drift velocity of $\sim 20 \text{ cm/s}$.
- d) Seasonal changes in the background atmosphere induce a winter maximum in the Na column density a factor of 1.4 higher than the summer minimum, in qualitative agreement with observations. Seasonal changes in the vertical eddy diffusion coefficient induce a seasonal variation in the Na column density and D-line emission of factors of 3 to 4, peaking at the equinoxes. This result is in agreement with low-latitude D-line observations but in disagreement with high-latitude data.
- e) Calculations of Li and K are hampered by a lack of kinetic data. Our results show K and Li consistent with the few available observations, if we adopt chemical schemes similar to those for Na and assume sources equal to 10^{-1} and 10^{-3} times that of Na , respectively.

Accession No.

NELI

DISTRICT

BRANCH

CITY

No.

Date

Amount

Remarks

BILL

A-1

DTIC
ELECTE
DEC 18 1986

EXECUTIVE SUMMARY

Studies of processes that determine the ion compositions of the ionosphere are of great practical interest in the field of long-range optical and radio communications. Apart from the major positive ions NO^+ and O_2^+ , relatively large amounts of metal ions are found in the D-region. It is believed that metal atoms are deposited by ablation from meteors and ionized by photoionization and charge transfer reactions.

Emission from neutral and ionic forms of metals have been identified in meteor spectra for sodium (Na), potassium (K), lithium (Li), magnesium (Mg), iron (Fe), and calcium (Ca). In addition, ions of Fe, Mg, Na, and Ca have been detected using a rocket-borne ion mass spectrometer.

Quantitative results on Na emissions from ground-based measurements have documented the seasonal and diurnal variations of the neutral sodium layer around 90 km. Among the metals, sodium is the most studied because of the large amount of data available on both neutral and ion distributions. Recent efforts at modeling the metal ions in the D-region have been helped by incorporation of a relatively sophisticated positive and negative ion chemistry in the calculation of the concentrations of the major positive and negative ions. However, attempts at studying the detailed diurnal behavior of the ions are hampered by the lack of knowledge of the diurnal variations of the neutral species such as O, O_3 , and NO.

A recent suggestion that certain atmospheric metals (particularly sodium) may play an important role in the stratospheric chlorine chemistry casts the studies of ion/neutral chemistry of metal in a new light. Below 90 km, the bulk of the metal species are in their neutral form. Once in the stratosphere, the metal may undergo a series of homogeneous and heterogeneous reactions to form metallic compounds and are ultimately removed from the atmosphere by rain-out or deposition in the troposphere. The question remains whether the metals of high reactivity are present in sufficient abundance as to affect the other chemical cycles in the stratosphere and mesosphere.

Three years ago, we proposed to initiate a modeling study program to set up a one-dimensional diurnal model of the stratosphere and mesosphere to study the chemistry of the metal neutrals and ions in the D and E regions. A necessary first step in the project is to use the model to simulate the

behavior of the background trace gases and ions. Since sodium is the species with most kinetic data and observation, we proposed to concentrate on sodium using the available observations as a way to validate the model results.

The results from our efforts are reported here. The report is organized into five parts. The key findings from each are summarized below:

- I. We have set up a one-dimensional model for the stratosphere and mesosphere encompassing the altitude range 60-120 km that calculates the altitude profiles and diurnal behavior of the background trace gases as well as metal neutrals and ions. A study was made on the simulation of the altitude distribution and diurnal behavior of neutral sodium in the atmosphere. The results were compared with the available observations with the purpose of identifying the photochemical reactions that control the behavior. At the start of the program, many of the key reaction rate constants had not been measured in the laboratory. Some of the reactions that we discussed have now been measured. With these rates, the calculated behavior of the sodium species is consistent with the available observations, indicating that the assumptions in the model concerning atmospheric inputs, and photochemical transformation are valid. We found that an estimated input of $2 \times 10^4 \text{ cm}^{-2} \text{ sec}^{-1}$ (1.2×10^2 tons/year) of sodium atom from ablation of meteor will produce a layer of neutral sodium atom around 90 km with concentration of $3-5 \times 10^3 \text{ cm}^{-3}$, in agreement with observations. Between 60-80 km, the sodium species are in the form of NaO_2 and NaOH . A value of $10^{-10} \text{ cm}^3 \text{ sec}^{-1}$ for the reaction of NaO with H_2O will yield a diurnal variation of 14 percent of the mean, consistent with the upper bound from observations.
- II. To estimate the impact of a metal on stratospheric chemistry, we must first establish how much metal enters into the stratosphere. The validation of the sodium results in the mesosphere support our estimates. Recent measurements of the rates for reactions of NaO_2 and NaOH with HCl and of the photoabsorption cross section of NaCl allow for realistic estimates of the impact of sodium chemistry on chlorine partitioning in the upper stratosphere. Calculated ClO concentrations near 50 km could increase by up to a factor of two with a corresponding decrease in calculated O_3 abundances of as much as 15 percent. The impact of ClO and O_3

depends crucially on the assumed meteoritic source of sodium, on transport from the mesosphere, and on transformation and removal of gaseous sodium in the stratosphere. Since the fluctuations in the abundance of gaseous sodium could induce O_3 variations comparable to those caused by changes in temperature and solar UV, consideration of the chemistry of sodium and other metals may be an important element in efforts toward early detection of trends in upper stratospheric O_3 . Future increases in stratospheric chlorine will magnify the impact of sodium species on ozone.

III. The diurnal photochemical model described in Part I has been utilized to calculate the diurnal variation of background and sodium ions between 60 and 120 km. Background ion species include the primary constituents NO^+ and O_2^+ . Densities of Na^+ are of order $2-3 \times 10^2 \text{ cm}^{-3}$ at 100 km, with a diurnal variation of factors of 400 and 3 at 90 and 100 km, respectively. The abundance of Na^+ above 90 km determines the topside scale height of the neutral sodium layer. This abundance is controlled by the rate for the clustering reaction of Na^+ with N_2 , which is the rate limiting step for conversion of Na^+ to Na. Downward transport of Na^+ due to ion drift is also effective in lowering Na densities above 90 km. The model can successfully simulate the observed topside scale height of the sodium layer by either using a slow rate for the clustering reaction $\sim 7 \times 10^{-32} \text{ cm}^6 \text{ sec}^{-1}$ at 200° K or adopting a downward ion drift velocity of 20 cm/s.

IV. Seasonal variations have been observed in the total column abundance of Na and the D-line emission rate. Previous studies by Garcia and Solomon (1985) have successfully explained seasonal variations in O and O_3 in terms of changes in the vertical diffusion coefficient K_{zz} induced by corresponding variations in breaking of gravity waves in the mesosphere. We have incorporated transport effects into our model and investigated the sensitivity of our results to changes in K_{zz} and background atmospheric density and temperature. Seasonal changes in the background atmosphere induce a winter maximum in the Na column density a factor of 1.4 higher than the summer minimum in qualitative agreement with observations. Seasonal changes in K_{zz} induce a seasonal variation of factors of three to four in the Na column abundance and the D-line emission, peaking

at the equinoxes. This result is in agreement with low-latitude D-line observations, but in disagreement with high-latitude D-line observations. We cannot thus reconcile the Na observations with the seasonal changes in K_{zz} within the context of the present photochemical model. The calculated diurnal variation of the Na column density is also sensitive to seasonal changes in background trace species, particularly O and H₂O.

- V. The diurnal variation and altitude profiles for Li and K have been calculated using our photochemical model. Lack of kinetic data precludes detailed analysis of the behavior of the above species. Our results are consistent with the few available observations, if we adopt chemical schemes similar to those for Na and assume sources equal to 10^{-1} and 10^{-3} times that of Na.

PART I

The Diurnal Variation of Neutral Sodium Species in the Upper Atmosphere

ABSTRACT

We have set up a one-dimensional model for the stratosphere and mesosphere encompassing the altitude range 60-120 km that calculates the altitude profiles and diurnal behavior of the background trace gases as well as metal neutrals and ions. A study was made on the simulation of the altitude distribution and diurnal behavior of neutral sodium in the atmosphere. The results were compared with the available observations with the purpose of identifying the photochemical reactions that control the behavior. At the start of the program, many of the key reaction rate constants had not been measured in the laboratory. By now, some of the reactions that we discussed have been measured. With these rates, the calculated behavior of the sodium species are consistent with the available observations, indicating that the assumptions in the model concerning atmospheric inputs, photochemical transformation are valid. We found that an estimated input of $2 \times 10^4 \text{ cm}^{-2} \text{ sec}^{-1}$ (1.2×10^2 tons/year) of sodium atom from ablation of meteor will produce a layer of neutral sodium atom around 90 km with concentration of $3-5 \times 10^3 \text{ cm}^{-3}$, in agreement with observations. Between 60-80 km, the sodium species are in the form of NaO_2 and NaOH . A value of $10^{-10} \text{ cm}^3 \text{ sec}^{-1}$ for the reaction of NaO with H_2O will yield a diurnal variation of 14 percent of the mean, consistent with the upper bound from observations.

Table of Contents

	<u>Page</u>
ABSTRACT	1
1. INTRODUCTION	2
2. SUMMARY OF PHOTOCHEMICAL SCHEME	2
3. SUMMARY OF OBSERVATIONS ON NEUTRAL IONS	5
4. DESCRIPTION OF MODEL	6
5. RESULTS	8
6. DISCUSSION AND CONCLUSIONS	11

1. INTRODUCTION

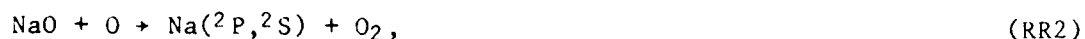
The existence of trace amounts of atomic sodium (Na) in the Earth's upper atmosphere was deduced in the earlier part of this century from observations of nighttime airglow in the D lines of Na (Chapman, 1939, and references there given). Subsequent measurements of resonance radiation in the D lines were carried out at twilight and during the day by numerous investigators in the period prior to 1970 (see review by Kvifte, 1973). These measurements deduced the concentration of atomic sodium in a narrow layer centered at around 90 km. The advent of laser radar techniques (lidar) has produced a wealth of information on the altitude distribution and the diurnal and seasonal variation of the sodium layer during the past 15 years (Gibson and Sandford, 1971, 1972; Megie and Blamont, 1977; Simonich et al., 1979; Clemesha et al., 1982; Granier and Megie, 1982; Gardner et al., 1986). Although different mechanisms were originally proposed to explain the origin of this sodium layer (Kvifte, 1973), experimental evidence and present theoretical models favor a source from ablation of meteorites occurring between 80 and 100 km (Megie and Blamont, 1977; Gadsden, 1968; Hunten et al., 1980).

We present in this report the results of our calculation of the diurnal variation of neutral sodium compounds. Comparison of our results with the observed properties that are determined by photochemical processes can place additional constraints on some of the reaction rates. In particular, we will see that the reaction of $\text{NaO}_2 + \text{O}$ must be slow and that the lower bound for the measured rate of $\text{NaO} + \text{H}_2\text{O}$ is consistent with present observations. Our study will also isolate the chemical cycles controlling the distribution and diurnal behavior of the sodium layer, thus estimating the sensitivity of our results to unknown kinetic rates and properties of the background atmosphere.

Sections 2 and 3 summarize the information about laboratory kinetic measurements and observations of atmospheric sodium available at present, respectively. Our model is described in Section 4, and the results of our calculations are presented in Section 5.

2. SUMMARY OF PHOTOCHEMICAL SCHEME

The first photochemical model for sodium compounds was proposed in 1939 by Chapman to explain the nighttime D-line emission. This mechanism proceeds through the oxidation-reduction cycle involving Na and sodium monoxide (NaO)



where the dissociation energy of O_2 is partially channelled into the excitation of Na to the ^2P state, with subsequent radiation in the D lines. The validity of the above mechanism has been confirmed by kinetic studies and atmospheric observations during the past 40 years. The evidence against the possibility of other mechanisms has been recently summarized by Bates and Ojha (1980).

The existence and chemistry of sodium compounds other than atomic sodium is more uncertain, because of a lack of laboratory kinetic data and atmospheric measurements. The nonproton-hydrate positive ions observed in the middle atmosphere by Arnold et al. (1978) were originally interpreted to be of the form $\text{NaOH}_2^+(\text{NaOH})_m(\text{H}_2\text{O})_n$ (Ferguson, 1978). This interpretation led Liu and Reid (1979) to postulate the production of NaOH through reactions such as



where NaO_2 is produced by the reaction



This model predicted rapid conversion of Na to NaOH below an altitude of 90 km. Direct production of NaOH from NaO was proposed by Murad and Swider (1979) through the reaction



A value of $(2 \pm 1) \times 10^{-10} \text{ cm}^3 \text{ sec}^{-1}$ for the rate of (RR7) has been recently obtained by Ager and Howard (1985). Although more recent measurements of stratospheric positive ions have eliminated the possibility of a sodium core (Arnold et al., 1981), the NaOH sources represented by reactions (RR10), (RR11), and particularly (RR7) are still realistic.

*RR numbers refer to reaction numbers in Table 1.

The abundance of NaOH is also of interest for stratospheric ozone chemistry. Murad and Swider (1979) and Murad, Swider, and Benson (1981) pointed out that the reaction



could constitute an important reaction pathway for stratospheric HCl if its rate were of the order of $10^{-12} \text{ cm}^3 \text{ s}^{-1}$, and if the NaOH concentration were $\sim 10^5 \text{ cm}^{-3}$. Furthermore, if NaCl were sufficiently stable to act as a nucleating agent and be incorporated into aerosols, reaction (1) could provide an important sink for stratospheric chlorine. The value of the rate for reaction (1) has recently been measured to be $2.5 \times 10^{-10} \text{ cm}^3 \text{ s}^{-1}$ (Silver, Stanton, Zahniser, and Kolb, 1984a). A more detailed discussion of the coupling to stratospheric chemistry will be given in Part II of this report.

More recently, the rate for (RR3) has been measured (Husain and Plane, 1982; Silver, Zahniser, Stanton, and Kolb, 1984b) to have a value three orders of magnitude higher than that used in Liu and Reid's model. Such high values for the rate of (RR3) raised the possibility of the existence of large amounts of NaO₂ in the upper atmosphere, with consequently low concentrations of atomic sodium. Analysis of the latest thermochemical data led Sze, Ko, Murad, and Swider (1982) to propose the reaction



as a potentially-fast recycling mechanism for NaO₂.

Our present understanding of the chemistry of sodium compounds is summarized in Figure 1, based on the scheme of Sze, Ko, Murad, and Swider (1982). Because of the difficulty in manipulating gas-phase Na in the laboratory, kinetic data for reactions involving sodium have become available only recently. Measurements are now available for the rates of (RR1), (RR3), (RR4), and (RR7), as well as other secondary reactions involving H₂ and O₃. Constraints can be placed on the Na(²P) branch of (RR2) from the measured background concentrations of O and O₃, the observed D-line emission, and kinetic considerations (Bates and Ojha, 1980). Additional constraints on other reaction rates can be obtained by comparing calculations with observations of the distribu-

tion (Liu and Reid, 1979; Sze, Ko, Murad, and Swider, 1982; Thomas, Isherwood, and Bowman, 1983) and diurnal variation of sodium (Kirchoff and Clemesha, 1983; Kirchoff, 1983). Estimated rates are given in Table 1 where laboratory measurements do not exist.

In Figure 1, the Na-NaO on the left-hand side represents the original Chapman scheme. The rates for (RR1) and (RR2) are sufficiently fast that the $[Na]/[NaO]$ should be proportional to the $[O]/[O_3]$ at any time of the day. Thus, in the absence of other sodium species, the diurnal behavior of the Na and NaO would be determined entirely by the diurnal variations of O and O_3 . The species NaO_2 and NaOH act as temporary reservoirs for the sodium species during the diurnal cycle. With the short photolysis lifetime for NaOH, diurnal variation of Na is expected if the density of NaOH is sufficiently high. The effect of NaO_2 on the diurnal variation of Na would depend on the magnitude of the recycling reactions (RR5) and (RR6).

3. SUMMARY OF OBSERVATIONS ON NEUTRAL IONS

An extensive data base now exists providing detailed information on the diurnal and seasonal behavior of the sodium layer. Some of these properties are directly attributable to transport phenomena on a seasonal (Gibson and Sandford, 1971; Megie et al., 1978; Kirchoff et al., 1981; Kirchoff and Clemesha, 1983) or diurnal time scale (Megie and Blamont, 1977; Clemesha et al., 1978; Kirchoff et al., 1981; Clemesha et al., 1982). Nevertheless, we can deduce from the data certain characteristics that have direct relevance to photochemical processes. The experimental data to be used in constraining our model are as follows:

- a) Total Abundance of Atomic Sodium: Lidar observations have constrained the diurnal variation of the Na column density to less than 15% (Gibson and Sandford, 1972; Clemesha et al., 1982). The absolute magnitude of the total abundance ranges from a summer minimum of $\sim 2 \times 10^9 \text{ cm}^{-2}$ to a winter maximum of $6-8 \times 10^9 \text{ cm}^{-2}$, yielding an average column density of $4 \times 10^9 \text{ cm}^{-2}$.
- b) Altitude Profiles of Atomic Sodium: Lidar observations of the sodium layer at different latitudes have consistently deduced a peak density of $3-5 \times 10^3 \text{ cm}^{-3}$ at 90-92 km during periods of low meteor-

itic activity (Megie and Blamont, 1977; Simonich et al., 1979). The peak height and density correlates with the seasonal change in total abundance, with high column densities corresponding to low peak altitudes and high peak densities (Gibson and Sandford, 1971).

Diurnal variations in the peak height have also been observed, but they are probably due to transport effects of gravity waves (Clemesha et al., 1982).

- c) Diurnal Variation of Local Densities of Atomic Sodium: The densities measured by lidar techniques exhibit a diurnal variation below 84 km (Simonich et al., 1979; Clemesha et al., 1982). The nocturnal decrease in sodium densities observed by these authors is about a factor of 2 at 83 km and 10 at 81 km.
- d) D-line Emission Rates: Measurements of the nighttime D-line emission in the southern hemisphere (low latitude) yield minimum values of 30 Rayleigh (R) during winter and 60 to 100 R at equinox (Kirchoff et al., 1981). Mean intensities in the northern hemisphere range from 35 to 100 R (Fukuyama, 1977). The equinox maximum in the northern hemisphere measurements is most pronounced at low latitudes, with amplitudes in agreement with the southern hemisphere results. High latitude measurements seem to exhibit a maximum in winter (Fukuyama, 1977). The emission rate also exhibits a small nocturnal variation of 30% symmetric around a minimum at midnight (Kirchoff et al., 1981).

A summary of the above experimental constraints is given in Table 2. We will concentrate on the diurnal variation of the above quantities. The seasonal behavior which will be useful for placing bounds on the experimental values used in comparison to our one-dimensional model will be discussed in Part IV.

4. DESCRIPTION OF MODEL

The one-dimensional model of mesospheric trace gases covers the altitude range from 60-120 km. It is an extension of the model previously used in studies of stratospheric chemistry (Sze, Ko, Specht, and Livshits, 1980). Concentrations of short-lived photochemical species are calculated using the grouping technique previously employed in stratospheric models (Sze et al., 1980).

The species calculated in our model include:

oxygen species, O_x : $O(^1D)$, O , O_3

odd hydrogen species, HO_x : H , OH , HO_2 , H_2O_2

odd nitrogen species, NO_x : N , NO , NO_2 , HNO_3 , NO_3 , N_2O_5 , HO_2NO_2

sodium species, NaX : Na , NaO , NaO_2 , $NaOH$

In addition, $O_2(^1\Delta_g)$ is also included. Although the NO_x species and $O_2(^1\Delta_g)$ are of minor importance in the neutral chemistry of the odd-oxygen and odd-hydrogen species, they are included in the chemistry scheme in anticipation of their roles in the ion chemistry. The effect of the odd-chlorine and methyl families on the above species is negligible at these altitudes; thus, they have not been included in the model.

Background species which are held fixed in the model include H_2 , H_2O , CO , N_2O , O_2 , and N_2 . Densities of the major constituents (N_2 and O_2) and temperatures are taken from the U.S. Standard Atmosphere (1976). The densities of the background trace species CO , H_2 , and H_2O , are taken from Allen, Lunine, and Yung (1984).

Photochemical lifetimes for HO_x and O_x are shorter than one day at altitudes below 80 km. The concentrations of all constituents are calculated from the time-dependent equation

$$\frac{dn_i}{dt} = P_i - L_i n_i, \quad (3)$$

where n_i , P_i , and L_i denote the density, production, and loss frequency for the i^{th} species. Equation (3) is solved subject to periodic boundary conditions over a 24-hour period,

$$n_i(t + 24 \text{ hrs.}) = n_i(t). \quad (4)$$

Note that the effect of transport is ignored in this region.

Time constants for HO_x , O_x , and NO_x become much longer than one day above 90 km. The densities of the above constituents are then determined by down-gradient diffusion. Although it is within the capability of the model to calculate the distribution of the long-lived species, we have fixed their densities in our calculations to the profiles given by Allen et al., (1984) for HO_x and O_x , and by Solomon, Crutzen, and Roble (1982) for NO_x . Slow species are

calculated in a self-consistent manner when we consider seasonal variations of the vertical eddy diffusion coefficient (see Part IV).

Sharp vertical gradients in the densities of O_x and HO_x result in very short (~ 1 day) transport time constants between 80 and 85 km. The diurnal variation of the above species is then determined by both photochemical and transport processes. The effects of transport are approximately accounted for in the present calculation by introducing an extra time-independent term, P_i^* in equation (3). The magnitude and sign of P_i^* is chosen such that the solutions of equation (3) at noon agree with the values calculated by Allen et al., (1984) at the same time.

The total density of sodium species (NaX) is calculated assuming an incoming flux of $2 \times 10^4 \text{ cm}^{-2} \text{ s}^{-1}$ at 100 km. The sodium is transported by diffusion into the troposphere where it is removed by heterogeneous processes with an effective lifetime of 10 days. The values of the diffusion coefficients below 70 km are the same as those used in the stratospheric model (Sze, Ko, Specht, and Livshits, 1980). Above 70 km, a value of $10^6 \text{ cm}^2 \text{ s}^{-1}$ is adopted as suggested by Hunten (1975). The calculated total NaX volume mixing ratio ranges from 2.3×10^{-9} at 100 km to 1×10^{-11} at 60 km.

The chemical scheme for the oxygen, hydrogen, and nitrogen species is similar to the one used in the stratospheric model. Reaction rates are taken from the latest NASA review (JPL, 1982), with the corrections suggested by Allen et al., (1984). The reactions involving sodium species are taken from Sze, Ko, Murad, and Swider (1982) as given in Table 1.

5. RESULTS

Diurnal profiles for the main O_x species (O , O_3) at 82, 84, 86, and 88 km are shown in Figures 2a, 2b, 2c, and 2d, respectively; similar profiles at the same altitudes are shown for the HO_x species, H , OH , and HO_2 in Figures 3a, 3b, 3c, and 3d. The calculations are performed for 38°N , summer solstice conditions. Our results are similar to the diurnal variation calculated by Allen et al., (1984). The O_x and HO_x families are dominated by O and H , respectively. The change in the diurnal behavior of these species with altitude illustrate the transition between the photochemically-controlled region below 82 km and the diffusion-controlled region above 90 km. Since the sodium chemistry above 60 km has very little effect on the background neutral chemistry, the

above profiles are used for all the different models of sodium considered below.

The results shown in Figure 2 indicate that the $[O]/[O_3]$ ratio is $10^2 - 10^3$ between 80 and 90 km. In the absence of temporary reservoirs, $[Na]$ and $[NaO]$ would be controlled by the Chapman scheme. The rates for (RR1) and (RR2) given in Table 1 would then imply a $[Na]/[NaO]$ ratio of $10^1 - 10^2$, placing the atomic sodium peak well below 80 km. Thus, the observed position of the Na peak and the constraints on (RR1) and (RR2) as suggested by thermal chemical data strongly suggest the existence of temporary reservoirs for atomic sodium.

In our previous study (Rodriguez et al., 1984), we focused on the interaction of the Na-NaO species with the temporary reservoirs, NaO_2 and $NaOH$. In the chemical scheme illustrated in Figure 1, the interaction between Na and NaO_2 is controlled by the rapid formation of NaO_2 , (reaction (RR3)), and recycling of NaO_2 to Na-NaO through (RR6). Similarly, coupling to $NaOH$ is controlled by (RR7) and the photolysis reaction (RR4). At that time, experimental data existed only on (RR3) (Silver et al., 1984b) and (RR4) (Rowland and Makide, 1982). Since then, (RR7) has been measured to have a value of $2 \pm 1 \times 10^{-10} \text{ cm}^3 \text{ sec}^{-1}$ (Ager and Howard, 1985). Given the sensitivity of the model results to (RR7), we examine here the sensitivity of results to (RR7) within the bounds of the experimental values in conjunction with (RR6).

Three models were considered, representing different strengths of coupling between the Na-NaO species and the NaO_2 and $NaOH$ temporary reservoirs. The adopted parameters for these models are listed in Table 3. Model A represents the conditions for weak coupling to temporary reservoirs consistent with measured kinetic rates. The value adopted for reaction (RR6) is small, but sufficient to recycle enough NaO_2 back to Na-NaO so that Na does not disappear completely (Sze et al., 1982) due to the fast rates measured for reaction (RR3). Model B adopts the mean measured rate for the formation of $NaOH$ (RR7), together with small coupling to the NaO_2 reservoir. Model C represents conditions of maximum coupling to the NaO_2 reservoir, with the rate of (RR6) near the kinetic limit.

Noon altitude profiles for Na are shown in Figure 4 for the different models. Measurements by Simonich et al. (1979) for midnight, and Granier and

Megie (1982) for noon are also shown at altitudes above 85 km. As indicated by the data, the diurnal variation of Na is negligible between 85 and 95 km. Agreement between these measurements and Model C is poor. Better agreement is obtained with Models A and B, especially in the region of the peak. The discrepancy between observation and the calculated results above 95 km is probably due to the effect of ion chemistry. We will discuss this in more detail in the Part III.

The diurnal variation of the total Na abundance is presented in Figure 5, again for all three models. The absolute magnitude of the abundance is in good agreement with observed values for Models A, B, and C. The diurnal variation of the total abundance is consistent with observations for Model A (14%) but is too large for Models B and C (23% and 31%, respectively). The larger diurnal variation in Model B is a result of increased abundances of NaOH due to the increase in the rate of (RR7) by a factor of 2 over Model A. The large diurnal variations calculated for Model C follow from the results that much of the atomic sodium is found below 82 km where the diurnal deviations of Na is the largest.

The results presented in Figures 4 and 5 suggest that Model C does not reproduce the observed Na altitude profile and diurnal variation of the sodium abundance. Models A and B yield very similar results for the altitude profile. Based on the diurnal variation of the column density, Model A is preferable to Model B. The diurnal variation in Model B is, however, close enough to the observational upper limit, and we cannot discriminate between values of 1 and $2 \times 10^{-10} \text{ cm}^3 \text{ sec}^{-1}$ for the rate of (RR7) without considering other second-order effects such as the effect of uncertainties in other unknown rates or background species, O and H₂O, in particular.

Figures 6a and 6b illustrate the diurnal variation of Na at 82, 84, and 86 km, for Models A (Figure 6a) and B (Figure 6b). Although the diurnal variation in Model B is slightly larger than in A, both models yield results in satisfactory agreement with experimental data below 85 km. We should note that the day-to-night ratio changes dramatically over an altitude range of 2 km in this region. This fact should be kept in mind in comparing theoretical results to lidar observations, since the latter typically have an altitude resolution of 1 - 2 km (Megie and Blamont, 1977; Simonich et al., 1979).

The interaction between the different sodium reservoirs is illustrated in Figures 7a through 7d. In the region 80-90 km, the $[\text{Na}]/[\text{NaO}_2]$ ratio can be estimated from the approximate chemical equilibrium conditions for NaO_2 :

$$k_3 [\text{Na}][\text{O}_2][\text{M}] \approx k_6 [\text{NaO}_2][\text{O}]. \quad (5)$$

In both Models A and B, Na is the most abundant species at 90 km during the day, with NaOH comparable to Na at night for Model B. At lower altitudes, with larger values for $[\text{O}_2]$ and $[\text{M}]$ and smaller values for $[\text{O}]$, NaO_2 becomes comparable to NaOH at 82 km. The $[\text{NaOH}]/[\text{NaO}_2]$ ratio can be obtained from the approximate relations

$$(J_4 + k_{12}[\text{H}])[\text{NaOH}] \approx [\text{NaO}_2] (k_{10}[\text{H}] + k_{11}[\text{OH}]) + k_7[\text{NaO}][\text{H}_2\text{O}] \quad (6)$$

$$k_1 [\text{Na}][\text{O}_3] \approx k_2 [\text{NaO}][\text{O}] \quad (7)$$

and equation (5). Rapid changes in $[\text{NaOH}]$ are expected at dawn and dusk due to the onset and disappearance of photolysis.

The diurnal variation of Na can be related to the variation in NaO_2 , O, and NaOH through (5) - (7). At 90 km, atomic oxygen exhibits no diurnal variation, and changes in NaO_2 and Na are due to rapid changes in NaOH from day to night. As we increase the rate of (RR7) from Model A to Model B, the NaOH/NaO_2 ratio increases, and the large diurnal changes in NaOH induce correspondingly larger variations in NaO_2 and Na near the sodium layer peak at 90 km. On the other hand, atomic oxygen exhibits a large diurnal variation at 82 km and determines the diurnal variation of Na to first order at that altitude.

6. DISCUSSION AND CONCLUSIONS

Results of Models A, B, and C are summarized in Table 4. The experimental results from Table 2 are included for comparison. Also shown in Table 4 is the midnight D-line emission rate. We note that the calculated D-line emission rate for a given model depends on the assumed branching ratio for production of $\text{Na}(^2\text{P})$ by reaction (RR2), for which only estimates exist (Sze et al., 1982; Bates and Ujha, 1980). We have adopted a value of .3 for the branch producing $\text{Na}(^2\text{P})$. Results on the D-line emission rate are reasonable for all models, and thus are inconclusive for our purposes. As noted previously, Model C agrees poorly with

observations of the peak height, peak density, the column density, and diurnal variation. We can therefore rule out Model C as an unrealistic description of sodium chemistry in the upper atmosphere. The rate for (RR6) ($\text{NaO}_2 + \text{O} \rightarrow \text{NaO} + \text{O}_2$) must therefore be significantly lower than $10^{-10} \text{ cm}^3 \text{ s}^{-1}$, closer to $10^{-13} \text{ cm}^3 \text{ s}^{-1}$.

It is harder to draw any definite conclusions for differentiating between Models A and B. The best basis for differentiation is the diurnal variation of local densities and total column densities of Na. Local density variations for both models are consistent with observations, given the altitude resolution of lidar measurements. Variations in the total column density for Models A and B are more sharply differentiated, and the question thus lies on the interpretation of the experimental data.

Early lidar measurements of the sodium layer yielded day-to-night ratios of at most 10% (Gibson and Sandford, 1972) or changes during the night of about 4% (Simonich et al., 1979). More recent observations of Clemesha et al. (1982) which were carried out on a continuous basis yielded diurnal variations with an amplitude of $\sim 15\%$ from the mean (30% peak-to-peak). The observations, however, exhibited a strong semidiurnal component, and the above authors suggested that the diurnal variation is due entirely to tidal effects. Thus, definite conclusions could be made only after incorporation of tidal effects into existing photochemical models, coupled with higher resolution measurements of the diurnal variation of Na. We thus cannot constrain the rate (RR7) ($\text{NaO} + \text{H}_2\text{O} \rightarrow \text{NaOH} + \text{OH}$) to more than a factor of two at this point. The lower bound used in Model A is consistent with measurements by Ager and Howard (1985).

Another consequence of the high rate for reaction (RR3) is that the diurnal variation of atomic sodium below the peak can be estimated to first order in Models A and B from the photochemical equilibrium relation between Na and NaO_2 given in equation (5). The diurnal variation of Na then follows that of atomic oxygen if NaO_2 does not change appreciably, a condition satisfied below the Na peak in Model A. Increased coupling to NaOH leads to a higher diurnal variation of NaO_2 in Model B. Comparison of the diurnal variation of O in Figure 2 and that of Na in Figure 6 suggests general agreement between both diurnal changes. The ratio $[\text{O}]_{\text{Dusk}}/[\text{O}]_{\text{Dawn}}$ is 5.3 at 82 km and 1.7 at 84 km. The additional coupling to NaOH is reflected in larger ratios for all models, particularly at 84 km. In Model C, the diurnal variation of atomic oxygen is no longer the

first-order process contributing to the variability of sodium, even at 82 km. In this case, the abundance of NaO_2 is much less than that of NaOH , and the diurnal variation of Na is determined by the interaction with the NaOH reservoir. As stated above, however, we feel that this model does not represent the chemistry of sodium species.

Given that the diurnal variation of atomic sodium depends crucially on the diurnal variation of atomic oxygen, the observed absence of appreciable diurnal change in the total Na abundance requires that the bulk of the sodium be located in a region where O is constant throughout the day, i.e., about 85 km. Once the total NaX is fixed, the position of the peak is determined to first order by the magnitude of (RR3). Lowering the peak by modifying the NaX profile through changes in the Na source or eddy diffusion coefficient could be reflected in a larger diurnal variation of the column density of sodium. Since the time constant for the Na-NaO_2 exchange ranges from seconds to a few minutes below 90 km, any modelling of transport effects (i.e., tides, gravity waves) must include a self-consistent treatment of the atomic oxygen variation.

The photolytic reactions,



could also play an important role in the diurnal variation of sodium if their values were very different from those assumed here. Reaction (RR5) could compete with the reaction with O (RR6) if $J_5 \sim 10^{-2} \text{ s}^{-1}$. In such a case, the recycling of NaO_2 to Na would occur via reaction (RR5), and the constraints derived here for reaction (RR6) can be easily translated into similar constraints for reaction (RR5). Photolysis of NaO_2 is also important in the stratosphere, where the concentration of atomic oxygen is small.

The value adopted for reaction (RR4) by Rowland and Makide (1982) assumes that all the observed EUV absorption of NaOH is due to photolysis. If this is not the case, and J_4 is smaller, our models would produce more NaOH , but its day-to-night change would be smaller and the effects of coupling of Na-NaO to the NaOH reservoir would be consequently reduced.

Ionization of atomic sodium can also affect our results in the region above the peak. Atomic sodium is ionized both by photons and by charge exchange with O_2^+ , with an effective J rate of $\sim 10^{-5} \text{ s}^{-1}$ (Swider, 1970; 1984). Loss of Na^+ occurs primarily through clustering with N_2 ,



followed by dissociative recombination of $\text{Na}^+ \cdot \text{N}_2$ (Richter and Sechrist, 1979). The partitioning between Na and Na^+ could thus be determined by the rate of the clustering reaction (7), which has not been measured. Vertical ion drifts could also change the Na/Na^+ ratio. This would reduce the amount of atomic Na calculated in the model, bringing the result into much better agreement with the measurements shown in Figure 4 above the peak. We will discuss this matter in more detail in Part III.

In conclusion, the results of our study point out the importance of the NaO_2 temporary reservoir in determining the diurnal variation of atomic sodium. The diurnal variation of atomic oxygen thus plays a dominant role in determining diurnal changes in Na. Present experimental data constrains the recycling of NaO_2 through reaction with O (RR6), limiting the rate to considerably less than $10^{-13} \text{ cm}^3 \text{ s}^{-1}$. Large amounts of NaOH are produced through the reaction of NaO with H_2O (reaction (RR7)), although the rate for this process has a factor of 3 uncertainty. Further clarification of this problem requires measurements of unknown reaction rates (in particular, (RR4), (RR5), and (RR6)), continuing high-resolution observations of sodium species in the upper atmosphere, and further modelling incorporating tidal and gravity wave effects on both sodium species and background trace gases.

Table 1: Reaction Scheme and Rate Constants

Reaction			Rate Coefficient ^a
1.	$\text{Na} + \text{O}_3$	$\rightarrow \text{NaO} + \text{O}_2$	3.5×10^{-10} [b]
2.	$\text{NaO} + \text{O}$	$\rightarrow \text{Na} (^2\text{P}, ^2\text{S}) + \text{O}_2$	4(-11) [c]
3.	$\text{Na} + \text{O}_2 + \text{N}_2$	$\rightarrow \text{NaO}_2 + \text{N}_2$	$1.9 \times 10^{-30} (\text{T}/300)^{-1.1}$ [d]
4.	$\text{NaOH} + h\nu$	$\rightarrow \text{Na} + \text{OH}$	2(-3) [e]
5.	$\text{NaO}_2 + h\nu$	$\rightarrow \text{Na} + \text{O}_2$	1(-4) [c]
6.	$\text{NaO}_2 + \text{O}$	$\rightarrow \text{NaO} + \text{O}_2$	1(-10), 1(-13) [c]
7.	$\text{NaO} + \text{H}_2\text{O}$	$\rightarrow \text{NaOH} + \text{OH}$	$(2 \pm 1) \times 10^{-10}$ [h]
8.	$\text{NaO} + \text{O}_3$	$\rightarrow \text{NaO}_2 + \text{O}_2$	1.8×10^{-10} [h]
9.	$\text{NaO} + \text{H}$	$\rightarrow \text{Na} + \text{OH}$	1(-14) [g]
10.	$\text{NaO}_2 + \text{OH}$	$\rightarrow \text{NaOH} + \text{O}_2$	1(-11) [f]
11.	$\text{NaO}_2 + \text{H}$	$\rightarrow \text{NaOH} + \text{O}$	1(-13) [g]
12.	$\text{NaOH} + \text{H}$	$\rightarrow \text{Na} + \text{H}_2\text{O}$	1.4(-12) [f]
13.	$\text{NaOH} + (^1\text{D})$	$\rightarrow \text{NaO} + \text{OH}$	1(-10) [g]
14.	$\text{Na} + \text{HO}_2$	$\rightarrow \text{NaOH} + \text{O}$	1(-10) [f]
15.	$\text{NaO} + \text{O}_3$	$\rightarrow \text{Na} + 2\text{O}_2$	1(-10) [h]
16.	$\text{NaO} + \text{HO}_2$	$\rightarrow \text{NaOH} + \text{O}_2$	1(-11) [f]
17.	$\text{NaO} + \text{H}_2$	$\rightarrow \text{Na} + \text{H}_2\text{O}$	1(-11) [h]
18.	$\text{NaO} + \text{H}_2$	$\rightarrow \text{NaOH} + \text{H}$	2.6(-11) [h]

^aRead 3(-10) as 3×10^{-10} . Units are $\text{cm}^3 \text{s}^{-1}$, except $\text{cm}^6 \text{s}^{-1}$ for (3) and s^{-1} for (4), (5), and (15). [b], Zahniser et al., (1985). [c], Sze et al. (1982). [d], Silver et al. (1984). [e], Rowland and Makide (1982). [f], Liu and Reid (1979). [g], Kirchoff and Clemesha (1983). [h] Ager and Howard (1985).

Table 2: Experimental Data on Sodium

		<u>References</u>
<u>Sodium Layer</u>		
Peak Altitude	90 - 92 km	Megie and Blamont, 1977;
Peak Density	$3-5 \times 10^3 \text{ cm}^{-3}$	Simonich et al., 1979
Total Abundance	$4 \times 10^9 \text{ cm}^{-2}$ ($2-8 \times 10^9 \text{ cm}^{-2}$)	Gibson and Sandford, 1972; Clemesha et al., 1982
<u>Diurnal Variation</u>		
Total Abundance ^a	< 15%	Gibson and Sandford, 1971; Clemesha et al., 1982
[Na] _{Dusk} /[Na] _{Dawn}	2 (83 km) 10 (81 km)	Simonich et al., 1979; Clemesha et al., 1982
<u>D-line Emission Rate</u>	~ 50 R (30-100 R)	Fukuyama, 1977; Kirchoff et al., 1981

^aPercent deviation from median abundance

Table 3: Adopted Models

	$k \text{ (NaO}_2 + \text{O)}$ ($\text{cm}^3 \text{ s}^{-1}$)	$k \text{ (NaO} + \text{H}_2\text{O)}$ ($\text{cm}^3 \text{ s}^{-1}$)
Model A	10^{-13}	10^{-10}
Model B	10^{-13}	2×10^{-10}
Model C	10^{-10}	10^{-10}

Table 4: Calculated Sodium Parameters for the Different Models

	Model B	Model A	Model C	Measured Value
Peak Altitude	90 km	90 km	86 km	90-92 km
Peak Density	$4.3 \times 10^3 \text{ cm}^{-3}$	$4.2 \times 10^3 \text{ cm}^{-3}$	$6.3 \times 10^3 \text{ cm}^{-3}$	$3-5 \times 10^3 \text{ cm}^{-3}$
Total Abundance ^a	$4.47 \times 10^9 \text{ cm}^{-2}$	$4.13 \times 10^9 \text{ cm}^{-2}$	$6.34 \times 10^9 \text{ cm}^{-2}$	$2-8 \times 10^9 \text{ cm}^{-2}$
Diurnal Variation, ^b Total Abundance	14%	23%	31%	<15%
[Na] _{Dusk} /[Na] _{Dawn}	7.1 (82 km)	7.4 (82 km)	25.5 (82 km)	10 (81 km)
	2.4 (84 km)	3.1 (84 km)	3.8 (84 km)	2 (83 km)
D-Line Emission Rate (night)	35 R	46 R	47 R	50 R

^aAveraged over one day.

^bPercent deviation from the median abundance.

References

- Ager, Joel W., III, and C. J. Howard (1985) Kinetic studies of some sodium reactions of atmospheric importance. E. O. S., 66, 317.
- Allen, M., J. I. Lunine, and Y. L. Yung (1984) The vertical distribution of ozone in the mesosphere and lower thermosphere, J. Geophys. Res., 89, 4841.
- Arnold, F., H. Böhrringer, and G. Henschen (1978) Composition measurements of stratospheric positive ions, Geophys. Res. Lett., 5, 653.
- Arnold, F., G. Henschen, and E. E. Ferguson (1981) Mass spectrometric measurements of fractional ion abundances in the stratosphere-positive ions, Planet. Space Sci., 29, 185.
- Bates, D. R., and P. C. Ojha (1980) Excitation of the Na D-doublet of the nightglow, Nature, 286, 790.
- Chapman, S. (1939) Notes on atmospheric sodium, Ap. J., 90, 309.
- Clemesha, B. R., V. W. J. H. Kirchoff, and D. M. Simonich (1978) Simultaneous observations of the Na 5893Å nightglow and the distribution of sodium atoms in the mesosphere, J. Geophys. Res. 239, 509.
- Clemesha, B. R., D. M. Simonich, P. O. Batista, and V. W. J. H. Kirchoff (1982) The diurnal variation of atmospheric sodium, J. Geophys. Res., 87, 181.
- Ferguson, E. E. (1978) Sodium hydroxide ions in the stratosphere, Geophys. Res. Lett., 5, 1035.
- Fukuyama, K. (1977) Airglow variations and dynamics in the lower thermosphere and upper mesosphere, II, Seasonal and long-term variations, J. Atmos. Terr. Phys., 39, 1.
- Gadsden, M. (1968) Sodium in the upper atmosphere: meteoritic origin, J. Atmos. Terr. Phys., 30, 151.
- Gardner, C. S., D. G. Boelz, C. R. Philbrick, and D. P. Sipler (1986) Simultaneous lidar measurements of the sodium layer at the Air Force Geophysics Laboratory and the University of Illinois. Submitted to J. Geophys. Res.
- Gibson, A. J., and M. C. W. Sandford (1971) The seasonal variation of the night-time sodium layer, J. Atmos. Terr. Phys., 33, 1675.
- Gibson, A. J., and M. C. W. Sandford (1972) Daytime laser radar measurements of the atmospheric sodium layer, Nature, 239, 509.
- Granier, C., and G. Megie (1982) Daytime lidar measurements of the mesospheric sodium layer. Planet. Space Sci. 30, 169.

- Hunten, D. M. (1975) Vertical transports in atmospheres. In Atmospheres of Earth and Planets. B. M. McCormac (ed.), Dordrecht, Holland, pp. 59-72.
- Hunten, D. M., R. P. Turco, and O. B. Toon (1980) Smoke and dust particles of meteoritic origin in the mesosphere and stratosphere, J. Atmos. Sci., 37, 1342.
- Husain, D., and J. M. C. Plane (1982) Kinetic investigation of the reaction between $\text{Na} + \text{O}_2 + \text{M}$ by time resolved atomic resonance absorption spectroscopy, J. Chem. Soc., Faraday Trans., 2, 78, 163.
- JPL (1982) Chemical kinetics and photochemical data for use in stratospheric modeling. Evaluation #5. JPL Publication 82-57.
- Kirchoff, V. W. J. H. (1983) Atmospheric sodium chemistry and diurnal variations: An update, Geophys. Res. Lett., 10, 721.
- Kirchoff, V. W. J. H., B. R. Clemesha, and D. M. Simonich (1981) Average nocturnal and seasonal variations of sodium nightglow at 23°S, 46°W, Planet. Space Sci., 29, 765.
- Kirchoff, V. W. J. H., and B. R. Clemesha (1983) The atmospheric neutral sodium layer, 2. Diurnal variations, J. Geophys. Res., 88, 442.
- Kolb, C. E., and J. B. Elgin (1976) Gas phase chemical kinetics of the Na in the upper atmosphere, Nature, 263, 488.
- Kvifte, G. (1973) Alkali chemistry problems of the upper atmosphere. In Physics and Chemistry of the Upper Atmosphere, B. M. McCormac (ed.), p. 158, Reidel, Dordrecht, Holland.
- Liu, S. C., and G. C. Reid (1979) Sodium and other minor constituents of meteoric origin in the atmosphere. Geophys. Res. Lett., 6, 283.
- Megie, G., and J. E. Blamont (1977) Laser sounding of atmospheric sodium: Interpretation in terms of global atmospheric parameters, Planet. Space Sci., 25, 1093.
- Megie, G., F. Bos, J. E. Blamont, and M. L. Chanin (1978) Simultaneous nighttime lidar measurements of atmospheric sodium and potassium, Planet. Space Sci., 26, 27.
- Murad, E., and W. Swider (1979) Chemistry of meteor metals in the stratosphere. Geophys. Res. Lett., 6, 929.
- Murad, E., W. Swider, and S. W. Bensen (1981) Possible role for metals in stratospheric chlorine chemistry. Nature, 289, 273.
- Richter, E. S., and C. F. Sechrist, Jr. (1979) A cluster ion chemistry for the mesospheric sodium layer. J. Atmos. Terr. Phys., 41, 579.
- Rodriguez, J. M., M. K. W. Ko, and N. D. Sze (1984) The diurnal variation of the neutral sodium species in the upper atmosphere: A model study. Report #AFGL-TR-84-0204, Air Force Geophysics Lab., Bedford, MA, ADA154988.

- Rowland, F. S., and Y. Makide (1982) Upper stratospheric photolysis of NaOH. Geophys. Res. Lett., 9, 473-475.
- Rowland, F. S., and P. J. Rogers (1982) Upper stratospheric photolysis of NaCl and KCl, Proc. Nat. Acad. Sci. USA, 79, 2737.
- Silver, J. A., A. C. Stanton, M. S. Zahniser, and C. E. Kolb (1984a) The gas phase reaction rate of sodium hydroxide with hydrochloric acid. J. Phys. Chem., 88, 3123.
- Silver, J. A., M. S. Zahniser, A. C. Stanton, and C. E. Kolb (1984b) Temperature-dependent termolecular reaction rate constants for potassium and sodium peroxide formation. Presented at the 20th International Symposium on Combustion, the Combustion Institute, Pittsburgh, PA.
- Simonich, D. M., B. R. Clemesha, and V. W. J. H. Kirchoff (1979) The mesospheric sodium layer at 23°S: Nocturnal and seasonal variations. J. Geophys. Res., 84, 1543.
- Solomon, S., P. J. Crutzen, and R. G. Roble (1982) Photochemical coupling between the thermosphere and the lower atmosphere. I. Odd nitrogen from 50 to 120 km. J. Geophys. Res., 87, 7206
- Swider, W. (1970) Ionic reactions for meteoritic elements, Ann. Geophys., 26, 595.
- Swider, W. (1984) Ionic and neutral concentrations of Mg and Fe near 92 km, Planet. Space Sci., 32, 307.
- Sze, N. D., M. K. W. Ko, R. Specht, and M. Livshits (1980) Modeling of chemical processes in the troposphere and stratosphere. AFGL-TR-80-0251, Contract No. F 19628-78-C-0215, ADA092704.
- Sze, N. D., M. K. W. Ko, W. Swider, and E. Murad (1982) Atmospheric sodium chemistry. I. The altitude region 70-100 km. Geophys. Res. Lett., 9, 1187-1190.
- Thomas, L., M. C. Isherwood, and M. R. Bowman (1983) A theoretical study of the height distribution of sodium in the mesosphere. J. Appl. Terr. Phys., 45, 587.
- U. S. Standard Atmosphere, 1976 (1976) NA00-S/T 76-1562, Washington, D.C.
- Zahniser, M. S., J. A. Silver, and C. E. Kolb (1985) Mesospheric chemistry of meteoric metals: Reaction rate measurements for Na + O₃. EOS (Trans. A.G.U.), 66, 317.

Figure Captions

- Figure 1. Chemical reactions controlling the behavior of sodium species in the mesosphere. The dotted box in the left-hand side represents the scheme proposed by Chapman (1939). Coupling to the temporary reservoirs NaO_2 and NaOH occurs primarily through the reactions denoted by solid arrows. The dotted arrows represent direct production of NaOH from NaO_2 (Liu and Reid, 1979). This mechanism is the primary source of NaOH if the reaction rate of NaO with H_2O is negligible.
- Figure 2. Diurnal variation of odd-oxygen species O and O_3 , calculated by our model at (a) 82 km, (b) 84 km, (c) 86 km, and (d) 88 km. Input parameters and assumptions of our model are discussed in the text.
- Figure 3. Diurnal variation of odd-hydrogen species H , OH , and HOX calculated at (a) 82 km, (b) 84 km, (c) 86 km, and (d) 88 km.
- Figure 4. Altitude profiles of atomic sodium at noon calculated for Models A, B, and C. The measurements of Simonich et al. (1979) at midnight (x) and of Granier and Megie (1982) at noon (o) are also included for comparison.
- Figure 5. Diurnal variation of the total column abundance of atomic sodium, calculated for Models A, B, and C.
- Figure 6. Diurnal variation of local densities of atomic sodium at 82, 84, and 86 km. Results are shown for Model A (6a) and Model B (6b).
- Figure 7. Diurnal variation of the local densities of sodium species at 82 and 90 km, calculated for Model A (7a and 7b) and Model B (7c and 7d).

SODIUM CHEMISTRY

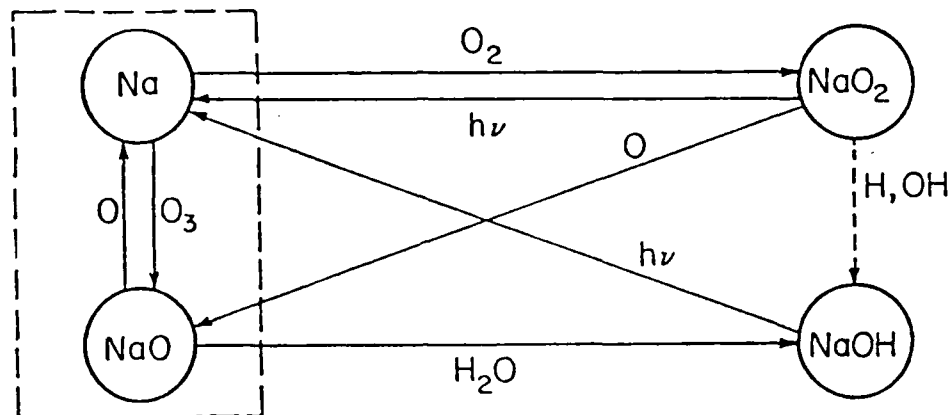


Figure 1. Chemical reactions controlling the behavior of sodium species in the mesosphere. The dotted box in the left-hand side represents the scheme proposed by Chapman (1939). Coupling to the temporary reservoirs NaO₂ and NaOH occurs primarily through the reactions denoted by solid arrows. The dotted arrows represent direct production of NaOH from NaO₂ (Liu and Reid, 1979). This mechanism is the primary source of NaOH if the reaction rate of NaO with H₂O is negligible.

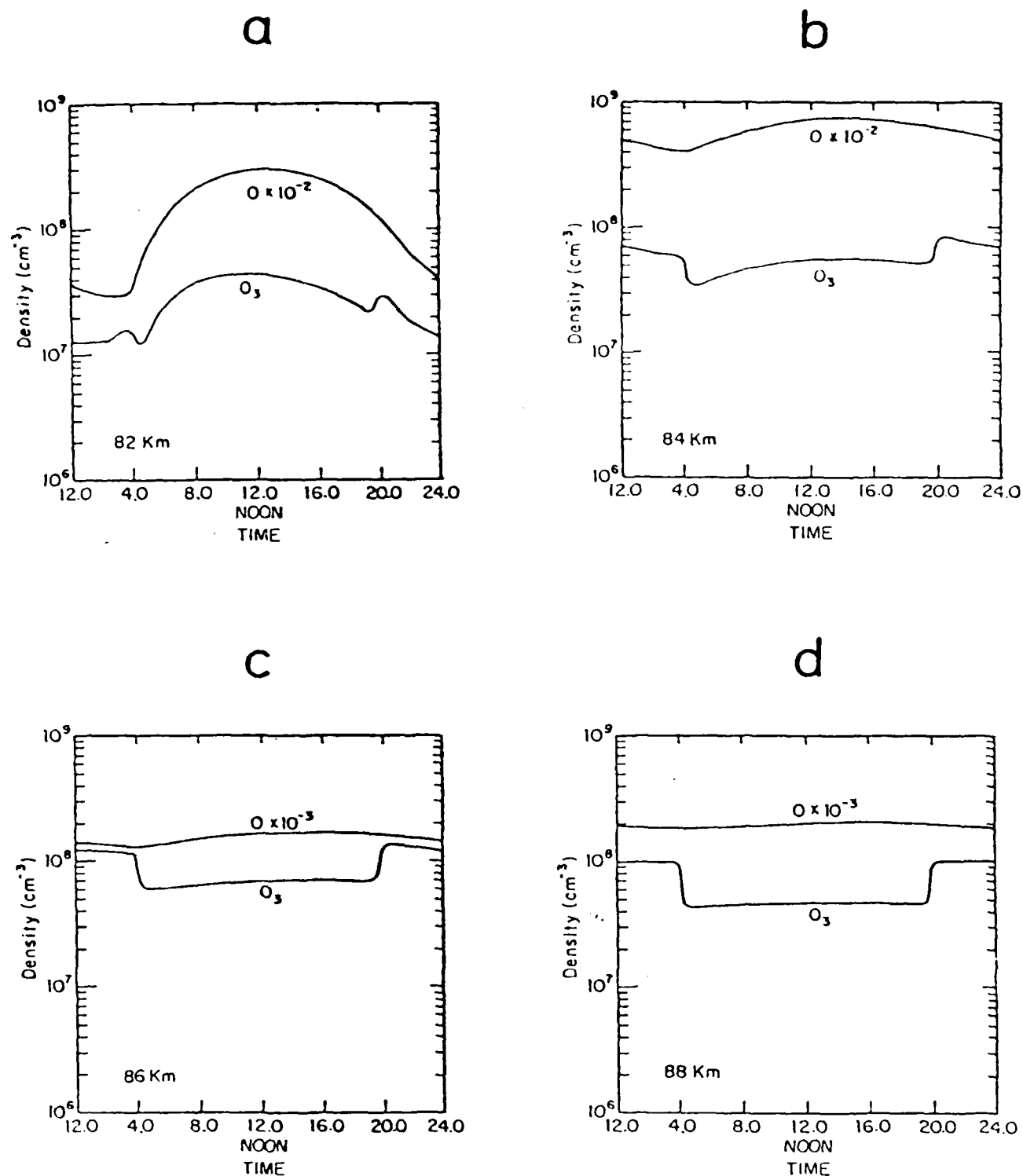


Figure 2. Diurnal variation of odd-oxygen species O and O_3 , calculated by our model at (a) 82 km, (b) 84 km, (c) 86 km, and (d) 88 km. Input parameters and assumptions of our model are discussed in the text.

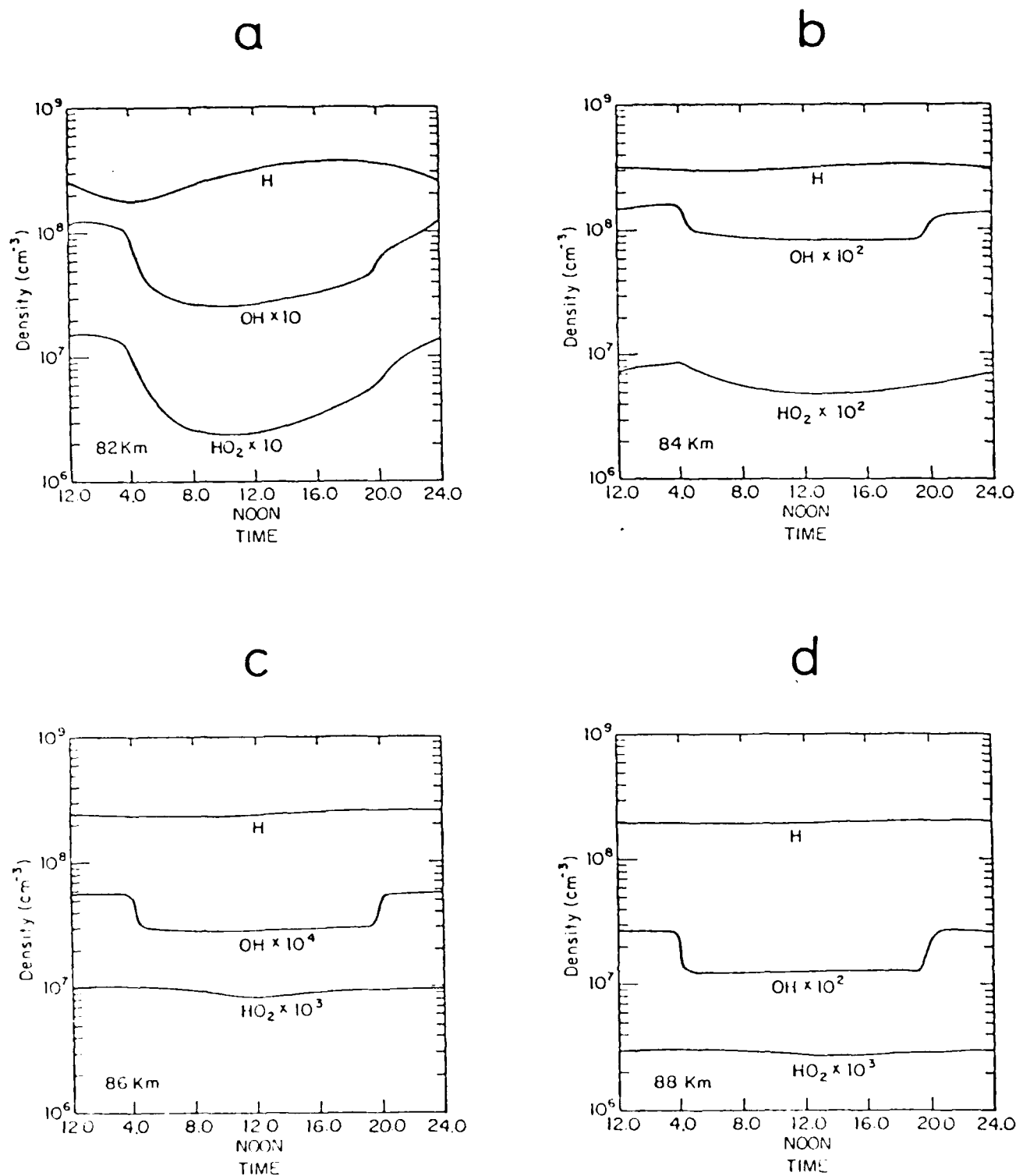


Figure 3. Diurnal variation of odd-hydrogen species H, OH, and HOX calculated at (a) 82 km, (b) 84 km, (c) 86 km, and (d) 88 km.

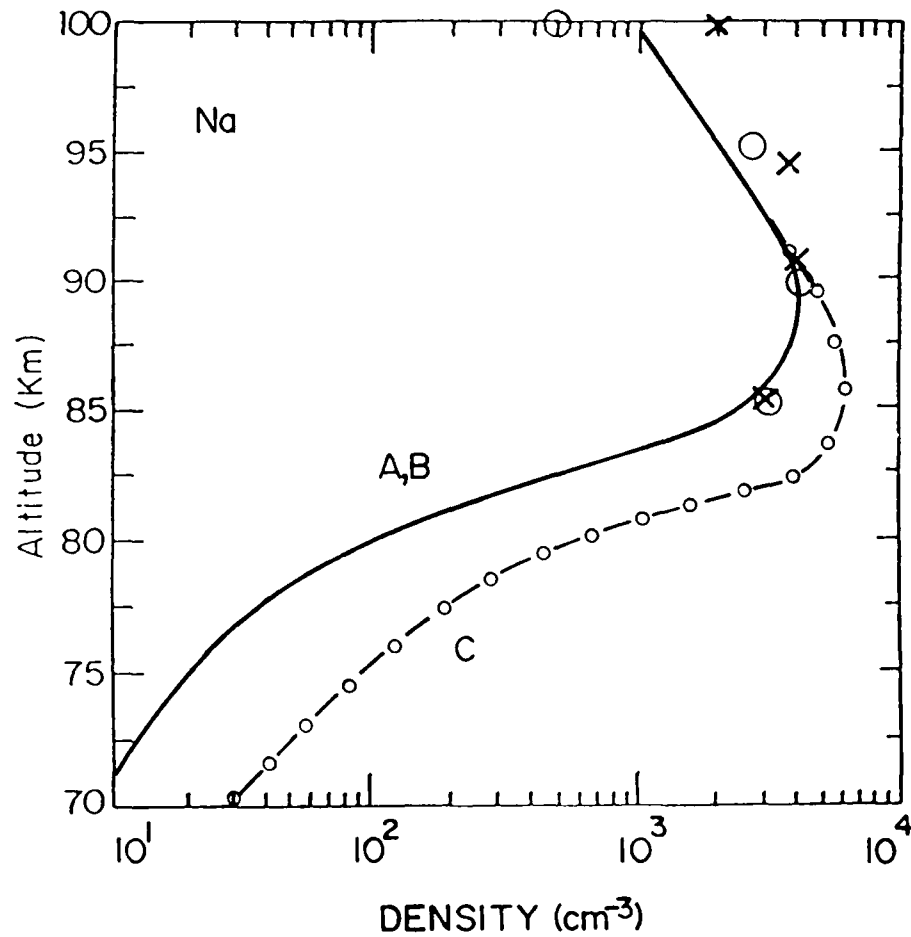


Figure 4. Altitude profiles of atomic sodium at noon calculated for Models A, B, and C. The measurements of Simonich et al. (1979) at midnight (x) and of Granier and Megie (1982) at noon (o) are also included for comparison.

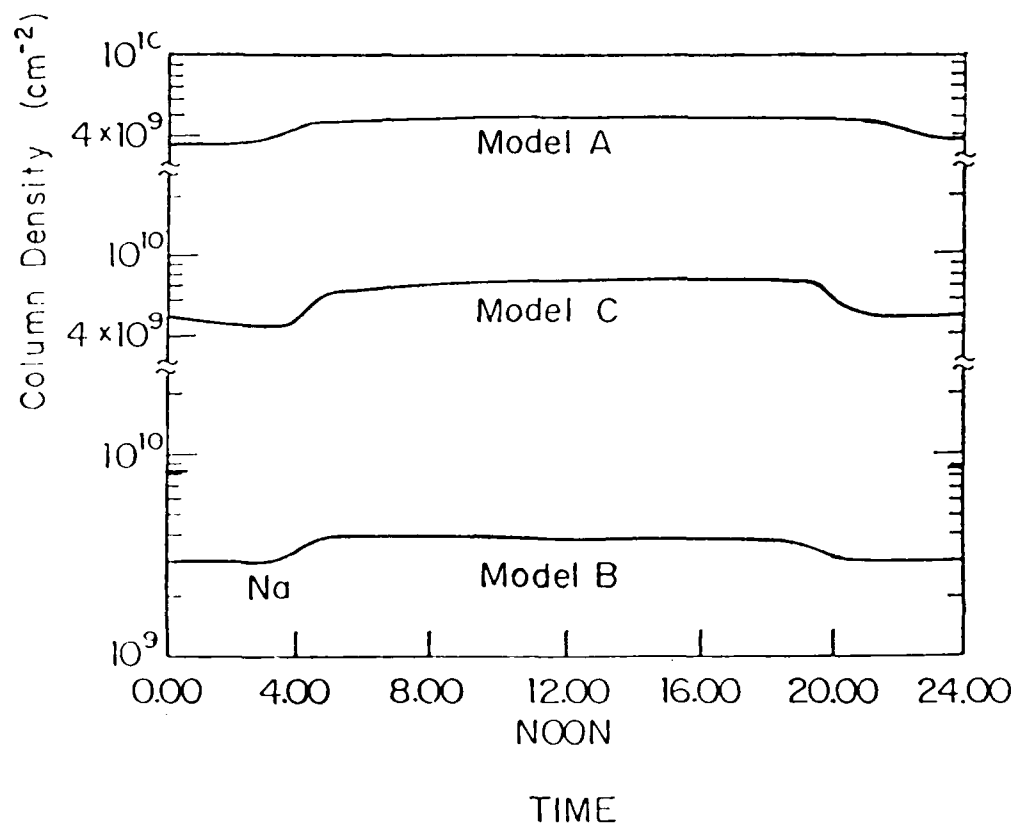


Figure 5. Diurnal variation of the total column abundance of atomic sodium, calculated for Models A, B, and C.

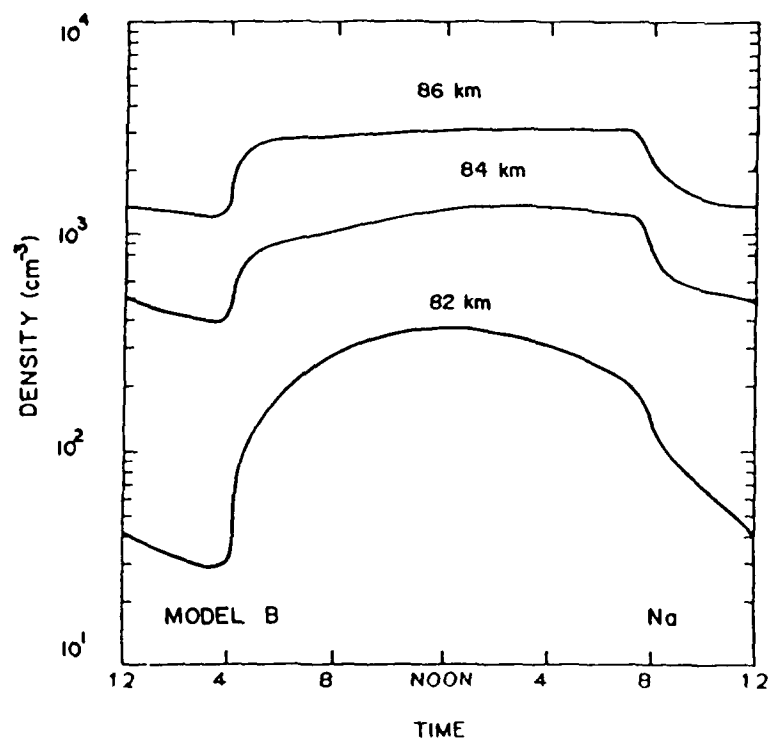
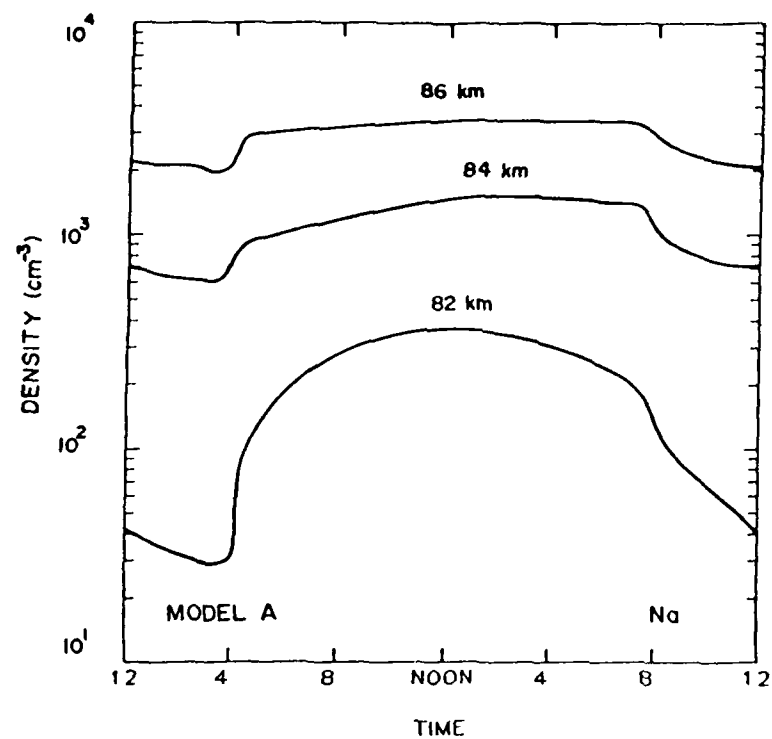


Figure 6. Diurnal variation of local densities of atomic sodium at 82, 84, and 86 km. Results are shown for Model A (6a) and Model B (6b).

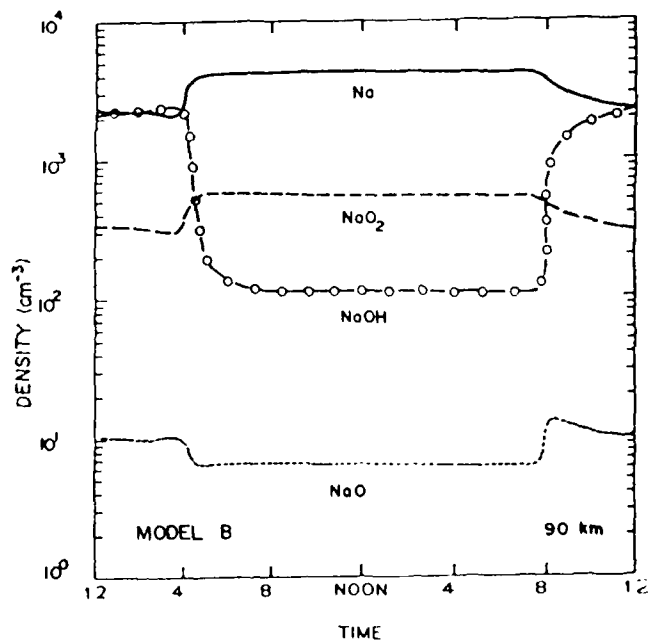
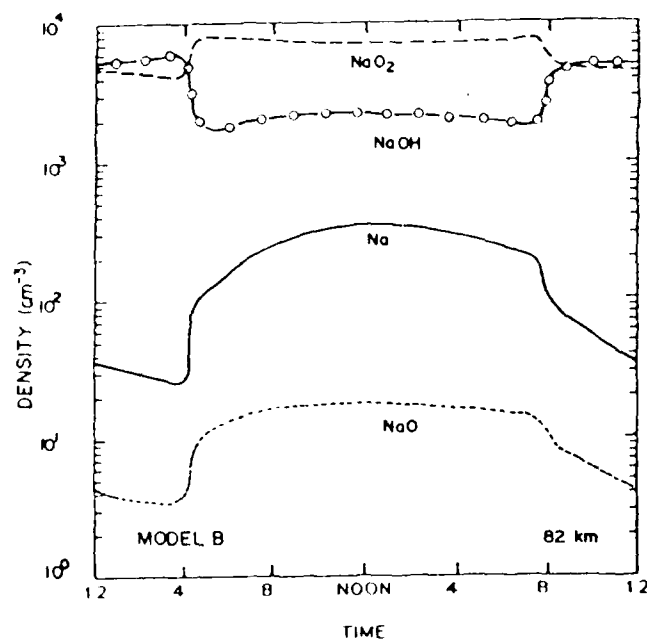
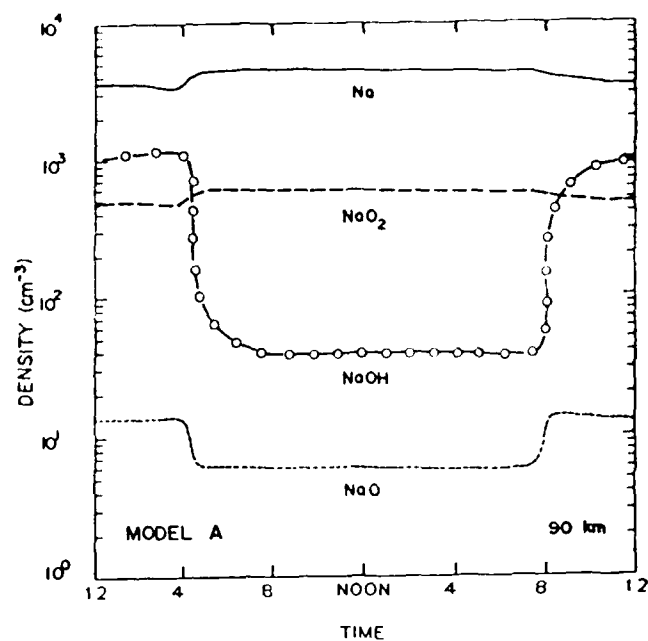
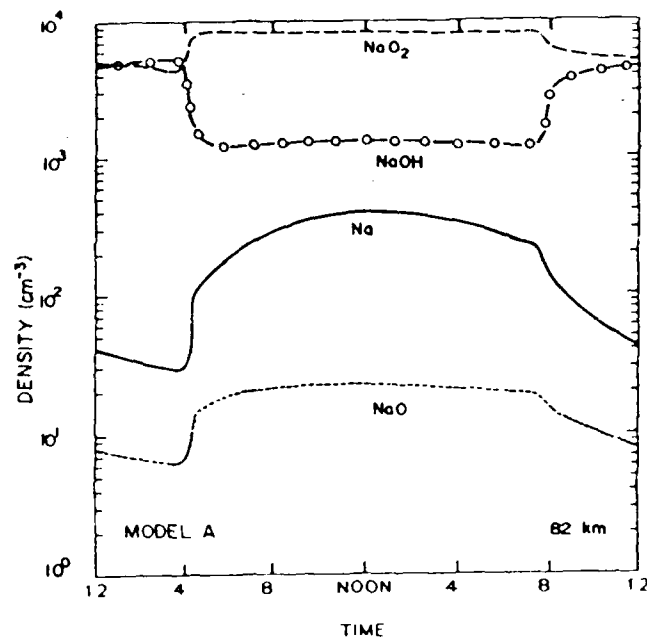


Figure 7. Diurnal variation of the local densities of sodium species at 82 and 90 km, calculated for Model A (7a and 7b) and Model B (7c and 7d).

PART II

Possible Impact of Sodium Species on ClO and O₃ in the Upper Stratosphere

ABSTRACT

Recent measurements of the rates for reactions of NaO₂ and NaOH with HCl and of the photoabsorption cross section of NaCl allow for realistic estimates of the impact of sodium chemistry on chlorine partitioning in the upper stratosphere. When sodium chemistry is incorporated into our one-dimensional model of the upper atmosphere, the results indicate that the calculated ClO concentrations near 50 km could increase by up to a factor of two with a corresponding decrease in calculated O₃ abundances of as much as 15 percent. The impact on ClO and O₃ depends crucially on the assumed meteoritic source of sodium, on transport from the mesosphere, and on transformation and removal of gaseous sodium in the stratosphere. Since the fluctuations in the abundance of gaseous sodium could induce O₃ variations comparable to those caused by changes in temperature and solar UV, consideration of the chemistry of sodium and other metals may be an important element in efforts toward early detection of trends in upper stratospheric O₃. Future increases in stratospheric chlorine will magnify the impact of sodium species on ozone.

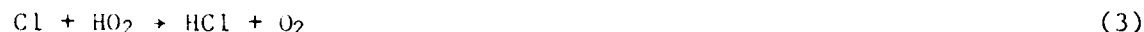
Table of Contents

	<u>Page</u>
ABSTRACT	29
1. INTRODUCTION	30
2. CHEMISTRY OF SODIUM SPECIES	31
3. IMPACT OF SODIUM CHEMISTRY ON CHLORINE SPECIES	32
4. DISCUSSION AND CONCLUSIONS	33

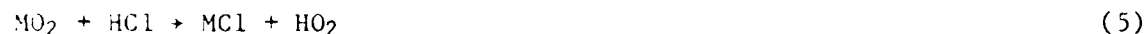
1. INTRODUCTION

The catalytic efficiency of chlorine compounds in removing stratospheric O_3 is particularly sensitive to the abundance of active-chlorine species (Cl , ClO). The chlorine catalytic cycle is most effective in the present atmosphere between 40 and 50 km, representing about one third of the total loss of O_3 at these altitudes. It is thus in this region where an early detection of ozone perturbations due to anthropogenic chlorine is most probable.

Our present understanding of chlorine chemistry indicates that the partition between active-chlorine and the reservoir species HCl is primarily determined by the reactions



Other processes which could affect the above partition include reactions of the type



where M denotes stratospheric metal species of meteoritic origin (Na , Ca , Ni , Mg , Al , Si , and Fe , among others). The potential importance of reaction (4) was first recognized by Murad et al. (1981) who suggested that the species MCl could act as an important reservoir of chlorine if its stratospheric abundance is comparable to that of HCl . On the other hand, reactions (4) and (5) followed by photolysis of MCl



could constitute a catalytic cycle for recycling HCl to active chlorine (Rowland and Rogers, 1982).

Realistic estimates of the effect of the above reactions have been hampered by a lack of kinetic data for metal species. Recent measurements of the rates of reactions of $NaOH$ and NaO_2 with HCl indicate very fast rates ap-

proaching the kinetic limit (Silver et al., 1984a; Silver and Kolb, 1986). These kinetic data can be combined with the latest measurement of the photolysis rate of NaCl (Silver et al., 1986) to provide a realistic assessment of the importance of (4) to (6) in the recycling of chlorine species by sodium. We report here results of such calculations.

2. CHEMISTRY OF SODIUM SPECIES

Direct observations of atomic sodium in the Earth's mesosphere have established the existence of a narrow layer of Na with average peak densities of $2-5 \times 10^3 \text{ cm}^{-3}$ near 90 km (cf. Clemesha et al., 1982). No other sodium compounds have been observed directly. Their atmospheric abundance, particularly in the stratosphere, must therefore be inferred from models incorporating sources, chemistry, and transport of Na species and constrained by the mesospheric observations.

We have incorporated the chemistry of active sodium species NaX (Na, NaO, NaO₂, NaOH, NaCl) into the AER 1-D model (Ko and Sze, 1984), now covering the altitude range 0-120 km. Adopted kinetic and photochemical data are listed in Table 1, and the chemical scheme is illustrated in Figure 1. Reactions R1 and R2 modulate rapid conversion between Na and NaO near 90 km and account for the sodium D-line nightglow (Chapman, 1939). Reaction of Na with O₂ and NaO with H₂O (R3 and R7) sequester most of the Na and NaO in the temporary reservoirs NaO₂ and NaOH between 60 and 85 km. The above reservoir species are in turn converted to NaCl below 60 km through reaction with HCl. The impact of chlorine chemistry on the sodium layer at 90 km is negligible.

Sodium is assumed to be produced in atomic form by meteor ablation between 80 and 90 km (Hunten, 1981). Estimates of the average influx range from 5×10^3 to $4 \times 10^4 \text{ cm}^{-2} \text{ s}^{-1}$ (Kirchoff and Clemesha, 1983; Hunten, 1981) depending primarily on the adopted mesospheric eddy diffusion coefficient and Na density at 90 km. We adopt in our model the shape of the production profile of Hunten (1981) and normalize it to a total influx of $2 \times 10^4 \text{ cm}^{-2} \text{ s}^{-1}$. The primary loss for active sodium is assumed to be washout in the troposphere with a lifetime of 10 days. Eddy diffusion coefficients in the mesosphere are those of Allen et al. (1981). Kinetic data and boundary conditions for other stratospheric trace gases are those used in the modeling of present-day conditions (Watson, 1986).

The model described above calculates peak densities of Na of $4 \times 10^3 \text{ cm}^{-3}$ at 90 km, and a diurnal variation of the column density of Na of less than 10 percent, in agreement with observations (Clemesha et al., 1982). Diurnally-averaged profiles for the major stratospheric NaX species (NaOH, NaO₂, NaCl) calculated by this model are shown in Figure 2. Sodium chloride is the major form of NaX below 60 km, exhibiting densities between 10^5 and 10^6 cm^{-3} . Such abundances (a few pptv) are small in comparison to those of HCl and ClO (> 100 pptv), implying a negligible role for NaCl as a temporary reservoir of chlorine.

Figure 1 also indicates other hypothetical net sinks for NaX in the stratosphere. These sinks, denoted by "?," include: formation of stable sodium bicarbonate (Murad and Swider, 1979), attachment to aerosol and smoke particles (Hunten, 1981), and formation of stable NaCl polymers (Lamb and Benson, 1986). The sensitivity of our calculated NaX to the polymerization process is illustrated in Figure 3. The solid-line profile assumes tropospheric washout to be the only sink of active sodium, as in Figure 2. The calculations denoted by the dashed line adopt the estimates of Lamb and Benson (1986) for the dimerization rate of NaCl, as well as their polymerization scheme. The dash-dot line represents NaX profiles calculated with a dimerization rate a factor of 10 smaller, thus allowing for uncertainties in the estimate and for possible reductions in the effective sink of NaX through photolysis of NaCl polymers or other chemical reactions. The relative partitioning of NaX species for all the above cases is the same as in Figure 2. The calculated NaX near 40 km can change by up to two orders of magnitude, depending on the adopted polymerization mechanism.

3. IMPACT OF SODIUM CHEMISTRY ON CHLORINE SPECIES

The effectiveness of the catalytic cycle (4) - (6) in converting HCl to Cl depends crucially on the abundance of NaCl and its photolysis rate. Figure 4 compares the calculated rate-limiting step for this cycle with the conventional recycling of HCl through reaction (1). The photolysis rates, which have been calculated from the UV cross sections recently measured by Silver et al. (1986), are smaller than the estimates of Rowland and Rogers (1982). The rates for the above mechanism are comparable near 50 km.

The effect of sodium chemistry on the calculated ClO is shown in Figure 5. Percent changes are calculated relative to the ClO profiles obtained with no sodium chemistry. The solid, dashed, and dash-dot profiles represent the same assumptions for the active-sodium sink as in Figure 3. We have also included in this figure a case with the NaX concentrations a factor of 2 higher than in Figure 2 and no polymerization sink. Given the uncertainties in the meteoritic input, the mesospheric vertical transport, and the observed peak Na densities, such concentrations of NaX cannot be ruled out. Changes in the ClO calculated above 40 km range from a few percent to almost a factor of two, depending on the assumed net sink of NaX.

The changes in the calculated ClO are reflected in the calculated O₃ above 40 km. Percent changes in the calculated O₃ are shown in Figure 6, for the same cases as in Figure 5. Maximum changes occur between 50 and 55 km. The calculated ozone could be reduced by as much as 10-15 percent at these altitudes, but the actual reduction will again be very sensitive to assumptions about the polymerization sink.

4. DISCUSSION AND CONCLUSIONS

The calculations presented above indicate that sodium chemistry may play an important role in determining the O₃ abundance in the upper stratosphere by influencing the partitioning of chlorine species. Variations in the stratospheric NaX abundances are expected due to seasonal changes in mesospheric transport (Garcia and Solomon, 1985), other dynamical processes or to sporadic changes in the sources and sinks. Sodium chemistry could then induce variations of up to a factor of two in the ClO and up to 15 percent in the ozone at 50 km. These changes in ozone are comparable to variations of order 5-10 percent due to dynamical, temperature, or solar cycle variations (cf. Keating et al., 1986) and would be even larger for an enhanced stratospheric chlorine burden. The possible effect of sodium chemistry on ozone variations should thus be included in efforts towards early detection of the perturbation to upper stratospheric ozone by increases in chlorine.

The calculated peak density of the sodium layer at 90 km, which is the only observational constraint on stratospheric Na abundances, depends not only on the adopted Na influx but also on the assumed eddy coefficient near the sodium peak (Liu and Reid, 1979) and on the relative magnitude of the rates of

reaction of Na with O_2 (R3) and of NaO_2 with O (R6) (Rodriguez et al., 1984). Better estimates of the stratospheric sodium abundance require better determinations of the flux, composition and ablation of meteorites and analysis of observations of mesospheric Na, O_3 , O, and sodium D line emission in conjunction with improved kinetic data on sodium and realistic models of the chemistry and dynamics of the mesosphere. Measurements of the polymerization rate of NaCl and of homogeneous and heterogeneous processes affecting gaseous sodium are also needed.

Observational validation of the calculations presented above could best be obtained by detection of gaseous NaCl in the upper stratosphere. Observations of O_3 and ClO above 50 km could also be analyzed to detect possible seasonal changes induced by seasonal variations in the transport of Na from the mesosphere by the mechanism of Garcia and Solomon (1985).

Our calculations also suggest the possible importance of other metals of meteoritic origin. The meteoritic abundance of metals such as Ca and Al are comparable to that of Na, while those of Si, Mg and Fe could be up to one order of magnitude higher (Mason, 1971). Very little is known about the chemistry and atmospheric distribution of the above species, although we may expect similar chemical schemes as that of sodium (Murad and Swider, 1979). The results presented here thus warrant further investigation of the role of these metals in the chemistry of the upper stratosphere.

Acknowledgements -- We would like to thank Drs. J. Silver and S. Benson for providing us with preprints of their papers, and Dr. M. J. Prather for valuable comments. This work is supported by the Air Force Geophysics Laboratory and the Fluorocarbon Program Panel of the Chemical Manufacturers Association.

Table 1
Reaction Scheme and Rate Constants

Reaction	Rate ^a
R1. $\text{Na} + \text{O}_3 \rightarrow \text{NaO} + \text{O}_2$	$3.5(-10)^b$
R2. $\text{NaO} + \text{O} \rightarrow \text{Na} (^2\text{P}, ^2\text{S}) + \text{O}_2$	$4(-11)^{h*}$
R3. $\text{Na} + \text{O}_2 + \text{N}_2 \rightarrow \text{NaO}_2 + \text{N}_2$ $\times (T/300)^{-1.1d}$	1.9×10^{-30}
R4. $\text{NaOH} + \text{HCl} \rightarrow \text{NaCl} + \text{H}_2\text{O}$	$2.0(-10)^c$
R5. $\text{NaO}_2 + \text{HCl} \rightarrow \text{NaCl} + \text{HO}_2$	$2.3(-10)^e$
R6. $\text{NaO}_2 + \text{O} \rightarrow \text{NaO} + \text{O}_2$	$1(-13)^{h*}$
R7. $\text{NaO} + \text{H}_2\text{O} \rightarrow \text{NaOH} + \text{OH}$	$2(-10)^g$
R8. $\text{NaO} + \text{O}_3 \rightarrow \text{NaO}_2 + \text{O}_2$	$1.8(-10)^g$
R9. $\text{NaO}_2 + \text{OH} \rightarrow \text{NaOH} + \text{O}_2$	$1(-11)^{h*}$
R10. $\text{NaO}_2 + \text{H} \rightarrow \text{NaOH} + \text{O}$	$1(-14)^{h*}$
R11. $\text{NaO} + \text{O}_3 \rightarrow \text{Na} + 2\text{O}_2$	$1(-10)^g$
R12. $\text{NaO} + \text{H}_2 \rightarrow \text{Na} + \text{H}_2\text{O}$	$1(-11)^g$
R13. $\text{NaO} + \text{H}_2 \rightarrow \text{NaOH} + \text{H}$	$2.6(-11)^g$
R14. $\text{NaOH} + h\nu \rightarrow \text{Na} + \text{OH}$	$2(-3)^i$
R15. $\text{NaO}_2 + h\nu \rightarrow \text{Na} + \text{O}_2$	$1(-4)^{h*}$
R16. $\text{NaCl} + h\nu \rightarrow \text{Na} + \text{Cl}$	• see text ^f

^aRead 3(-10) as 3×10^{-10} . Units are $\text{cm}^3 \text{s}^{-1}$, except $\text{cm}^6 \text{s}^{-1}$ for (3) and s^{-1} for (14), (15), and (16). ^bZahniser et al. (1985). ^cSilver et al. (1984a). ^dSilver et al. (1984b). ^eSilver and Kolb (1986). ^fSilver et al. (1986). ^gAger and Howard (1985). ^hSze et al. (1982). ⁱRowland and Makide (1982). *Estimated rates.

References

- Ager, Joel W., III, and C. J. Howard (abstract), Kinetic studies of some sodium reactions of atmospheric importance. EOS (Trans. A.G.U.), 66, 317, 1985.
- Allen, Mark, Y.L. Yung, and J.W. Waters, Vertical transport and photochemistry in the terrestrial mesosphere and lower thermosphere (50-120 km), J. Geophys. Res., 86, 3617, 1981.
- Chapman, S., Notes on atmospheric sodium, Ap. J., 90, 309, 1939.
- Clemesha, B. R., D. M. Simonich, P. O. Batista, and V. W. J. H. Kirchoff, The diurnal variation of atmospheric sodium, J. Geophys. Res., 87, 181, 1982.
- Garcia, R. R., and S. Solomon, The effect of breaking gravity waves on the dynamics and chemical composition of the mesosphere and lower thermosphere. J. Geophys. Res., 90, 3850, 1985.
- Hunten, D. M., A meteor-ablation model of the sodium and potassium layers. Geophys. Res. Lett., 8, 369, 1981.
- Keating, G. M., G. R. Brasseur, J. Y. Nicholson III, and A. DeRudder, Detection of the response of ozone in the middle atmosphere to short-term solar ultraviolet variations. Geophys. Res. Lett., 12, 449, 1985.
- Kirchhoff, V. W. J. H., and B. R. Clemesha, Eddy diffusion coefficients in the lower thermosphere. J. Geophys. Res., 88, 5765-5768, 1983.
- Ko, M. K. W., and N. D. Sze, Diurnal variation of ClO: Implications for the Stratospheric Chemistries of ClONO₂, HOCl, and HCl. J. Geophys. Res., 89, 11619-11632, 1984.
- Lamb, J. J., and S. W. Benson, Some kinetic and thermochemical aspects of sodium in the stratosphere. J. Geophys. Res. (in press), 1986.
- Liu, S. C., and G. C. Reid, Sodium and other minor constituents of meteoric origin in the atmosphere. Geophys. Res. Lett., 6, 283, 1979.
- Mason, B. (ed.), Handbook of Elemental Abundances in Meteorites. Gordon & Breach, New York, NY, 1971.
- Murad, E., and W. Swider, Chemistry of meteor metals in the stratosphere. Geophys. Res. Lett., 6, 929, 1979.
- Murad, E., W. Swider, and S. W. Benson, Possible role for metals in stratospheric chlorine chemistry. Nature, 289, 273, 1981.
- Rodriguez, J. M., M. K. W. Ko, and N. D. Sze, The diurnal variation of the neutral sodium species in the upper atmosphere: A model study. Report #AFGL-TR-84-0204, Air Force Geophysics Lab., Bedford, MA, 1984, ADA154988.
- Rowland, F. S., and Y. Makide, Upper stratospheric photolysis of NaO₂. Geophys. Res. Lett., 9, 473-475, 1982.

- Rowland, F. S., and P. J. Rogers, Upper stratospheric photolysis of NaCl and KCl. Proc. Nat. Acad. Sci. USA, 79, 2737, 1982.
- Silver, J. A., A. C. Stanton, M. S. Zahniser, and C. E. Kolb, The gas phase reaction rate of sodium hydroxide with hydrochloric acid, J. Phys. Chem., 88, 3123, 1984.
- Silver, J. A., M. S. Zahniser, A. C. Stanton, and C. E. Kolb, Temperature-dependent termolecular reaction rate constants for potassium and sodium peroxide formation. Presented at the 20th International Symposium on Combustion, the Combustion Institute, Pittsburgh, PA, p. 605, 1984.
- Silver, J. A., and C. E. Kolb, Gas-phase reaction rate of sodium superoxide with hydrochloric acid. J. Phys. Chem. (in press), 1986.
- Silver, J. A., D. R. Worsnop, A. Freedman, and C. E. Kolb, Absolute photodissociation cross sections of gas-phase sodium chloride at room temperature. J. Chem. Phys., 84, 4378, 1986.
- Sze, N. D., M. K. W. Ko, W. Swider, and E. Murad, Atmospheric Sodium Chemistry. I. The Altitude Region 70-100 km. Geophys. Res. Lett., 9, 1187-1190, 1982.
- Watson, R. J. (ed.), Atmospheric ozone: Assessment of our understanding of the processes controlling its present distribution and changes. WMO/NASA, 1986 (in press).
- Zahniser, M. S., J. A. Silver, and C. E. Kolb (abstract), Mesospheric chemistry of meteoric metals: Reaction rate measurements for Na + O₃. EOS (Trans. A.G.U.), 66, 317, 1985.

Figure Captions

- Fig. 1. Chemistry of sodium species in the stratosphere and mesosphere. Rates for processes denoted by dotted lines have not been measured.
- Fig. 2. Calculated diurnally-averaged densities of sodium species in the upper stratosphere. The species NaO_2 and NaOH disappear at night in this altitude range, while NaCl exhibits little diurnal variation. The only loss of NaX is by washout in the troposphere.
- Fig. 3. Calculated mixing ratio of NaX ($\text{Na} + \text{NaO} + \text{NaO}_2 + \text{NaOH} + \text{NaCl}$) for different rates for the polymerization sink. The solid-line profile corresponds to the calculations in Fig. 2 (no polymerization). The dashed line assumes the polymerization mechanism of Lamb and Benson (1986) with their estimate for the dimerization rate K_d . Calculations denoted by the dash-dot line assume a dimerization rate a factor of 10 smaller.
- Fig. 4. Rates ($\text{cm}^{-3} \text{ s}^{-1}$) for conversion of HCl to active chlorine (Cl , ClO) in the upper stratosphere. Conversion is primarily achieved in present models through reaction of OH with HCl (1). The rate limiting step for the sodium-catalyzed cycle is photolysis of NaCl (6). We adopt the NaCl profile in Fig. 2 and the J rates calculated from cross sections of Silver et al. (1986).
- Fig. 5. Percent change in calculated ClO densities. The change is calculated relative to a baseline with no sodium chemistry. Solid, dashed, and dash-dot lines represent the same assumptions for the sodium sink as in Fig. 3. The open circles denote calculations with twice the sodium abundance and no polymerization sink.
- Fig. 6. Percent change in calculated O_3 densities. Calculations correspond to the ClO profiles in Fig. 5.

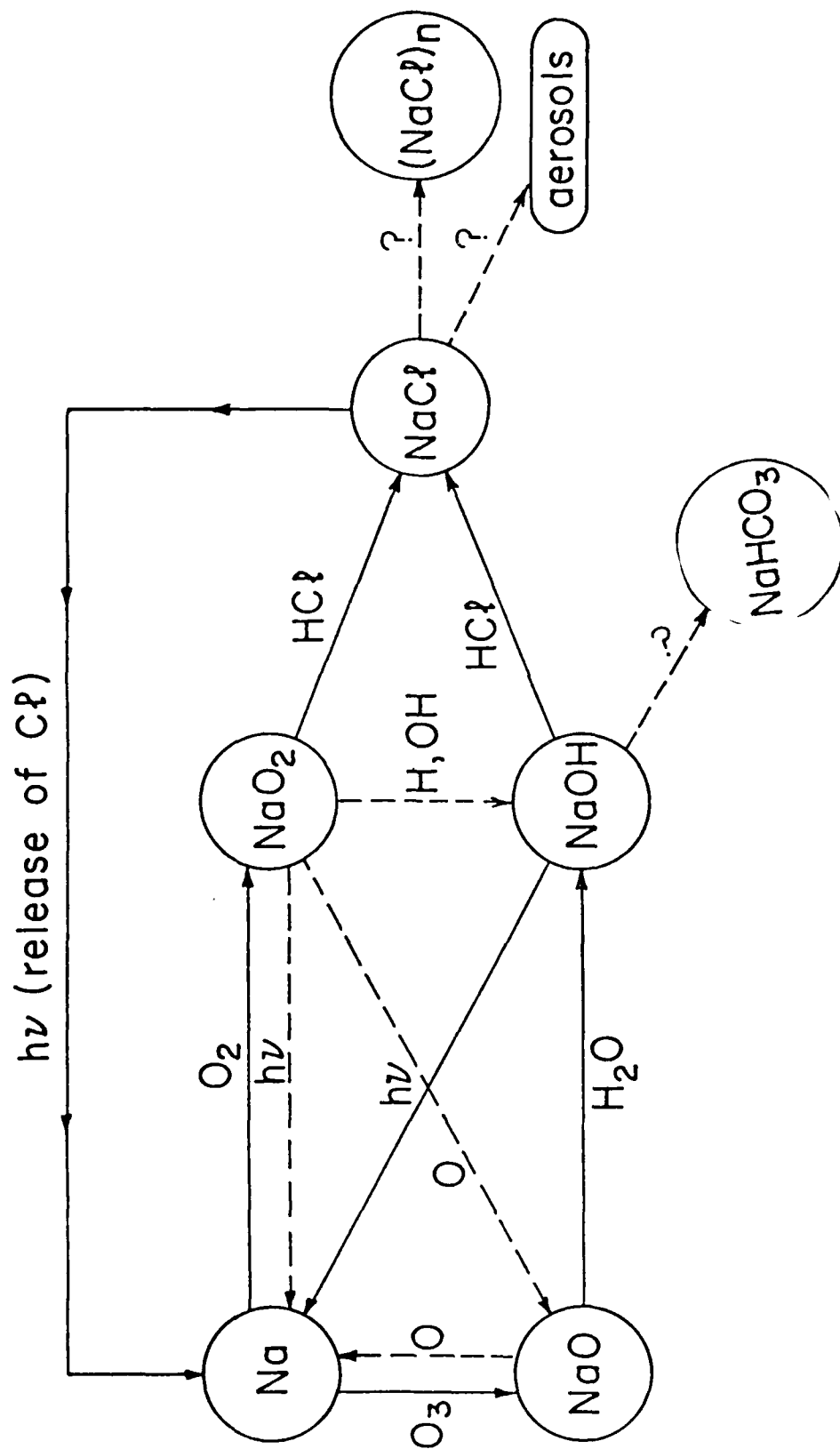


Figure 1. Chemistry of sodium species in the stratosphere and mesosphere. Adopted rates are listed in Table 1. Rates for processes denoted by dotted lines have not been measured. Formation of $(\text{NaCl})_n$, NaHCO_3 , and attachment to aerosols act as permanent sinks of gaseous sodium species.

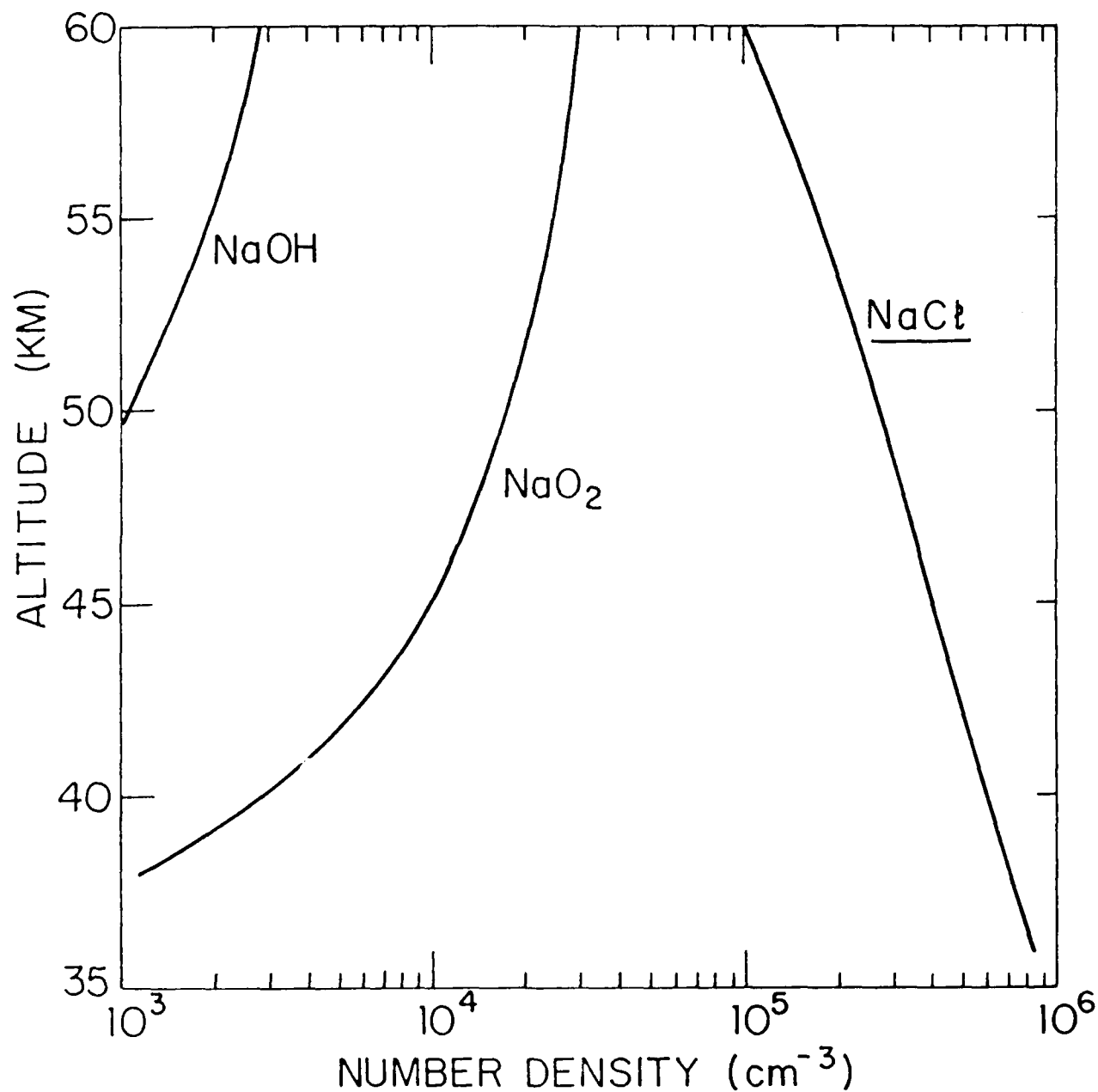


Figure 2. Calculated diurnally-averaged densities of sodium species in the upper stratosphere. The species NaO₂ and NaCl disappear at night in this altitude range, while NaCl exhibits little diurnal variation. Loss of NaX is by washout in the troposphere. Other possible sinks of NaX are neglected. Model input and assumptions are discussed in the text.

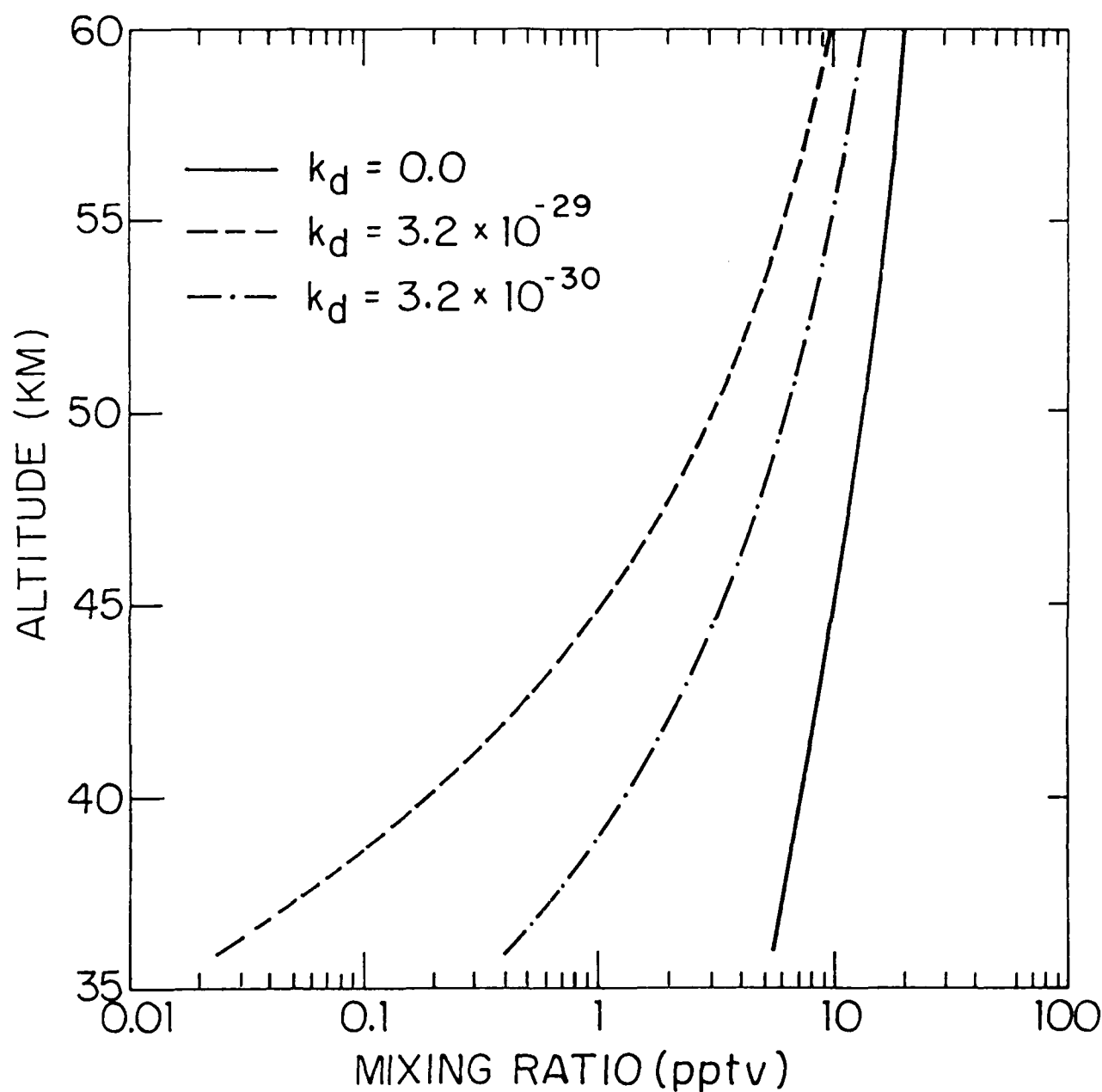


Figure 3. Calculated mixing ratio of NaX (Na + NaO + NaO₂ + NaOH + NaCl) for different rates for the polymerization sink. The solid-line profile corresponds to the calculations in Figure 2 (no polymerization). The dashed line assumes the polymerization mechanism of Lamb and Benson (1986) with their estimate for the dimerization rate K_d . Calculations denoted by the dash-dot line assume a dimerization rate a factor of 10 smaller than in Lamb and Benson (1986).

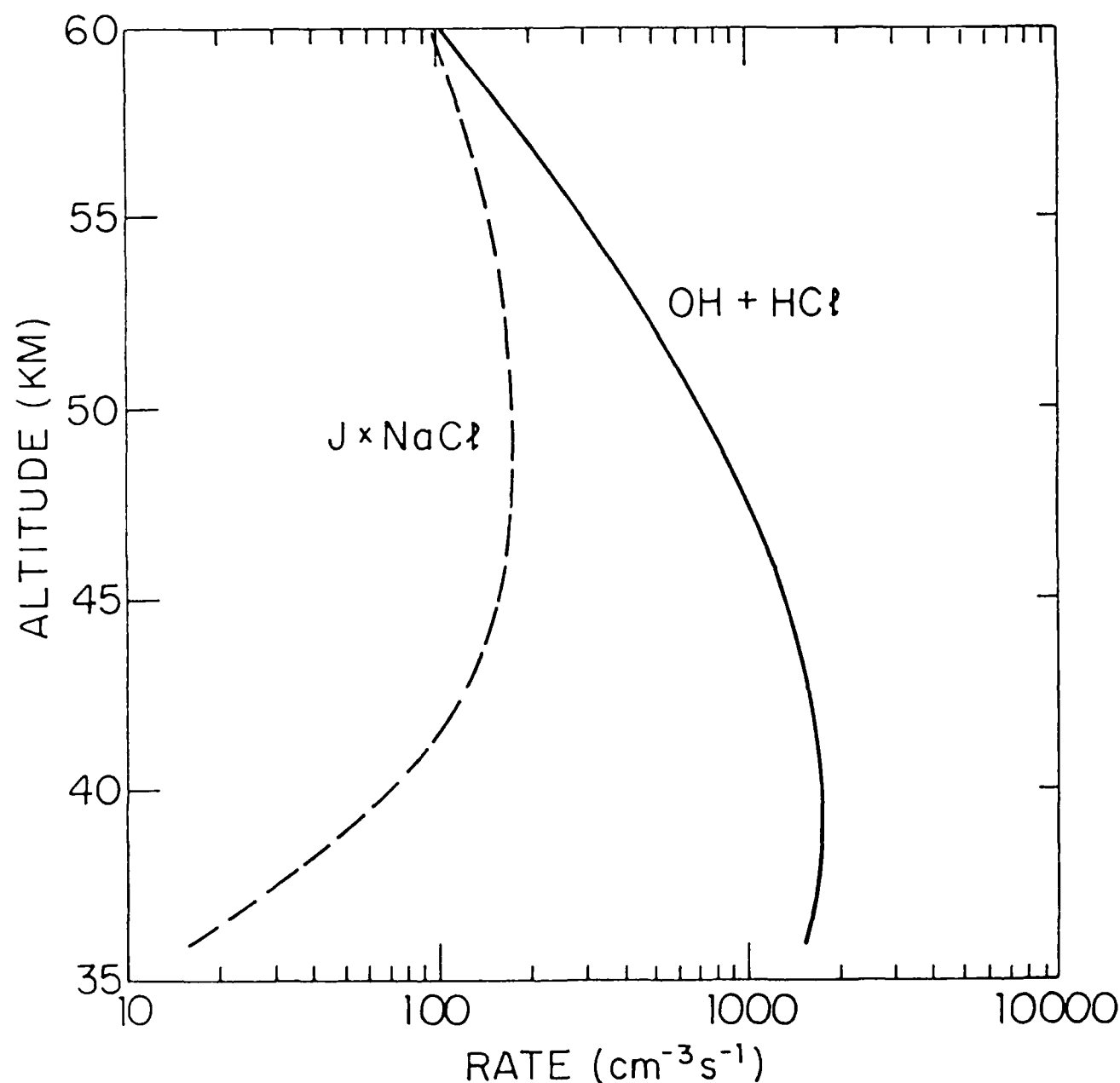


Figure 4. Rates ($\text{cm}^{-3} \text{s}^{-1}$) for conversion of HCl to active chlorine (Cl, ClO) in the upper stratosphere. Conversion is primarily achieved in present models through reaction of OH with HCl (1). The rate limiting step for the sodium-catalyzed cycle is photolysis of NaCl (6). We adopt the NaCl profile in Figure 2 and the J rates calculated from cross sections of Silver et al. (1986).

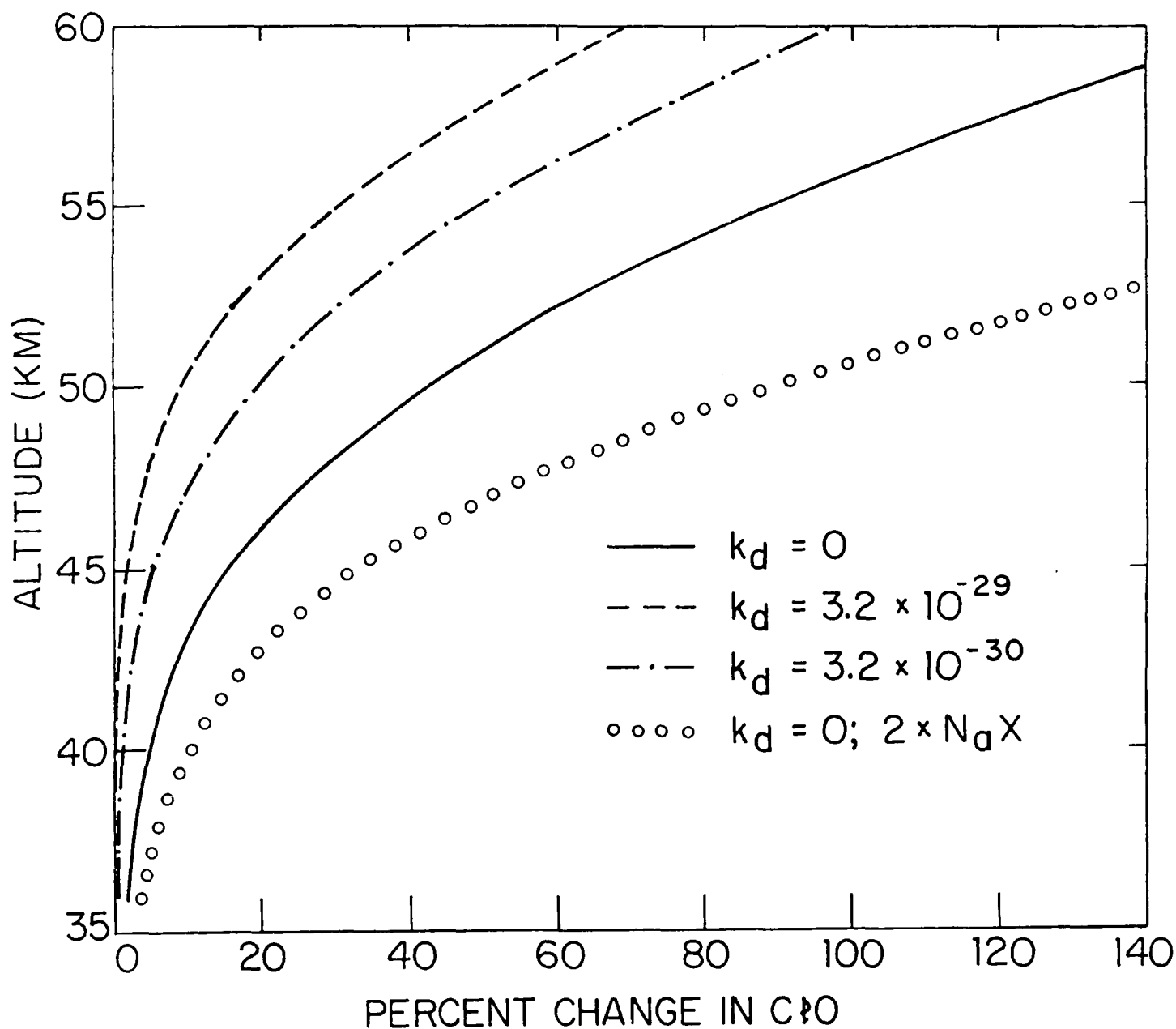


Figure 5. Percent change in calculated ClO densities. The change is calculated relative to a baseline with no sodium chemistry. Solid, dashed, and dash-dot lines represent the same assumptions for the sodium sink as in Figure 4. The open circles denote calculations with twice the sodium abundance and no polymerization sink.

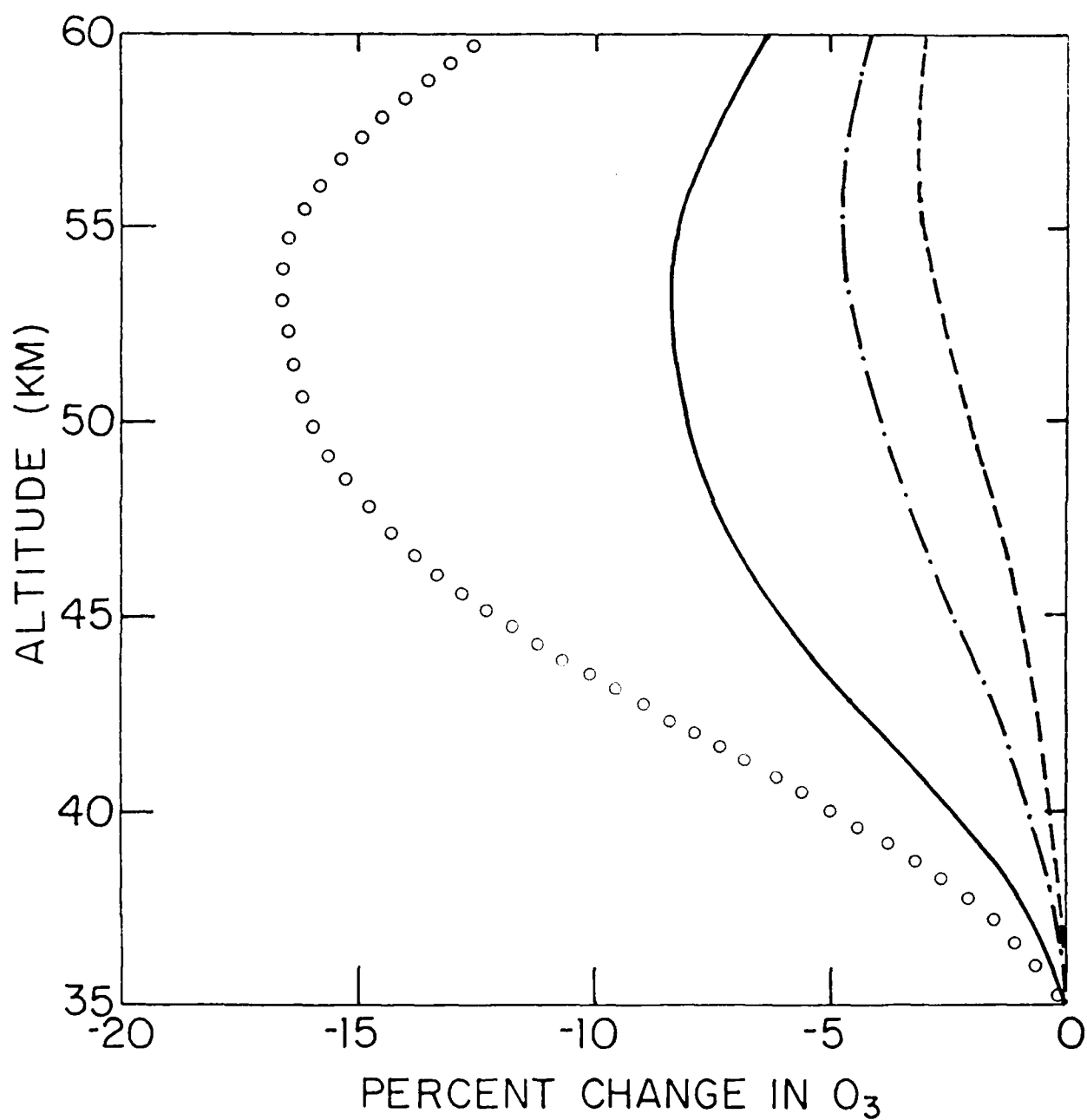


Figure 6. Percent change in calculated O_3 densities. Calculations correspond to the C10 profiles in Figure 5.

PART III

The Neutral/Ion Chemistry of Sodium in the Statosphere and Mesosphere

ABSTRACT

This report presents results from our model calculation of the diurnal behavior of the neutral and ionic sodium species. It is shown that the concentration of Na^+ above 90 km exerts a direct influence on the topside scale height of the atomic sodium layer in the mesosphere. The abundance of Na^+ is controlled by the reaction rate for the clustering reaction which is the rate limiting step for the conversion of Na^+ to Na. Downward transport of Na^+ due to ion drift is also effective in reducing the sodium abundance around 90 km. The model can successfully simulate the observed topside scale height of the sodium layer by either using a slow rate for the clustering reaction or incorporating transport of Na^+ .

Table of Contents

	<u>Page</u>
ABSTRACT	45
1. INTRODUCTION	46
2. IONS IN THE D AND LOWER E REGIONS	46
3. MODEL FOR THE BACKGROUND IONS	49
4. DIURNAL MODEL FOR SODIUM NEUTRALS AND IONS	52
5. SODIUM ION CHEMISTRY AND THE SCALE HEIGHT OF THE NEUTRAL ATOMIC SODIUM LAYER	53
6. CONCLUDING REMARKS	56
References	59
Figures	67

1. INTRODUCTION

In Part I, we presented results from our diurnal simulation of the concentrations of the sodium species based on neutral chemistry. We now extend the discussion to include ion chemistry of sodium species.

Positively charged ions of atomic weight 23 have been observed in the E region during several rocket flights (see Swider, 1984, and references therein). These observations have been interpreted as positively-charged Na ion (Na^+). Sodium ions are produced by photo-ionization as well as by charge exchange reactions with the major positive ions O_2^+ and NO^+ (Swider, 1969a). Dissociative recombination of molecular ions, produced by clustering of Na^+ with N_2 and CO_2 (Richter and Sechrist, 1979) ultimately removes Na^+ ions. The clustering rate decreases rapidly with altitude resulting in inefficient removal of ions at high altitudes. Although there are insufficient data to obtain any detailed information on the diurnal and seasonal behavior of the ions, they can nonetheless affect the behaviour of the neutral sodium. In particular, the departure of the observed scale height of atomic sodium from the scale height of the atmosphere above 90 km (Gibson and Sanford, 1970; Simonich et al., 1979) is thought to be controlled by the amount of Na^+ ions present (Hanson and Donaldson, 1967).

In order to calculate the production and removal rates of the sodium ions, one needs to know the distributions of the background ions. In Sections 2 and 3, we will present the model for calculating the diurnal behavior of the background ions in the D and lower E region. Section 4 will present the results of the calculated diurnal behavior of the sodium ions. The effects of the ions on the observations of the scale height of atomic sodium above 90 km and other impact on sodium will be discussed in Section 5.

2. IONS IN THE D AND LOWER E REGIONS

Since our primary interest is in the effect of metal ions' chemistry on the neutral chemistry around 90 km, we will use a version of the ion chemistry appropriate for the D and lower E regions. In the lower E region, production of O_2^+ , N_2^+ and O^+ by x-ray and Lyman- β dominates. However, the N_2^+ and O^+ are converted rapidly to O_2^+ by charge exchange. Some O^+ is converted to NO^+ , which is also formed by the charge exchange reaction of NO with O_2^+ . In the D region, production of NO^+ by Lyman- α is important, making this ion the most

important ionic constituent near 80 km. In the lower D region (60-80 km), there are evidence from mass-spectrometric measurements that hydrated cluster ions are common (Narcisi and Bailey, 1965; Goldberg and Aikin, 1971; Krankowsky et al., 1972). Swider and Narcisi (1983) suggested that carbon dioxide may be an important agent in hastening the formation of these clustered ions.

Negative ions are produced through a chain of reactions initiated by electron attachment to O_2 :



Although observations show conflicting results making the identifications of the ions difficult, it is relatively certain that the major ions are CO_3^- and NO_3^- (Swider and Narcisi, 1983). For the problem at hand, it is not crucial that the identity of the negative ions is precisely known.

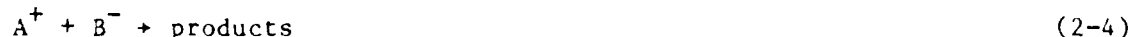
Positive ions are destroyed mainly by dissociative recombination,



where AB^+ denotes a molecular ion. Rates for dissociative recombination are usually very fast ($\sim 10^{-6} \text{ cm}^3 \text{ sec}^{-1}$), and result in lifetimes of the order of minutes for positive molecular ions near 90 km. Removal of negative ions is effected by photodetachment reactions



As the concentrations of the negative ions become much higher below 80 km at night, positive-negative ion recombination



becomes an important loss mechanism.

A simplified model of the reaction schemes for positive and negative ions appropriate for the D and lower E region are given in Figures 1 and 2 respectively. The photo-ionization sources incorporated in our model include the following:

For daytime condition:

- a)† X-rays: Absorption and ionization cross sections of O, O₂, and N₂ are taken from Swider (1969b), for wavelengths between 1 and 100Å. The solar fluxes for quiet conditions are also from Swider (1969b).
- b,c) Lyman-β ionization of O₂ and Lyman-α ionization of NO: Absorption cross sections, ionization cross sections, and fluxes are taken from Swider (1969a, 1983) for quiet conditions.
- d) Energetic electrons: Spectra of energetic electrons at 300 km measured by the AE-C satellite have been presented by Torr et al. (1976). These authors estimated an ion production rate of $10 \text{ cm}^{-3} \text{ s}^{-1}$ at for nighttime 90 km although the rate for daytime could be considerably higher. We have assumed that the ion production profile has the shape of the theoretical calculation of Berger et al. (1974; Figure 6, for 5 keV e-folding energy); this profile is normalized to a peak production rate of $10 \text{ cm}^{-3} \text{ s}^{-1}$ at 90 km. The above total production rate was subdivided into 90% O₂⁺ and 10% NO⁺ production as suggested by Swider (1969a, 1983) for cosmic rays. Because of the large uncertainties, production of ions from energetic electrons is not included in most of our calculations. However, they are included in Figure 3 for completeness.
- e) Ionization of O₂ (¹Δ): We have used the parameterization suggested by Paulsen et al. (1972).
- f) Cosmic rays: The parameterization given by Swider (1983) for mid-latitude condition is used.

For night time conditions:

- b,c) Lyman-β and Lyman-α scattered by the geocorona: The scattered fluxes as a function of altitude and solar zenith angle are taken from Strobel et al. (1974, 1980).
- d) Energetic electrons: see discussion for dayside ion condition.
- f) Cosmic rays: As on the dayside.

A constant production rate of $10^{-3} \text{ cm}^{-3} \text{ s}^{-1}$ at all altitudes due to galactic x-rays (Torkar and Friedrich, 1983) is included. The production of ions by starlight (Strobel et al., 1974, 1980) has been ignored since it is only important above ~ 110 km.

†Alphabet refers to labels on Figure 3.

The adopted production rates for ions are presented for noon in Figures 3(a) and 3(b) and 3(c) for midnight. These calculations assume 45° latitude, equinox conditions. Ionization by x-rays and Lyman- β are dominant above an altitude of 90 km on the dayside. The nightside sources are dominated by ionization by energetic electrons if values from Torr et al. (1976) are adopted. We must note, however, that this source is quite variable (Torr et al., 1976). The profiles for ion production by energetic electrons presented in Figure 3 should thus be considered as upper bounds. Values for these production rates smaller than ionization by Lyman- α and Lyman- β cannot be ruled out. Uncertainties also exist in the production by Lyman- α and Lyman- β at night, since the fluxes at these wavelengths are obtained from extrapolation of radiative transfer calculations (Strobel et al., 1974, 1980).

The list of two- and three-body reactions included in the model is given in Table 1. The values for the reaction rates are taken from Swider and Narcsi (1983). Note that we have assumed that the production of O_2^+ ions is due only to photo-ionization processes. The additional production from charge exchange with N_2^+ and O^+ is incorporated into the same term (Swider, 1969a). The production of NO^+ is from both photo-ionization and charge exchange.

3. MODEL FOR THE BACKGROUND IONS

The basic structure of our ion code is illustrated by the flow chart in Figure 4. This code was adapted from the mesospheric code described in Part I. The local concentrations of the electron, the positive and the negative ions, are governed by the system of equations:

$$\frac{d[N_i]}{dt} = P_i - L_i[N_i] \quad (3-1)$$

$$[e] + [NSUM] = [PSUM] \quad (3-2)$$

where P_i , L_i , and $[N_i]$ are the local production rate, loss frequency, and number density of the i^{th} ionic species, $[e]$ is the electron density, and $[NSUM]$ and $[PSUM]$ are the sum of the negative and positive ions concentrations, respectively. Equation (3-1) corresponds to the local approximation of the continuity equation for each ionic species whereas (3-2) serves to determine $[e]$ by charge conservation. The numerical scheme adopted to solve the system can be used for any arbitrary grouping of the ionic species and does not assume a chain structure for the ion chemistry.

Equation (3-1) is solved at a series of discrete time steps using the fully implicit scheme described by Sze et al. (1980). The initial values for the electron and positive ion densities at noon are taken from our steady state calculation. At other time steps, the initial values are taken to be the electron and positive ion densities calculated at the previous time step. At each time step, the equations are solved using an iteration scheme similar to the one used by Swider and Foley (1978). The values for $[e]_{j+1}$ and $[PSUM]_{j+1}$ for the $j+1^{th}$ iteration are updated via (Swider & Foley, 1978)

$$\begin{aligned} [e]_{j+1} &= \{ [e]_j + [PSUM]_j / (1 + \lambda) \} / 2, \\ [PSUM]_{j+1} &= \{ [e]_j + [NSUM]_j + [PSUM]_j \} / 2 \end{aligned} \quad (3-3)$$

with

$$\lambda = [NSUM]_j / [e]_j.$$

The process is repeated until equations (3-3) are satisfied to some specified accuracy. The solution is propagated forward using time steps of one hour during the day, two hours at night, and 30 minutes around sunrise and sunset. After 24 hours, the solutions are tested for periodicity, and the calculation is repeated if periodicity is not achieved to within 1%. Due to the small time constants for ionic processes, our solutions usually become periodic in one to two diurnal cycles.

The neutral background atmosphere is obtained from the diurnal calculation described in Part I. The effect of the ion chemistry on neutral background trace gases is negligible under most conditions.

Results of our calculations for the background ions and electrons at 45°N for equinox condition are presented below. The diurnal variation of the electron density is presented in Figure 5 at altitudes of 86, 90, 94, and 100 km. Similar results for the same altitudes are shown in Figure 6 for O_2^+ and NO^+ , which are the main positive ion constituents in this region. The electron densities exhibit a day-to-night ratio of about 20 - 30 between 86 and 94 km, increasing to about 50 at 100 km. There is considerable variation during the daytime, with the electron density increasing by factors of 2 to 5 between sunrise and noon. NO^+ densities are larger than O_2^+ densities over most of this region; the diurnal behavior of NO^+ is thus positively correlated with that of the electrons. Below 95 km, O_2^+ densities exhibit a larger day-to-

night ratio (greater than 200). This is due to the conversion of O_2^+ to NO^+ at night through charge exchange with NO.

Our results during the day are in good agreement with diurnal calculations presented by Torkar and Friedrich (1983). We note that the magnitude of the diurnal variation, however, will depend on the model's assumptions for nightside sources. The ionization by energetic electrons exhibits great variability. In these calculations, we neglect ion production by energetic electrons. The Lyman- α and Lyman- β sources are computed from radiative transfer models which become uncertain below ~ 100 km (Strobel et al., 1974, 1980). Our results should be interpreted only as the general diurnal behavior of electrons and ions. More detailed information on the nightside ionization sources at specific times is needed to pinpoint the diurnal variation to a greater accuracy.

Profiles for electron and total negative ion densities for day and night are shown in Figure 7 for the same conditions as in Figures 5 and 6. In light of the possibly large variability in the electron flux, we also include the calculated profiles for which the ionization from energetic electrons at night is included (curves e, f). The figure illustrates that variability of this source can induce changes in the electron density of more than factors of 4 above 90 km.

The distributions of negative ions for daytime and nighttime conditions are given in Figure 8. The total negative ion density in the daytime remains smaller than the electron density down to about 60 km. During the night, the concentration of the negative ions becomes larger in the absence of photodetachment reaction (2-4). The density of NO_3^- grows to more than 10^3 cm^{-3} , reflecting the increase in concentrations of NO_2 and O_3 which favors the transfer to NO_3^- via O_3^- and CO_3^- . Hydrated negative ions are not included in the calculation since the rates for the reactions involving these ions are uncertain.

Profiles of positive ions for day- and nighttime conditions are given in Figures 9 and 10. The positive ions are mostly in the form of O_2^+ and NO^+ above 90 km. Below 90 km, various hydrated ions are formed in appreciable amounts. Densities for these ions are shown in Figure 10. Formation of these hydrated ions is initiated by the clustering reactions (Swider and Narcisi, 1983):



followed by switching reactions of the form

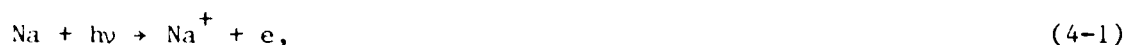


The profiles in Figures 9 and 10 are calculated using the H_2O mixing ratios of Bevilacqua et al. (1983), which are up to an order of magnitude smaller than those of Allen et al. (1984) above 80 km. Variations in upper mesospheric water will affect the calculated densities of the hydrated positive ions. The results in Figures 9 and 10 reproduce the general characteristics of calculations by other models (Swider and Foley, 1978; Swider, 1983; Swider and Narcisi, 1983).

4. DIURNAL MODEL FOR SODIUM NEUTRALS AND IONS

The ionic sodium species considered are: Na^+ , NaO^+ , NaO_2^+ , $\text{Na}^+ \cdot \text{N}_2$, $\text{Na}^+ \cdot \text{CO}_2$, and $\text{Na}^+ \cdot \text{H}_2\text{O}$. The chemical scheme for this family is illustrated in Figure 11. This scheme combines the reactions proposed by Murad (1978) and Richter and Sechrist (1979). The latter paper proposed the clustering scheme that recycles the Na^+ back to neutral Na.

The Na^+ ion is produced by



and



Molecular ions are formed via



which in turn yields the more stable $\text{Na}^+ \cdot \text{CO}_2$ and $\text{Na}^+ \cdot \text{H}_2\text{O}$ through the switching reactions:



and



The cluster ions are converted back to neutral atomic sodium by dissociative recombination. Reaction (4-4) is the rate limiting step for the sequence of reactions (4-4) through (4-6).

The ion reactions shown in Figure 11 are added to our diurnal model for the sodium species (Part I), and the diurnal behavior and altitude distributions of the ionic and neutral sodium species are calculated in a self-consistent manner. In these calculations, the background neutral and ionic constituents are not recalculated, since they are not affected by the sodium chemistry. Parameters used in calculating the reaction rates in our sodium model are shown in Table 2, with the rates for the neutral species as documented in Part I and those for the ionic species taken from Murad (1978) and Richter and Sechrist (1979). As in the case of the neutral chemistry, most of the ion reactions have not been measured, and the values proposed are deduced from measured values of similar reactions.

The diurnal variation of Na^+ is shown in Figure 12 for 90, 94, and 100 km. The day-to-night ratio ranges from 400 (90 km) to 3 (100 km). The factor of 10 variation for the altitude range 90 to 110 km suggested by the data as presented by Swider (1984) is thus consistent with our results, although the large changes in diurnal variation over a small altitude range preclude drawing any definitive conclusions about the validity of our chemical scheme.

Altitude profiles at noon for Na^+ and Na are shown in Figure 13. Atomic sodium is converted into Na^+ at high altitudes where their densities are comparable. As we shall see in the next section, processes that affect the concentration of Na^+ can then indirectly alter the distributions of Na at these altitudes. Densities of the other ionic species are smaller by factors of 100 or more. In particular, the $[\text{NaO}^+]/[\text{Na}^+]$ value is $\sim 10^{-7}$ to 10^{-8} , in agreement with the estimations of Murad (1978).

5. SODIUM ION CHEMISTRY AND THE SCALE HEIGHT OF THE NEUTRAL ATOMIC SODIUM LAYER

The topside scale height of the sodium layer has been observed to be much smaller than that of the background atmosphere (Gibson and Sandford, 1971;

Megie and Blamont, 1977; Simonich et al., 1979; Granier and Megie, 1982), decreasing to about 2-4 km at 100 km altitude. A possible explanation for this small scale height is the conversion of Na to Na⁺ by photoionization or charge exchange with O₂⁺ (Hanson and Donaldson, 1967; Gadsden, 1968; Richter and Sechrist, 1979).

This sensitivity of the scale height of atomic Na ion chemistry is illustrated in Figure 14 which gives the calculated profiles of Na with different assumptions for the Na⁺ abundance. As discussed in Section 4, reaction (4-4) constitutes the rate-limiting step for recombination of sodium ions and is assumed to be of the form (Richter and Sechrist, 1979):

$$K_S = K^* \left(\frac{300}{T} \right)^{1.5} \text{ cm}^6 \text{ s}^{-1}. \quad (5-1)$$

A value of $K^* = 2 \times 10^{-31} \text{ cm}^6 \text{ s}^{-1}$ was suggested by Richter and Sechrist (1979) by analogy to similar reactions involving NO⁺. Reaction (4-4) has also been measured at 130° K in a helium buffer by Perry et al. (1980); their value of $2.6 \times 10^{-30} \text{ cm}^6 \text{ s}^{-1}$ implies a value of $K^* = 7 \times 10^{-31} \text{ cm}^6 \text{ s}^{-1}$ if the temperature dependence in eq. (5-1) is valid. The Na profiles in Figure 14 are calculated using different values for K^* . The noontime profile from the calculation without ionic species (-o-) is compared with the cases calculated with value of K^* from Richter and Sechrist (1979) ($K^* = 2 \times 10^{-31} \text{ cm}^6 \text{ s}^{-1}$,) and Perry et al. (1980) ($K^* = 7 \times 10^{-31} \text{ cm}^6 \text{ s}^{-1}$, ---). We have also considered the hypothetical situation with $K^* = 4 \times 10^{-32} \text{ cm}^6 \text{ s}^{-1}$ (xxx). As expected, the scale height of neutral sodium increases with increasing K^* , reflecting the more efficient rate for reconversion of Na⁺ to Na. The observed small scale heights about 90 km could thus be explained by the ion chemistry without having to invoke transport processes (as in Hanson and Donaldson, 1967, for example) if K_S is sufficiently fast.

Local values for the topside scale height are given in Table 3 for the cases considered in Figure 14. A comparison with observations indicates an upper limit of $2 \times 10^{-31} \text{ cm}^6 \text{ s}^{-1}$ for K^* if the small topside scale heights are to be explained solely by ion-neutral chemistry. Such small values of K^* are not likely, however, given the measurements of Perry et al. (1980) and that the faster clustering rate are expected when N₂ is the buffer gas (Jegou et al., 1984; Heimerl, 1976). An alternative mechanism to reduce the topside

scale height is the downward transport of Na^+ from the region prior to its conversion to Na . Vertical ion drifts with velocities of 10 to 50 cm s^{-1} have been suggested by Hunten (1981) and Kirchoff and Batista (1984) and could be effective.

Ionic species could acquire a vertical velocity through electromagnetic interactions. These include electrostatic forces from the ionospheric electric fields (Kirchoff and Batista, 1984) and $\bar{\mathbf{v}} \times \bar{\mathbf{B}}$ type forces from the magnetic field because of the motions in the horizontal plane associated with the zonal wind (Jegou et al., 1984) and tides (Kirchoff and Batista, 1984). Ion drift could provide an effective way for the vertical transport of Na species in the mesosphere, particularly when a significant portion of the sodium species is in ionic form.

A detailed calculation of these effects would require the incorporation of the above parameters in our model. In lieu of a full calculation, we examined the response of the topside layer to typical net vertical downward velocities for ions by modifying the continuity equation for the NaX species to have the form

$$\frac{d\phi}{dz} + \frac{d\left(\left[\frac{\text{Na}^+}{\text{NaX}}\right] \cdot [\text{NaX}] \cdot W_D\right)}{dz} = P - L, \quad (5-2)$$

where ϕ is the flux due to molecular and eddy diffusion, P and L denote the production and loss mechanisms for NaX , and W_D represents the vertical ion drift velocity. The relative abundance $[\text{Na}^+]/[\text{NaX}]$ is independent of the assumed drift velocity if the time constant for the vertical drift is larger than the time constant for the removal of Na^+ as given by the rate limiting step (4-4). This condition is valid below 100 km, where the time constant for the vertical drift is $\sim 10^4$ s, while the time constant for Na^+ clustering is $\sim 10^3$ s.

Figure 15 shows the results of our calculations for constant drift velocities equal to 0, -5, -10, and -20 cm/s between 120 and 90 km. The small topside scale height observed (2-3 km, Gibson and Sandford, 1981; Clemesha et al., 1982) can be modeled using downward velocities between 10 and 20 cm/s. The effect of vertical ion drift is thus an important contributing factor in controlling the topside sodium layer.

6. CONCLUDING REMARKS

We have presented the results of a fully diurnal model for ion species in the D and lower E regions. When coupled with our previous model of the neutral species, our present model allows for the self-consistent calculation of background neutral and ionic species between 60 and 120 km. Results of our calculations are in good agreement with those of other models.

Production of Na^+ occurs primarily through photoionization below 100 km, and through charge exchange with O_2^+ at higher altitudes. The main loss mechanism is dissociative recombination of sodium cluster ions. A self-consistent calculation thus requires knowledge of the O_2^+ and e densities in the above altitude regimes. Our code has been applied to the calculation of the density and diurnal variation of sodium species above 90 km. The calculated diurnal variation of Na^+ (factor of 10-100 between 90 and 100 km) and daytime densities ($\sim 10^2 \text{ cm}^{-3}$) are in good agreement with rocket data (Swider, 1984).

We have also investigated the effect of ion chemistry on the abundance of neutral sodium above 90 km. In particular, the small scale height (2-3 km) observed in the topside sodium layer seems to require either downward ion drifts velocities of order $10\text{-}20 \text{ cm s}^{-1}$ above 90 km or a rate of clustering of Na^+ with N_2 a factor of 5 smaller than the value suggested by Richter and Sechrist (1979). Further elucidation of this question will require measurements of the clustering rate at mesospheric temperatures as well as incorporation of more realistic scenarios for ion drifts into our model.

Since we have included a complete treatment of the ion chemistry in the D region, the model presented above is also suited to studies of the D region ion chemistry and its possible effect on neutral constituents during disturbed conditions (Swider and Keneshea, 1973; Solomon et al., 1983). The model also allows for each extension to the calculation of other metallic ion species.

Table 1

List of Reactions and Reaction Rates for the Background Ions

TYPE ^a	PAR1	PAR2	PAR3	REACTIONS
1 7.	1.00E-28	-3.00E+00	0.00E+00	$H^+.(H_2O)_3 + CO_2 + M = H^+.(H_2O)_3.CO_2 + M, 7$
2 1.	1.00E-09	0.00E+00	0.00E+00	$H^+.(H_2O)_3.CO_2 + H_2O = H^+.(H_2O)_4 + CO_2, 1$
3 1.	4.50E-10	0.00E+00	0.00E+00	$O_2^+ + NO = NO^+ + O_2, 1$
4 7.	1.60E-30	-3.20E+00	0.00E+00	$O_2^+ + O_2 + M = O_4^+ + M, 7$
5 1.	3.00E-10	0.00E+00	0.00E+00	$O_4^+ + O = O_2^+ + O_3, 1$
6 1.	1.50E-09	0.00E+00	0.00E+00	$O_4^+ + H_2O = O_2^+.H_2O + O_2, 1$
7 1.	1.00E-09	0.00E+00	0.00E+00	$O_2^+.H_2O + H_2O = H^+.H_2OOH + O_2, 1$
8 1.	2.00E-10	0.00E+00	0.00E+00	$O_2^+.H_2O + H_2O = H^+.H_2O + OH, 1$
9 1.	1.40E-09	0.00E+00	0.00E+00	$H^+.H_2OOH + H_2O = H^+.(H_2O)_2 + OH, 1$
10 7.	1.40E-30	-2.00E+00	0.00E+00	$H^+.H_2O + N_2 + N_2 = H^+.H_2O.N_2 + N_2, 7$
11 1.	1.00E-09	0.00E+00	0.00E+00	$H^+.H_2O.N_2 + CO_2 = H^+.H_2O.CO_2 + N_2, 1$
12 1.	1.00E-09	0.00E+00	0.00E+00	$H^+.H_2O.CO_2 + H_2O = H^+.(H_2O)_2 + CO_2, 1$
13 7.	5.00E-28	-3.00E+00	0.00E+00	$H^+.(H_2O)_2 + CO_2 + M = H^+.(H_2O)_2.CO_2 + M, 7$
14 1.	1.00E-09	0.00E+00	0.00E+00	$H^+.(H_2O)_2.CO_2 + H_2O = H^+.(H_2O)_3 + CO_2, 1$
15 7.	3.50E-27	-3.00E+00	0.00E+00	$H^+.H_2O + H_2O + M = H^+.(H_2O)_2 + M, 7$
16 7.	2.20E-27	-3.00E+00	0.00E+00	$H^+.(H_2O)_2 + H_2O + M = H^+.(H_2O)_3 + M, 7$
17 7.	2.30E-27	-3.00E+00	0.00E+00	$H^+.(H_2O)_3 + H_2O + M = H^+.(H_2O)_4 + M, 7$
18 7.	1.00E-29	-2.30E+00	0.00E+00	$NO^+ + CO_2 + N_2 = NO^+.CO_2 + N_2, 7$
19 1.	1.00E-09	0.00E+00	0.00E+00	$NO^+.CO_2 + H_2O = CO_2 + NO^+.H_2O, 1$
20 7.	1.10E-27	-4.70E+00	0.00E+00	$NO^+.H_2O + H_2O + N_2 = NO^+.(H_2O)_2 + N_2, 7$
21 7.	1.60E-27	-4.70E+00	0.00E+00	$NO^+.(H_2O)_2 + H_2O + N_2 = NO^+.(H_2O)_3 + N_2, 7$
22 1.	7.00E-11	0.00E+00	0.00E+00	$NO^+.(H_2O)_3 + H_2O = H^+.(H_2O)_3 + XX, 1$
23 7.	4.00E-07	-1.00E+00	0.00E+00	$NO^+ + E = N + O, 7$
24 7.	2.10E-07	-6.30E-01	0.00E+00	$O_2^+ + E = O + O, 7$
25 1.	2.00E-06	0.00E+00	0.00E+00	$O_4^+ + E = O_2 + O_2, 1$

^aThe parameterization and values for the reaction constants are taken from Swider and Narcisi (1983). The reaction rates are calculated as follows:

Type 1: $k = PAR1$

Type 7: $k = PAR1 \cdot (300/T)^{-PAR2}$

Type 8: $k = PAR1 \cdot (300/T)^{-PAR2} \cdot \exp(PAR3/T)$.

TYPE	PAR1	PAR2	PAR3	REACTIONS	
26	1.	1.50E-06	0.00E+00	0.00E+00	$O_2^+.H_2O + E = O_2 + H_2O, 1$
27	1.	2.00E-06	0.00E+00	0.00E+00	$H^+.H_2OOH + E = H_2O + H_2O, 1$
28	1.	1.30E-06	0.00E+00	0.00E+00	$H^+.H_2O + E = H_2 + OH, 1$
29	1.	2.50E-06	0.00E+00	0.00E+00	$H^+.(H_2O)_2 + E = H_2O + H_2 + OH, 1$
30	1.	3.00E-06	0.00E+00	0.00E+00	$H^+.(H_2O)_3 + E = OH + XX, 1$
31	1.	3.60E-06	0.00E+00	0.00E+00	$H^+.(H_2O)_4 + E = OH + XX, 1$
32	1.	1.50E-06	0.00E+00	0.00E+00	$H^+.H_2O.N_2 + E = H + XX, 1$
33	1.	2.00E-06	0.00E+00	0.00E+00	$H^+.H_2O.CO_2 + E = H + XX, 1$
34	1.	3.00E-06	0.00E+00	0.00E+00	$H^+.(H_2O)_2CO_2 + E = H + XX, 1$
35	1.	1.50E-06	0.00E+00	0.00E+00	$NO^+.CO_2 + E = NO + CO_2, 1$
36	1.	1.50E-06	0.00E+00	0.00E+00	$NO^+.H_2O + E = NO + H_2O, 1$
37	1.	2.00E-06	0.00E+00	0.00E+00	$NO^+.(H_2O)_2 + E = NO + XX, 1$
38	1.	3.00E-06	0.00E+00	0.00E+00	$NO^+.(H_2O)_3 + E = NO + XX, 1$
39	8.	3.30E-06	-4.00E+00	-5.03E+03	$O_4^+ + M = O_2^+ + O_2 + M, 8$
40	7.	2.00E-31	-4.40E+00	0.00E+00	$NO^+ + N_2 + N_2 = NO^+.N_2 + N_2, 7$
41	1.	1.00E-09	0.00E+00	0.00E+00	$NO^+.N_2 + CO_2 = NO^+.CO_2 + N_2, 1$
42	8.	1.00E-08	-5.40E+00	-2.10E+03	$NO^+.N_2 + N_2 = NO^+ + N_2 + N_2, 8$
43	7.	2.00E-31	-4.40E+00	0.00E+00	$NO^+.H_2O + N_2 + N_2 = NO^+.H_2O.N_2 + N_2, 7$
44	1.	1.00E-09	0.00E+00	0.00E+00	$NO^+.H_2O.N_2 + CO_2 = NO^+.H_2OCO_2 + N_2, 1$
45	1.	1.00E-09	0.00E+00	0.00E+00	$NO^+.H_2O.CO_2 + H_2O = NO^+.(H_2O)_2 + CO_2, 1$
46	7.	2.00E-31	-4.40E+00	0.00E+00	$NO^+.(H_2O)_2 + N_2 + N_2 = NO^+.(H_2O)_2.N_2 + N_2, 7$
47	1.	1.00E-09	0.00E+00	0.00E+00	$NO^+.(H_2O)_2.N_2 + CO_2 = NO^+.(H_2O)_2.CO_2 + N_2, 1$
48	1.	1.00E-09	0.00E+00	0.00E+00	$NO^+.(H_2O)_2.CO_2 + H_2O = NO^+.(H_2O)_3 + CO_2, 1$
49	8.	1.20E-01	-4.00E+00	-8.80E+03	$H^+.(H_2O)_4 + M = H^+.(H_2O)_3 + H_2O + M, 8$
50	8.	2.00E-05	-3.30E+00	-5.50E+03	$NO^+.CO_2 + M = NO^+ + CO_2 + M, 8$
51	8.	5.00E-08	-5.40E+00	-2.10E+03	$NO^+.H_2O.N_2 + M = NO^+.H_2O + N_2 + M, 8$
52	8.	2.00E-04	-3.30E+00	-5.50E+03	$NO^+.H_2O.CO_2 + M = NO^+.H_2O + CO_2 + M, 8$
53	8.	5.00E-07	-5.40E+00	-2.10E+03	$NO^+.(H_2O)_2.N_2 + M = NO^+.(H_2O)_2 + N_2 + M, 8$
54	8.	2.00E-03	-3.30E+00	-5.50E+03	$NO^+.(H_2O)_2.CO_2 + M = NO^+.(H_2O)_2 + CO_2 + M, 8$
55	8.	1.00E-02	-5.70E+00	-6.80E+03	$NO^+.(H_2O)_3 + M = NO^+.(H_2O)_2 + H_2O + M, 8$
56	8.	1.00E-02	-5.70E+00	-8.10E+03	$NO^+.(H_2O)_2 + M = NO^+.H_2O + H_2O + M, 8$
57	1.	5.00E-10	0.00E+00	0.00E+00	$O_2^- + O_3 = O_3^- + O_2, 1$
58	8.	1.40E-29	-1.00E+00	-6.00E+02	$O_2 + E + O_2 = O_2^- + O_2, 8$
59	1.	1.00E-31	0.00E+00	0.00E+00	$O_2 + E + N_2 = O_2^- + N_2, 1$

	TYPE	PAR1	PAR2	PAR3	REACTION
60	1.	1.50E-10	0.00E+00	0.00E+00	$O_2^- + O = O_3 + E, 1$
61	1.	1.50E-10	0.00E+00	0.00E+00	$O_2^- + O = O^- + O_2, 1$
62	1.	2.00E-10	0.00E+00	0.00E+00	$O_2^- + O_2(^1\Delta) = O_2 + O_2 + E, 1$
63	7.	2.50E-30	-2.50E+00	0.00E+00	$O_2^- + O_2 + O_2 = O_4^- + O_2, 7$
64	1.	4.30E-10	0.00E+00	0.00E+00	$O_4^- + CO_2 = CO_4^- + O_2, 1$
65	1.	1.30E-10	0.00E+00	0.00E+00	$CO_4^- + O_3 = O_3^- + CO_2 + O_2, 1$
66	1.	4.80E-11	0.00E+00	0.00E+00	$CO_4^- + NO = NO_3^- + CO_2, 1$
67	1.	1.50E-10	0.00E+00	0.00E+00	$CO_4^- + O = CO_3^- + O_2, 1$
68	1.	3.20E-10	0.00E+00	0.00E+00	$O_3^- + O = O_2^- + O_2, 1$
69	1.	5.50E-10	0.00E+00	0.00E+00	$O_3^- + CO_2 = CO_3^- + O_2, 1$
70	1.	1.10E-10	0.00E+00	0.00E+00	$CO_3^- + O = O_2^- + CO_2, 1$
71	1.	1.10E-11	0.00E+00	0.00E+00	$CO_3^- + NO = NO_2^- + CO_2, 1$
72	1.	2.00E-10	0.00E+00	0.00E+00	$CO_3^- + NO_2 = NO_3^- + CO_2, 1$
73	1.	9.00E-11	0.00E+00	0.00E+00	$NO_2^- + O_3 = NO_3^- + O_2, 1$
74	7.	5.00E-30	-1.90E+00	0.00E+00	$O^- + O_2 + O_2 = O_3^- + O_2, 7$
75	1.	2.00E-10	0.00E+00	0.00E+00	$O^- + O = O_2 + E, 1$
76	1.	3.00E-10	0.00E+00	0.00E+00	$O^- + O_2(^1\Delta) = O_3 + E, 1$
77	1.	4.40E-10	0.00E+00	0.00E+00	$O^- + O_3 = O_3^- + O, 1$
78	1.	4.40E-10	0.00E+00	0.00E+00	$O^- + O_3 = O_2^- + O_2, 1$
79	1.	6.00E-08	0.00E+00	0.00E+00	$O_2^+ + [NSUM]^b = XX, 1$
80	1.	6.00E-08	0.00E+00	0.00E+00	$O_4^+ + [NSUM] = XX, 1$
81	1.	6.00E-08	0.00E+00	0.00E+00	$O_2 + H_2O + [NSUM] = XX, 1$
82	1.	6.00E-08	0.00E+00	0.00E+00	$H^+.H_2O.OH + [NSUM] = XX, 1$
83	1.	6.00E-08	0.00E+00	0.00E+00	$H^+.H_2O + [NSUM] = XX, 1$
84	1.	6.00E-08	0.00E+00	0.00E+00	$H^+.H_2O.N_2 + [NSUM] = XX, 1$
85	1.	6.00E-08	0.00E+00	0.00E+00	$H^+.H_2O.CO_2 + [NSUM] = XX, 1$
86	1.	6.00E-08	0.00E+00	0.00E+00	$H.(H_2O)_2^+ + [NSUM] = XX, 1$
87	1.	6.00E-08	0.00E+00	0.00E+00	$H.(H_2O)_2.CO_2 + [NSUM] = XX, 1$
88	1.	6.00E-08	0.00E+00	0.00E+00	$H^+.(H_2O)_3 + [NSUM] = XX, 1$
89	1.	6.00E-08	0.00E+00	0.00E+00	$H^+.(H_2O)_3.CO_2 + [NSUM] = XX, 1$
90	1.	6.00E-08	0.00E+00	0.00E+00	$H^+.(H_2O)_4 + [NSUM] = XX, 1$
91	1.	6.00E-08	0.00E+00	0.00E+00	$NO^+ + [NSUM] = XX, 1$

^b[NSUM] denotes the total density of negative ions.

	TYPE	PAR1	PAR2	PAR3	REACTION
92	1.	6.00E-08	0.00E+00	0.00E+00	$\text{NO}^+ \cdot \text{N}_2 + [\text{NSUM}] = \text{XX}, 1$
93	1.	6.00E-08	0.00E+00	0.00E+00	$\text{NO}^+ \cdot \text{CO}_2 + [\text{NSUM}] = \text{XX}, 1$
94	1.	6.00E-08	0.00E+00	0.00E+00	$\text{O}_2^- + [\text{PSUM}]^c = \text{XX}, 1$
95	1.	6.00E-08	0.00E+00	0.00E+00	$\text{O}^- + [\text{PSUM}] = \text{XX}, 1$
96	1.	6.00E-08	0.00E+00	0.00E+00	$\text{O}_4^- + [\text{PSUM}] = \text{XX}, 1$
97	1.	6.00E-08	0.00E+00	0.00E+00	$\text{O}_3^- + [\text{PSUM}] = \text{XX}, 1$
98	1.	6.00E-08	0.00E+00	0.00E+00	$\text{CO}_3^- + [\text{PSUM}] = \text{XX}, 1$
99	1.	6.00E-08	0.00E+00	0.00E+00	$\text{CO}_4^- + [\text{PSUM}] = \text{XX}, 1$
100	1.	6.00E-08	0.00E+00	0.00E+00	$\text{NO}_2^- + [\text{PSUM}] = \text{XX}, 1$
101	1.	6.00E-08	0.00E+00	0.00E+00	$\text{NO}_3^- + [\text{PSUM}] = \text{XX}, 1$
102	1.	6.00E-08	0.00E+00	0.00E+00	$\text{NO}^+ \cdot \text{H}_2\text{O} + [\text{NSUM}] = \text{XX}, 1$
103	1.	6.00E-08	0.00E+00	0.00E+00	$\text{NO}^+ \cdot (\text{H}_2\text{O})_2 + [\text{NSUM}] = \text{XX}, 1$
104	1.	6.00E-08	0.00E+00	0.00E+00	$\text{NO}^+ \cdot (\text{H}_2\text{O})_3 + [\text{NSUM}] = \text{XX}, 1$
105	1.	6.00E-08	0.00E+00	0.00E+00	$\text{NO}^+ \cdot \text{H}_2\text{O} \cdot \text{N}_2 + [\text{NSUM}] = \text{XX}, 1$
106	1.	6.00E-08	0.00E+00	0.00E+00	$\text{NO}^+ \cdot \text{H}_2\text{O} \cdot \text{CO}_2 + [\text{NSUM}] = \text{XX}, 1$
107	1.	6.00E-08	0.00E+00	0.00E+00	$\text{NO}^+ \cdot (\text{H}_2\text{O})_2 \cdot \text{N}_2 + [\text{NSUM}] = \text{XX}, 1$
108	1.	6.00E-08	0.00E+00	0.00E+00	$\text{NO}^+ \cdot (\text{H}_2\text{O})_2 \cdot \text{CO}_2 + [\text{NSUM}] = \text{XX}, 1$

^c[PSUM] denotes the total density of positive ions.

Table 2
List of Reactions for the Sodium Species

	TYPE ^a	PAR1	PAR2	PAR3	REACTIONS
1	1.	3.00E-10	0.00E+00	0.00E+00	$\text{Na} + \text{O}_3 = \text{NaO} + \text{O}_2, 1$
2	1.	4.00E-11	0.00E+00	0.00E+00	$\text{NaO} + \text{O} = \text{Na} + \text{O}_2, 1$
3	2.	8.00E-31	-2.90E+02	0.00E+00	$\text{Na}^+\text{O}_2 + \text{M} = \text{NaO}_2 + \text{M}, 2$
4	1.	1.00E-13	0.00E+00	0.00E+00	$\text{NaO}_2 + \text{O} = \text{NaO} + \text{O}_2, 1$
5	1.	0.00E+00	0.00E+00	0.00E+00	$\text{NaO} + \text{H}_2\text{O} = \text{NaOH} + \text{OH}, 1$
6	1.	5.00E-11	0.00E+00	0.00E+00	$\text{NaO} + \text{O}_3 = \text{NaO}_2 + \text{O}_2, 1$
7	1.	1.00E-14	0.00E+00	0.00E+00	$\text{NaO} + \text{H} = \text{Na} + \text{OH}, 1$
8	1.	1.00E-11	0.00E+00	0.00E+00	$\text{NaO}_2 + \text{OH} = \text{NaOH} + \text{O}_2, 1$
9	1.	1.00E-13	0.00E+00	0.00E+00	$\text{NaO}_2 + \text{H} = \text{NaOH} + \text{O}, 1$
10	1.	1.40E-12	0.00E+00	0.00E+00	$\text{NaOH} + \text{H} = \text{Na} + \text{H}_2\text{O}, 1$
11	1.	1.00E-10	0.00E+00	0.00E+00	$\text{NaOH} + \text{O}^1\text{D} = \text{NaO} + \text{OH}, 1$
12	1.	1.40E-11	0.00E+00	0.00E+00	$\text{Na} + \text{HO}_2 = \text{NaOH} + \text{O}, 1$
13	1.	1.00E-10	0.00E+00	0.00E+00	$\text{NaO} + \text{O}_3 = \text{Na} + \text{XX}, 1$
14	1.	1.00E-11	0.00E+00	0.00E+00	$\text{NaO} + \text{HO}_2 = \text{NaOH} + \text{XX}, 1$
15	1.	6.00E-10	0.00E+00	0.00E+00	$\text{Na} + \text{O}_2^+ = \text{Na}^+ + \text{O}_2, 1$
16	1.	8.00E-11	0.00E+00	0.00E+00	$\text{Na} + \text{NO}^+ = \text{Na}^+ + \text{NO}, 1$
17	7.	2.00E-31	-1.50E+00	0.00E+00	$\text{Na}^+ + \text{N}_2 + \text{M} = \text{Na}^+\text{.N}_2 + \text{M}, 7$
18	8.	9.00E-07	-2.50E+00	-4.75E+03	$\text{Na}^+\text{.N}_2 + \text{M} = \text{Na}^+ + \text{N}_2 + \text{N}_2, 8$
19	7.	2.00E-29	-1.50E+00	0.00E+00	$\text{Na}^+ + \text{CO}_2 + \text{M} = \text{Na}^+\text{.CO}_2 + \text{M}, 7$
20	8.	6.00E-06	-2.50E+00	-6.25E+03	$\text{Na}^+\text{.CO}_2 + \text{M} = \text{Na}^+ + \text{CO}_2 + \text{M}, 8$
21	7.	5.00E-32	-1.50E+00	0.00E+00	$\text{Na}^+ + \text{O}_2 + \text{M} = \text{NaO}_2^+ + \text{M}, 7$
22	8.	8.00E-09	-2.50E+00	-2.85E+03	$\text{NaO}_2^+ + \text{M} = \text{Na}^+ + \text{O}_2 + \text{M}, 8$
23	7.	1.00E-28	-1.50E+00	0.00E+00	$\text{Na}^+ + \text{H}_2\text{O} + \text{M} = \text{Na}^+\text{.H}_2\text{O} + \text{M}, 7$

^aThe parameterization and values for the reaction constants are taken from Murad (1978) and Richter and Schrist (1979). The reaction rates are calculated as follows:

Type 1: $k = \text{PAR1}$

Type 2: $k = \text{PAR1} \cdot \exp(-\text{PAR2}/T)$

Type 7: $k = \text{PAR1} \cdot (300/T)^{-\text{PAR2}}$

Type 8: $k = \text{PAR1} \cdot (300/T)^{-\text{PAR2}} \cdot \exp(\text{PAR3}/T)$.

	TYPE	PAR1	PAR2	PAR3	REACTIONS
24	1.	1.00E-09	0.00E+00	0.00E+00	$\text{Na}^+.\text{N}_2 + \text{CO}_2 = \text{Na}^+.\text{CO}_2 + \text{N}_2, 1$
25	1.	1.00E-09	0.00E+00	0.00E+00	$\text{Na}^+.\text{CO}_2 + \text{H}_2\text{O} = \text{Na}^+.\text{H}_2\text{O} + \text{CO}_2, 1$
26	7.	1.00E-06	-5.00E-01	0.00E+00	$\text{Na}^+.\text{CO}_2 + \text{E} = \text{Na} + \text{CO}_2, 7$
27	7.	1.00E-06	-5.00E-01	0.00E+00	$\text{Na}^+.\text{H}_2\text{O} + \text{E} = \text{Na} + \text{H}_2\text{O}, 7$
28	7.	1.00E-06	-5.00E-01	0.00E+00	$\text{Na}^+.\text{N}_2 + \text{E} = \text{Na} + \text{N}_2, 7$
29	7.	1.00E-06	-5.00E-01	0.00E+00	$\text{NaO}_2^+ + \text{E} = \text{NaO}_2 + , 7$
30	1.	1.00E-10	0.00E+00	0.00E+00	$\text{NaO}_2^+ + \text{O} = \text{NaO}^+ + \text{O}_2, 1$
31	1.	5.00E-10	0.00E+00	0.00E+00	$\text{NaO}^+ + \text{O} = \text{Na}^+ + \text{O}_2, 1$
32	1.	1.00E-09	0.00E+00	0.00E+00	$\text{NaO} + \text{O}_2^+ = \text{NaO}^+ + \text{O}_2, 1$
33	1.	1.00E-09	0.00E+00	0.00E+00	$\text{NaO} + \text{NO}^+ = \text{NaO}^+ + \text{NO}, 1$
34	1.	4.00E-07	0.00E+00	0.00E+00	$\text{NaO}^+ + \text{E} = \text{Na} + \text{O}, 1$
35	1.	6.00E-08	0.00E+00	0.00E+00	$\text{Na}^+ + [\text{NSUM}]^b = \text{Na} + \text{XX}, 1$
36	1.	6.00E-08	0.00E+00	0.00E+00	$\text{Na}^+.\text{N}_2 + [\text{NSUM}] = \text{Na} + \text{XX}, 1$
37	1.	6.00E-08	0.00E+00	0.00E+00	$\text{Na}^+.\text{CO}_2 + [\text{NSUM}] = \text{Na} + \text{XX}, 1$
38	1.	6.00E-08	0.00E+00	0.00E+00	$\text{Na}^+.\text{H}_2\text{O} + [\text{NSUM}] = \text{Na} + \text{XX}, 1$
39	1.	6.00E-08	0.00E+00	0.00E+00	$\text{NaO}^+ + [\text{NSUM}] = \text{NaO} + \text{XX}, 1$
40	1.	6.00E-08	0.00E+00	0.00E+00	$\text{NaO}_2^+ + [\text{NSUM}] = \text{Na} + \text{XX}, 1$

^b[NSUM] denotes the total density of negative ions.

Table 3
Calculated Local Topside Scale Heights (km)

Altitude (km)	Scale Height [†] (km)			
	No ions	$K^* = 7 \times 10^{-31} \uparrow \uparrow$	$K^* = 2 \times 10^{-31}$	$K^* = 4 \times 10^{-32}$
92	9.2	8.13	7.84	6.85
94	6.72	6.52	6.11	5.23
96	6.13	5.74	5.12	4.31
98	5.85	4.99	4.27	3.31
100	5.73	4.26	3.60	2.48

[†]Local scale height is obtained from the gradient of Na profile.

^{††} $\text{Na}^+ + \text{N}_2 + \text{M} \rightarrow \text{Na}^+ + \text{N}_2 + \text{M}$ with reaction rate $K_S = K^* \left(\frac{300}{T}\right)^{1.5}$. Units for K^* are $\text{cm}^6 \text{ s}^{-1}$.

Experimental Results

Gibson and Sandford (1970): 4 km (98 km), 3 km (100 km), 2 km (102 km).

Megie and Blamont (1977): 2-5 km average scale height above peak.

Simonich et al. (1979): 2.5-5 km at 100 km (scale height changes during night).

References Cited:

- Allen, M., J. I. Lunine, and Y. L. Yung (1984) The vertical distribution of ozone in the mesosphere and lower thermosphere. J. Geophys. Res., 89, 4841.
- Berger, M. J., S. M. Seltzer, and K. Maeda (1974) Some new results on electron transport in the atmosphere. J. Atmos. Terr. Phys., 36, 591.
- Bevilacqua, R. M., J. J. Olivero, P. R. Schwartz, C. J. Gibbins, J. M. Bologna, and D. J. Thacker (1983) An observational study of water vapor in the mid-latitude mesosphere using ground-based microwave techniques. J. Geophys. Res., 88, 8523.
- Clemesha, B. R., D. M. Simonich, P. O. Batista, and V. W. J. H. Kirchoff (1982) The diurnal variation of atmospheric sodium. J. Geophys. Res., 87, 181.
- Gibson, A. J., and M. C. W. Sandford (1971) The seasonal variation of the night-time sodium layer. J. Atmos. Terr. Phys., 33, 1675.
- Goldberg, R. A., and A. C. Aikin (1971) Studies of positive ion composition in the equatorial D region ionosphere. J. Geophys. Res., 76, 8352.
- Granier, C., and G. Megie (1982) Daytime Lidar Measurements of the Mesospheric Sodium Layer. Planet. Space Sci. 30, 169.
- Hanson, W. B., and J. S. Donaldson (1967) Sodium distribution in the upper atmosphere. J. Geophys. Res., 72, 5513.
- Heimerl, J. M. (1976) Report #1917, U.S.A. Ballistic Research Lab., Maryland.
- Hunten, D. M. (1981) A meteor-ablation model of the sodium and potassium layers. Geophys. Res. Lett., 8, 369.
- Jegou, J. P., C. Granier, M. L. Chanin, and G. Megie (1984) General theory of the alkali metals present in the Earth's upper atmosphere. I. Transit model: Chemical and dynamical processes. Submitted to Annales de Geophysique.
- Kirchoff, V. W. J. H., and P. P. Batista (1983) Calculation of the vertical drift of the sodium ion. Annales Geophysicae, 1, 509.
- Krankowsky, D. F., F. Arnold, H. Wider, J. Kissel, and J. Zähringer (1972) Positive ion chemistry in the lower ionosphere. Radio Science, 1, 83.
- Megie, G., and J. E. Blamont (1977) Laser sounding of atmospheric sodium: Interpretation in terms of global atmospheric parameters. Planet. Space Sci., 25, 1093.
- Murad, E. (1978) Problems in the chemistry of metallic species in the D and E regions. J. Geophys. Res., 83, 5525.

- Narcisi, R. S., and A. D. Bailey (1965) Mass spectrometric measurements of positive ions at altitudes from 64 to 112 km. J. Geophys. Res., 70, 3687.
- Paulsen, D. E., R. E. Huffman, and J. C. Larrabee (1972) Improved photoionization rates of $O_2(^1\Delta_g)$ in the D region. Radio Sci., 7, 51.
- Perry, R. A., A. A. Viggiano, D. L. Albritton, E. E. Ferguson, and F. C. Fehsenfeld (1980) Laboratory measurements of stratospheric sodium ion reactions. Geophys. Res. Lett., 7, 693.
- Rodriguez, J. M., M. K. W. Ko, and N. D. Sze (1984) The diurnal variation of the neutral sodium species in the upper atmosphere: A model study. Report #AFGL-TR-84-0204, Air Force Geophys. Lab., Bedford, MA., ADA 154988.
- Richter, E. S., and C. F. Sechrist, Jr. (1979) A cluster ion chemistry for the mesospheric sodium layer. J. Atmos. Terr. Phys., 41, 579.
- Simonich, D. M., B. R. Clemesha, and V. W. J. H. Kirchoff (1979) The Mesospheric Sodium Layer at 23°S: Nocturnal and Seasonal Variations. J. Geophys. Res. 84, 1543.
- Solomon, S., G. C. Reid, D. W. Rusch, and R. J. Thomas (1983) Mesospheric ozone depletion during the solar proton event of July 13, 1982. Part II: Comparison between theory and measurements. Geophys. Res. Lett., 10, 257.
- Strobel, D. F., T. R. Young, R. R. Meier, T. P. Coffey, and A. W. Ali (1974): The nighttime ionosphere: E region and lower F region. J. Geophys. Res., 79, 3171.
- Strobel, D. F., C. B. Opal, and R. R. Meier (1980) Photoionization rates in the nighttime E- and F-region ionosphere. Planet. Space Sci., 28, 1027-1033.
- Swider, W. (1969a) Processes for meteoric elements in the E region. Planet. Space Sci., 17, 1233-1246.
- Swider, W. (1969b) Ionization rates due to the attenuation of 1-100 Å nonflare solar X-rays in the terrestrial atmosphere. Rev. Geophys., 7, 573.
- Swider, W. (1983) Latitudinal influences on the quiet daytime D region. Adv. Space Res., 2, 213.
- Swider, W. (1984) Ionic and neutral concentrations of Mg and Fe near 92 km. Planet. Space Sci., 32, 307.
- Swider, W., and W. A. Dean (1975) Effective electron loss coefficient of the disturbed daytime D region. J. Geophys. Res., 80, 1815.
- Swider, W., and T. J. Keneshea (1973) Decrease of ozone and atomic oxygen in the lower mesosphere during a PCA event. Planet. Space Sci., 21, 1969-1973.

- Swider, W., and R. S. Narcisi (1983) Steady-state model of the D-region during the February 1979 eclipse. J. Atm. Terr. Phys., 45, 493.
- Sze, N. D., M. K. W. Ko, R. Specht, and M. Livshits (1980) Modeling of Chemical Processes in the Troposphere and Stratosphere. AFGL-TR-80-0251, Contract No. F 19628-78-C-0215, ADA092704.
- Torkar, K. M., and M. Friedrich (1983) Tests of an ion-chemical model of the D- and lower E-regions. J. Atm. Terr. Phys., 45, 369.
- Torr, D. G., M. R. Torr, R. A. Hoffman, and J. C. G. Walker (1976) Global characteristics of 0.2 to 26 keV charged particles at F region altitudes. Geophys. Res. Lett., 3, 305.

Figure Captions

- Figure 1. Schematic diagram for the chemical scheme of the positive ions in the D and lower E regions. The ions are grouped into two families with O_2^+ and NO^+ being the primary ions in each group.
- Figure 2. Schematic diagram for the chemical scheme of the negative ions in the D and lower E regions.
- Figure 3. The production rates for positive ions for daytime and nighttime conditions: A) Day (45° Solar Zenith Angle (SZA)), altitude range 90-120 km; B) Day (45° SZA), altitude range 60-90 km; c) Night (180° SZA), altitude range 60-120 km. An altitude-independent production rate of $10^{-3} \text{ cm}^3 \text{ s}^{-1}$ due to galactic x-rays is also included in the model. The curves are: a) x-ray, b) Lyman- β , c) Lyman- α , d) energetic electrons, e) ionization of $O_2(^1\Delta)$, and f) cosmic rays.
- Figure 4. Flow chart for the diurnal model of neutral and ionic sodium species.
- Figure 5. Calculated diurnal variation of electron density. Profiles are calculated at (a) 86 km, (b) 90 km, (c) 94 km, and (d) 100 km.
- Figure 6. Calculated diurnal variation of the densities of NO^+ and O_2^+ . Profiles are calculated at (a) 86 km, (b) 90 km, (c) 94 km, and (d) 100 km.
- Figure 7. Calculated total electron and negative ion densities for daytime and nighttime. The positive ion densities are equal to the sum of the electron and the negative ion densities. Curves (a) and (b) are the calculated altitude profiles for electrons for day and night, respectively. The corresponding day and night profiles for the negative ions are given by curves (c) and (d). Curves (e) and (f) are the profiles for electron and negative ions calculated for nighttime including the production of ions from energetic electrons.
- Figure 8. Calculated altitude profiles of negative ions for day (A) and night (B). The curves are O_2^- (—), CO_3^- (---), CO_4^- (···), NO_3^- (-·-·-), NO_2^- (-o-o-), O^- (-Δ-Δ-).
- Figure 9. Calculated altitude profiles of O_2^+ ("a" for day, "b" for night) and NO^+ ("c" for day and "d" for night).
- Figure 10. Calculated day (A) and night (B) altitude profiles of the dominant positive ions below 100 km. The curves are $H^+.(H_2O)_4$ (—), $NO^+.(H_2O)$ (---), $NO^+.(H_2O)_2$ (···), $NO^+.(CO_2)$ (-·-·-), $H^+.(H_2O)_3$ (-o-o-).
- Figure 11. Schematic diagram for the chemical scheme of sodium neutral and ionic species.

Figure 12. Calculated diurnal variation of the Na^+ density at (a) 90 km, (b) 94 km, and (c) 100 km.

Figure 13. Calculated altitude profiles for Na and Na^+ at noon.

Figure 14. Calculated altitude profiles of atomic sodium using different rates for reaction (4-4). The curves correspond to values of $K^* = 2 \times 10^{-31} \text{ cm}^6 \text{ s}^{-1}$ (—), $K^* = 7 \times 10^{-31} \text{ cm}^6 \text{ s}^{-1}$ (---), $K^* = 4 \times 10^{-32} \text{ cm}^6 \text{ s}^{-2}$ (-x-), and the case where no Na^+ is present (-o-o-).

Figure 15. Calculated profiles of the Na layer, assuming vertical ion drift velocities of 0 (—), -4 (-Δ-Δ-), -10 (-o-o-), and -20 (-x-x-) cm/s.

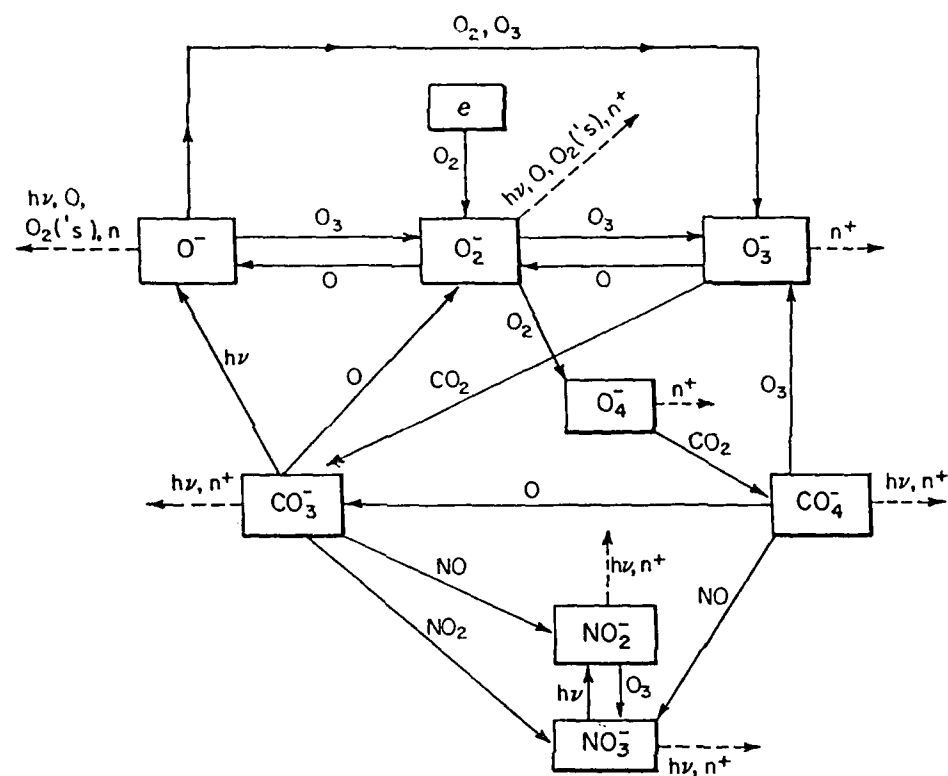


Figure 2. Schematic diagram for the chemical scheme of the negative ions in the D and lower E regions.

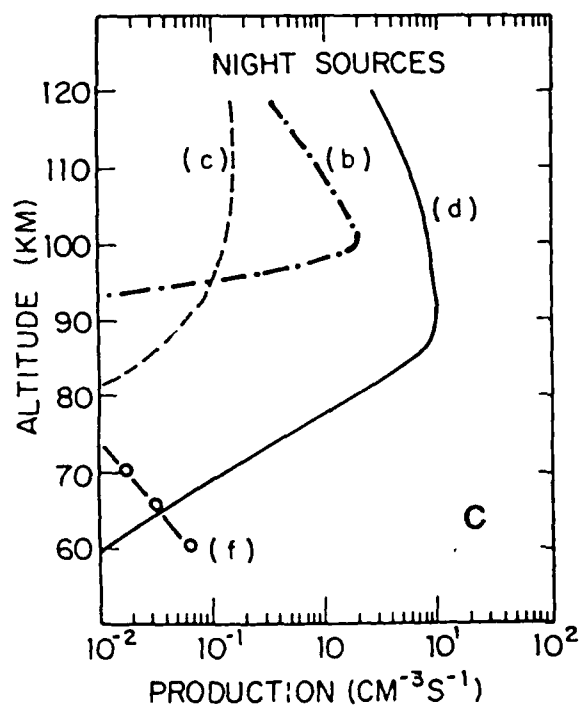
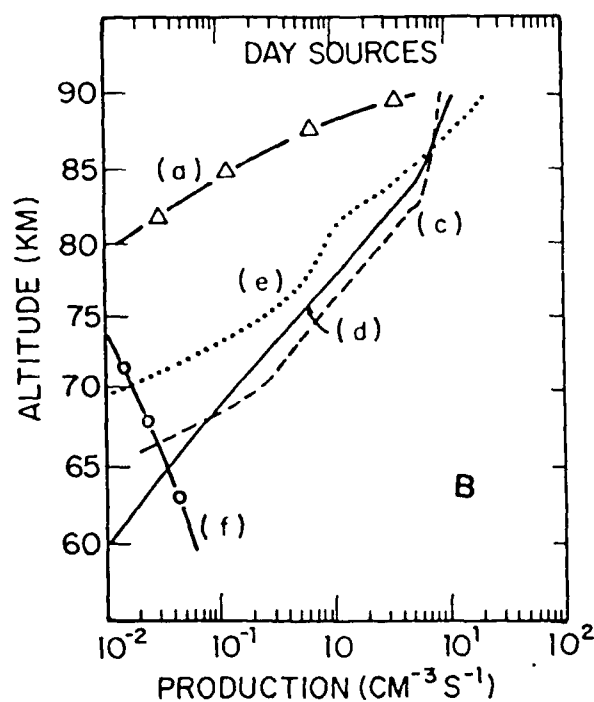
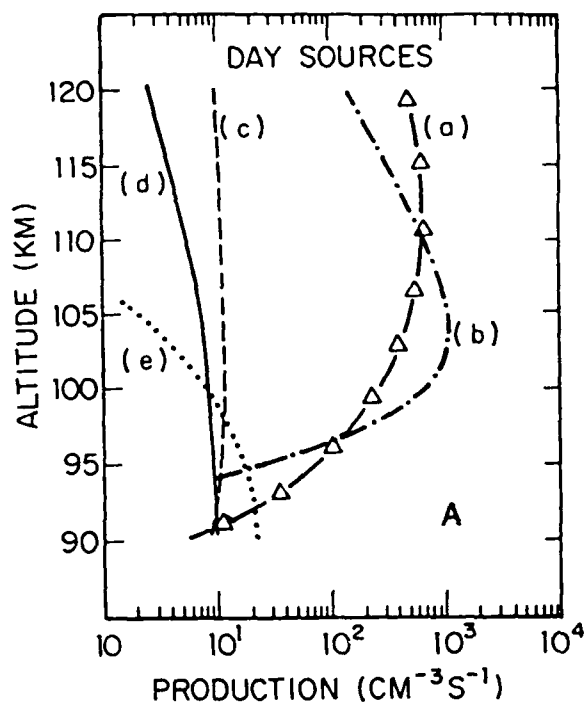


Figure 3. The production rates for positive ions for daytime and nighttime conditions: A) Day (45° Solar Zenith Angle (SZA)), altitude range 90-120 km); B) Day (45° SZA), altitude range 60-90 km; c) Night (180° SZA), altitude range 60-120 km. An altitude-independent production rate of $10^{-3} \text{ cm}^{-3} \text{ s}^{-1}$ due to galactic x-rays is also included in the model. The curves are: a) x-ray, b) Lyman- β , c) Lyman- α , d) energetic electrons, e) ionization of $\text{O}_2(^1\Delta)$, and f) cosmic rays.

Ion Chemistry - Diurnal Option

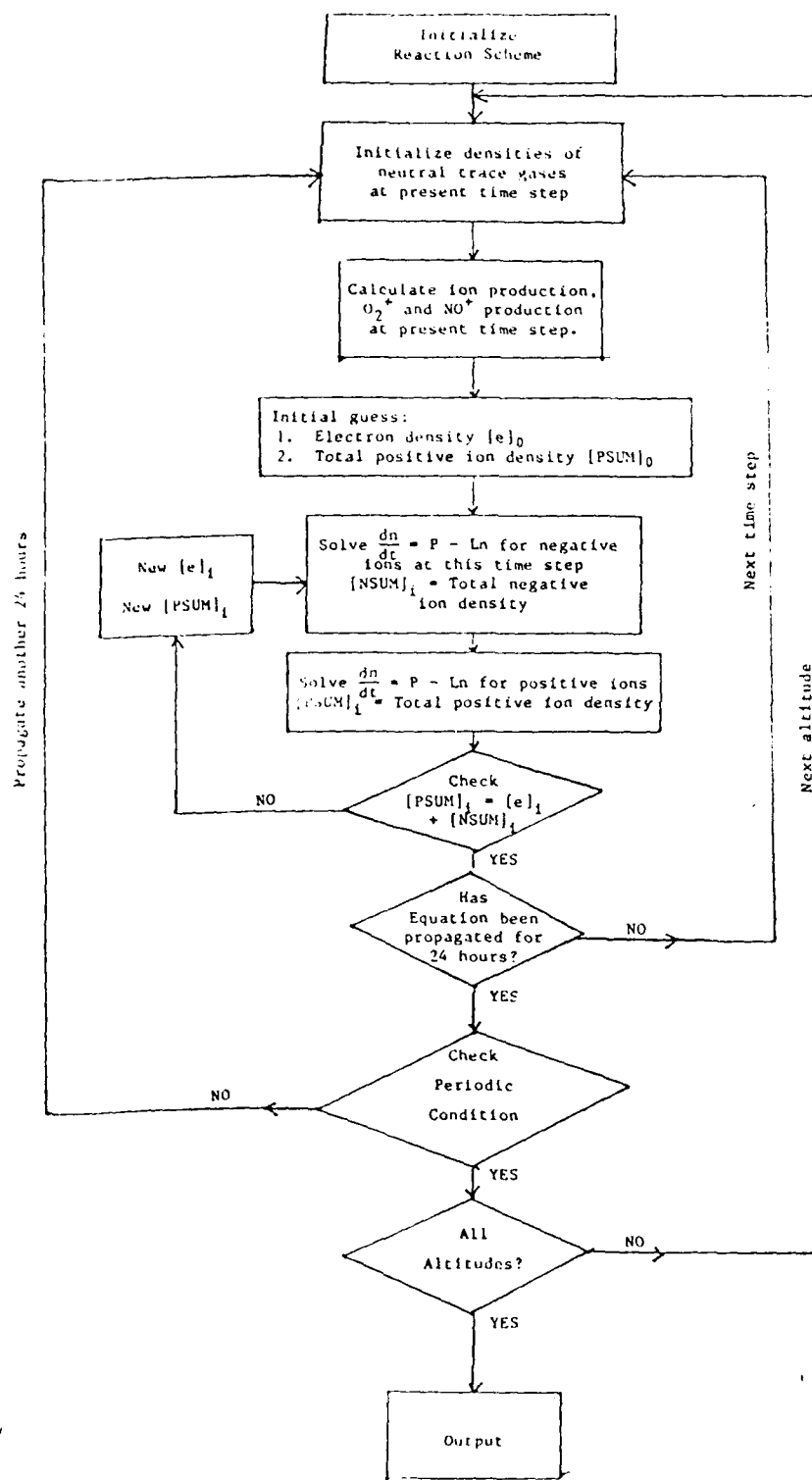


Figure 4. Flow chart for the diurnal model of neutral and ionic sodium species.

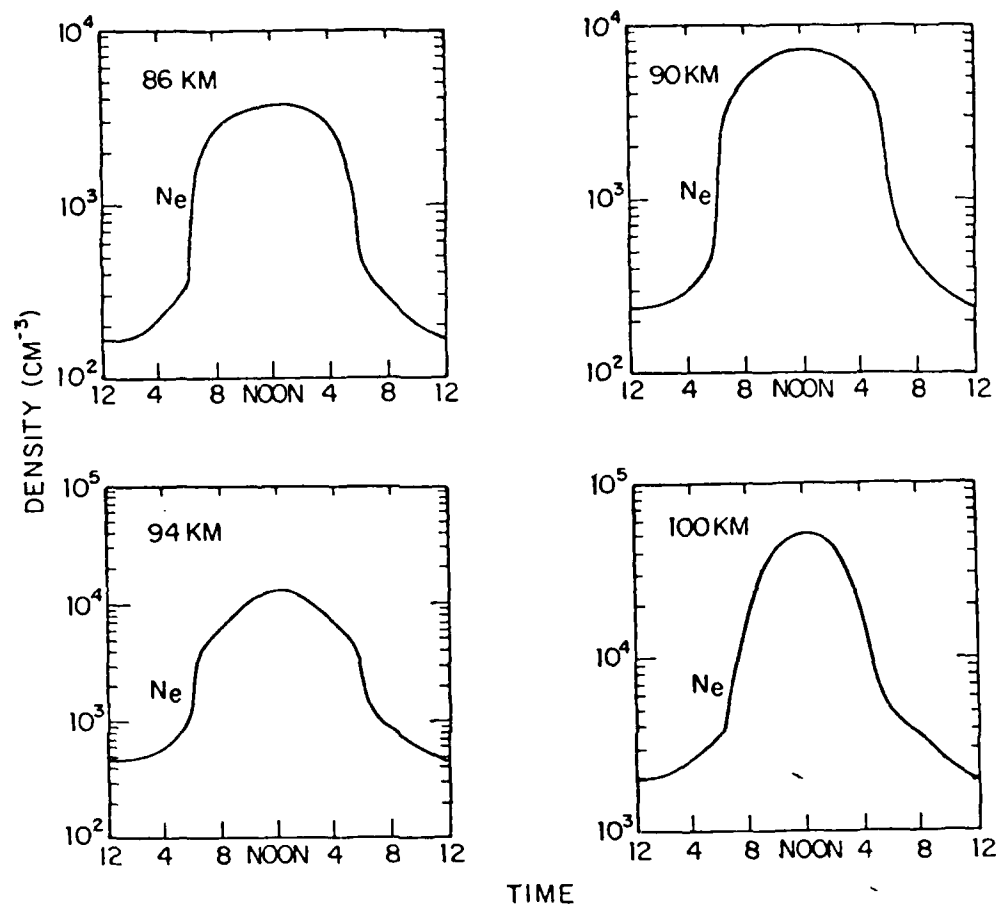


Figure 5. Calculated diurnal variation of electron density. Profiles are calculated at (a) 86 km, (b) 90 km, (c) 94 km, and (d) 100 km.

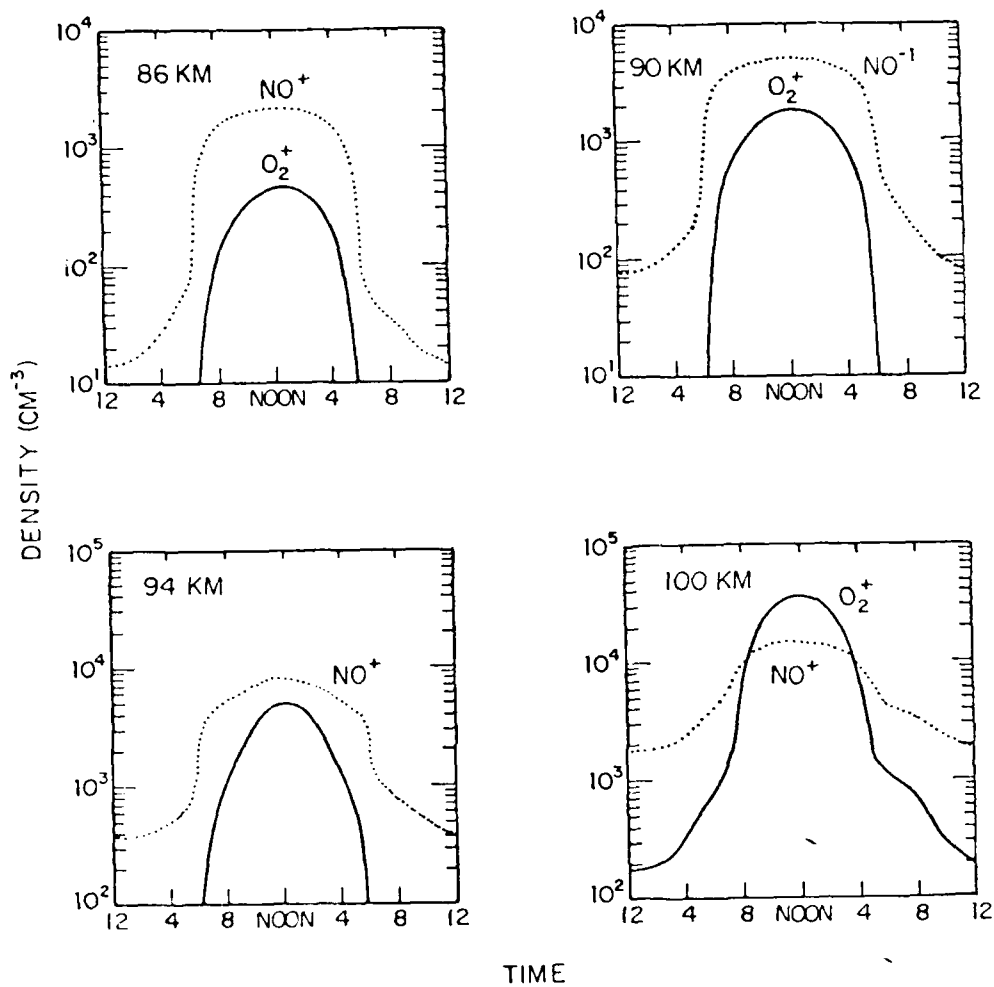


Figure 6. Calculated diurnal variation of the densities of NO⁺ and O₂⁺. Profiles are calculated at (a) 86 km, (b) 90 km, (c) 94 km, and (d) 100 km.

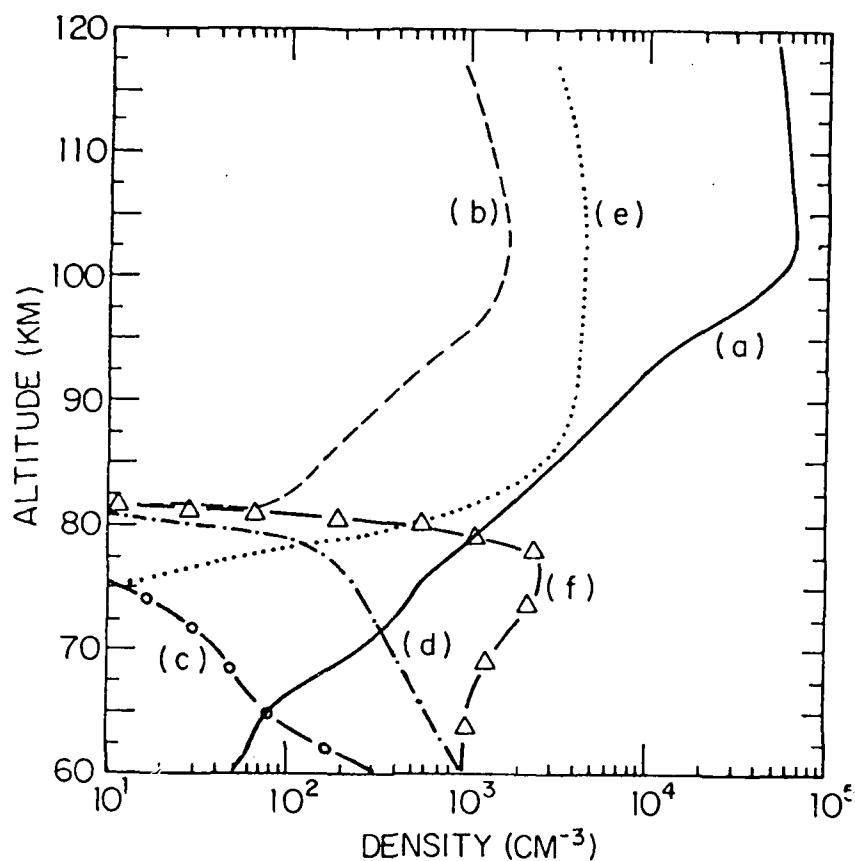


Figure 7. Calculated total electron and negative ion densities for daytime and nighttime. The positive ion densities are equal to the sum of the electron and the negative ion densities. Curves (a) and (b) are the calculated altitude profiles for electrons for day and night, respectively. The corresponding day and night profiles for the negative ions are given by curves (c) and (d). Curves (e) and (f) are the profiles for electron and negative ions calculated for nighttime including the production of ions from energetic electrons.

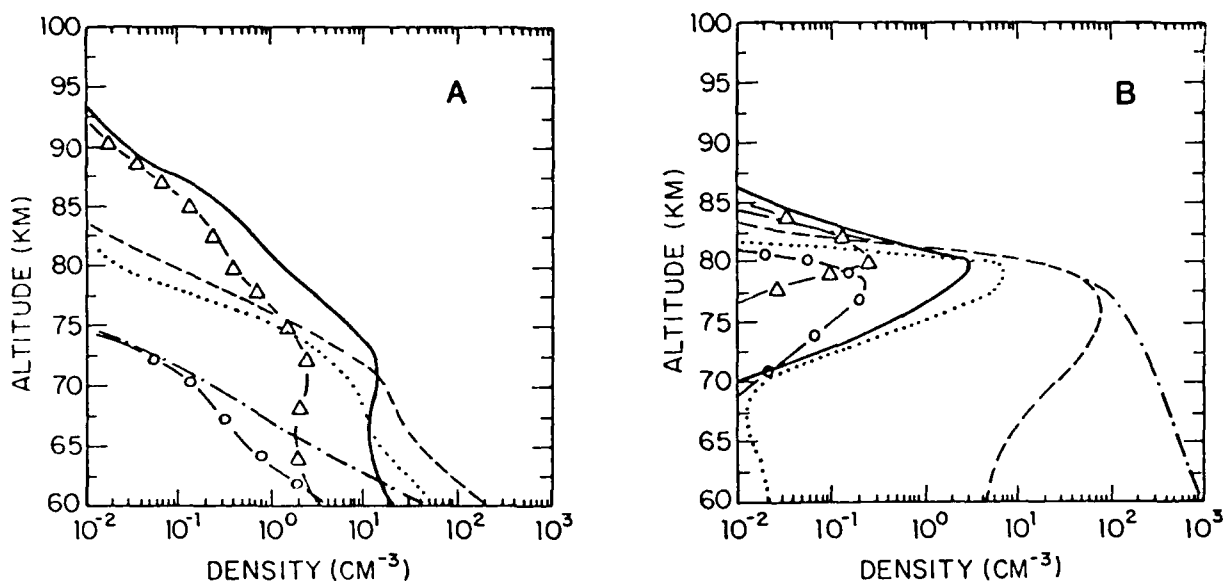


Figure 8. Calculated altitude profiles of negative ions for day (A) and night (B). The curves are O₂⁻ (—), CO₃⁻ (---), CO₄⁻ (···), NO₃⁻ (-·-·-), NO₂⁻ (-o-o-), O⁻ (-Δ-Δ-).

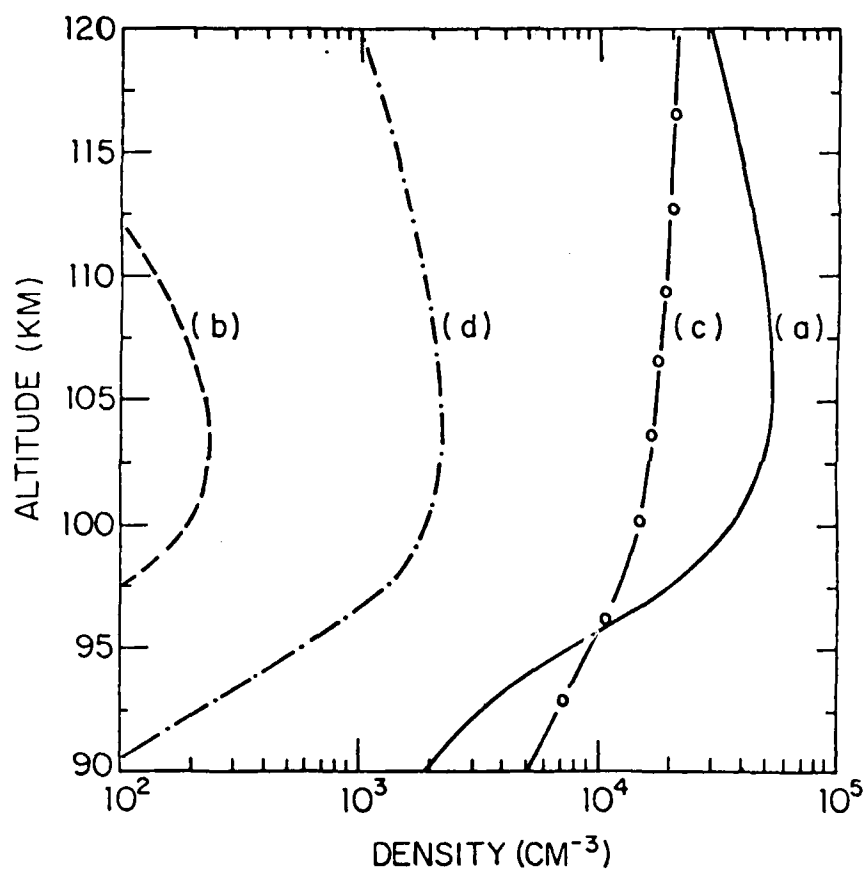


Figure 9. Calculated altitude profiles of O_2^+ ("a" for day, "b" for night) and NO^+ ("c" for day and "d" for night).

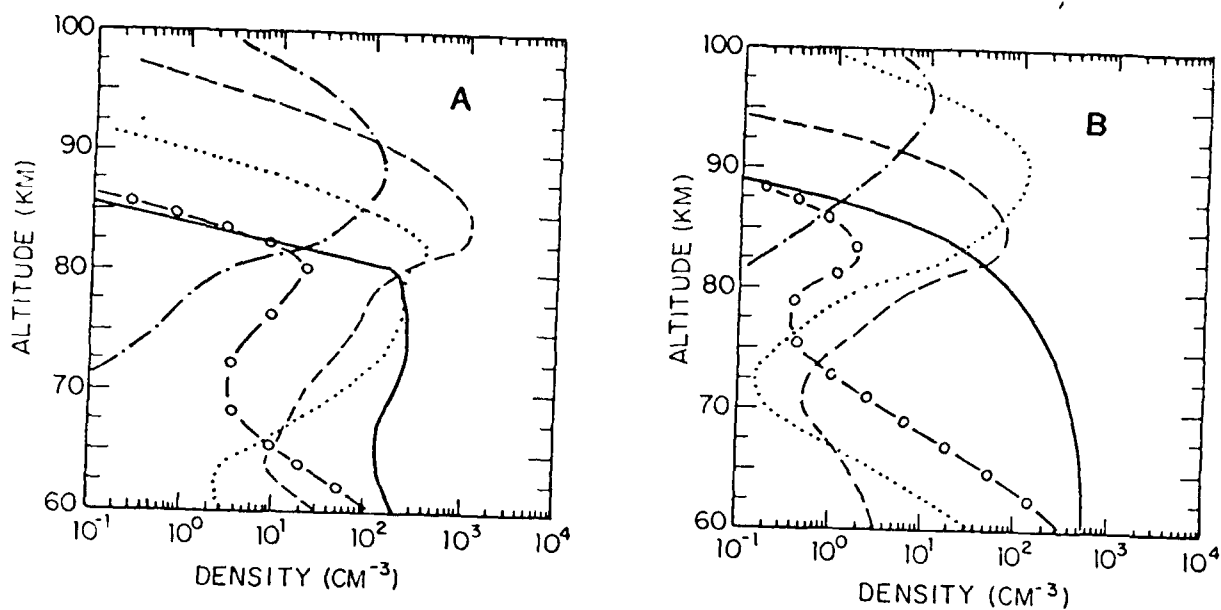


Figure 10. Calculated day (A) and night (B) altitude profiles of the dominant positive ions below 100 km. The curves are $\text{H}^+ \cdot (\text{H}_2\text{O})_4$ (—), $\text{NO}^+ \cdot (\text{H}_2\text{O})$ (---), $\text{NO}^+ \cdot (\text{H}_2\text{O})_2$ (···), $\text{NO}^+ \cdot (\text{CO}_2)$ (-·-·-), $\text{H}^+ (\text{H}_2\text{O})_3$ (-o-o-).

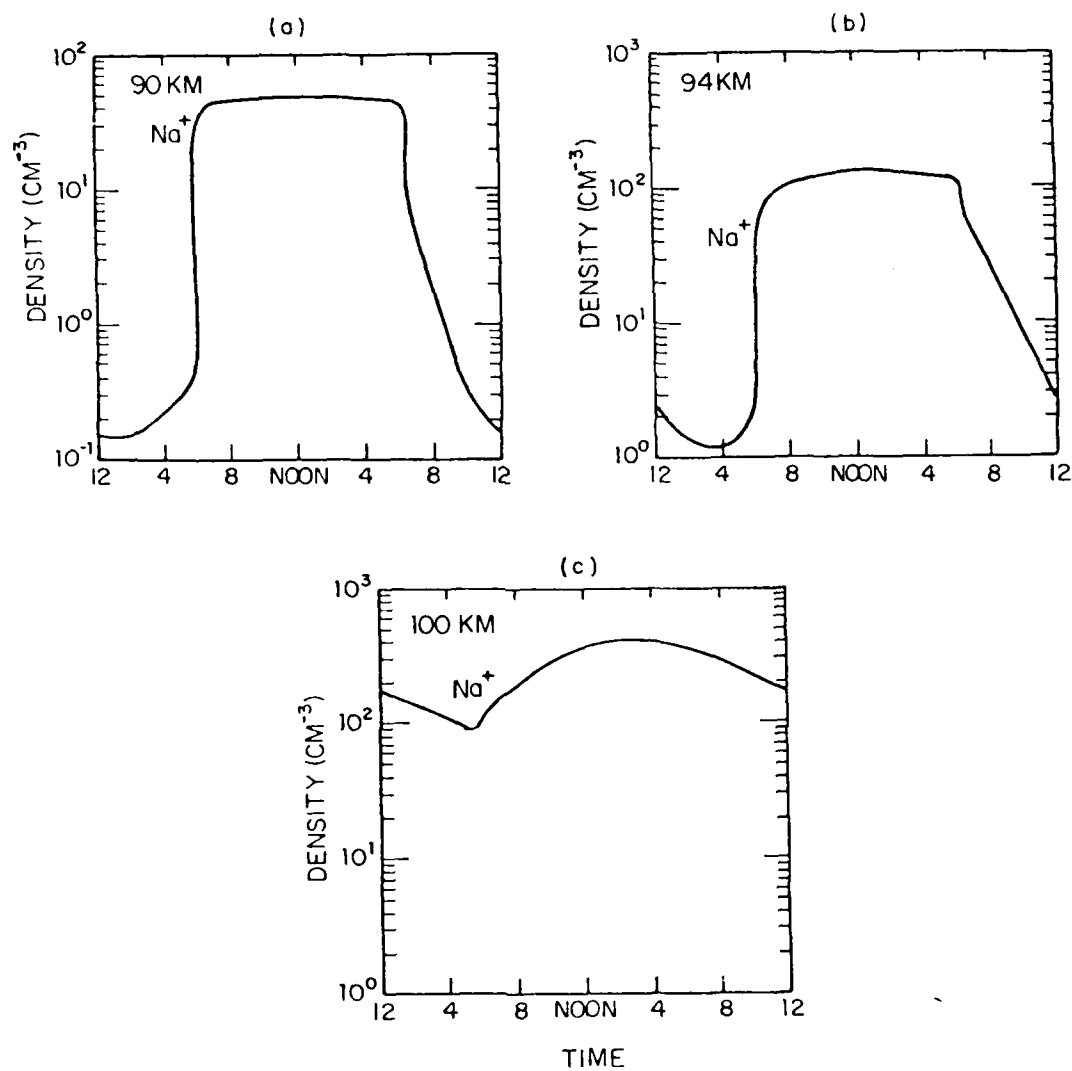


Figure 12. Calculated diurnal variation of the Na^+ density at (a) 90 km, (b) 94 km, and (c) 100 km.

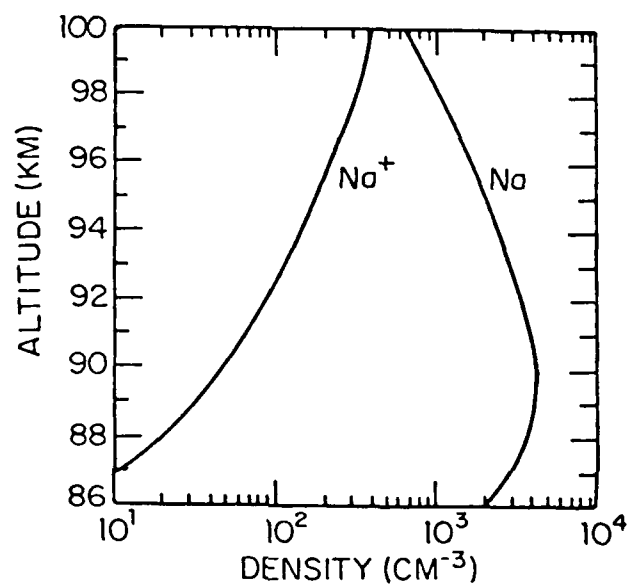


Figure 13. Calculated altitude profiles for Na and Na⁺ at noon.

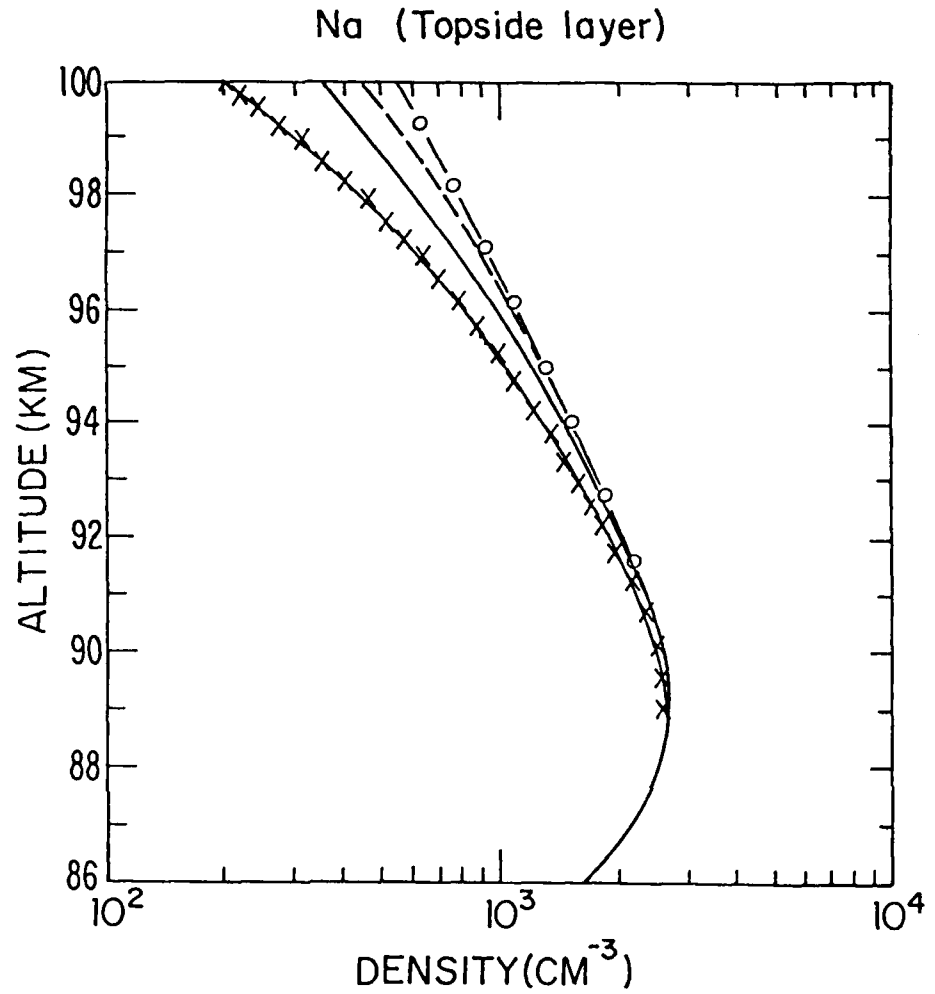


Figure 14. Calculated altitude profiles of atomic sodium using different rates for reaction (4-4). The curves correspond to values of $K^* = 2 \times 10^{-31} \text{ cm}^6 \text{ s}^{-1}$ (—), $K^* = 7 \times 10^{-31} \text{ cm}^6 \text{ s}^{-1}$ (---), $K^* = 4 \times 10^{-32} \text{ cm}^6 \text{ s}^{-2}$ (-x-), and the case where no Na^+ is present (-o-o-).

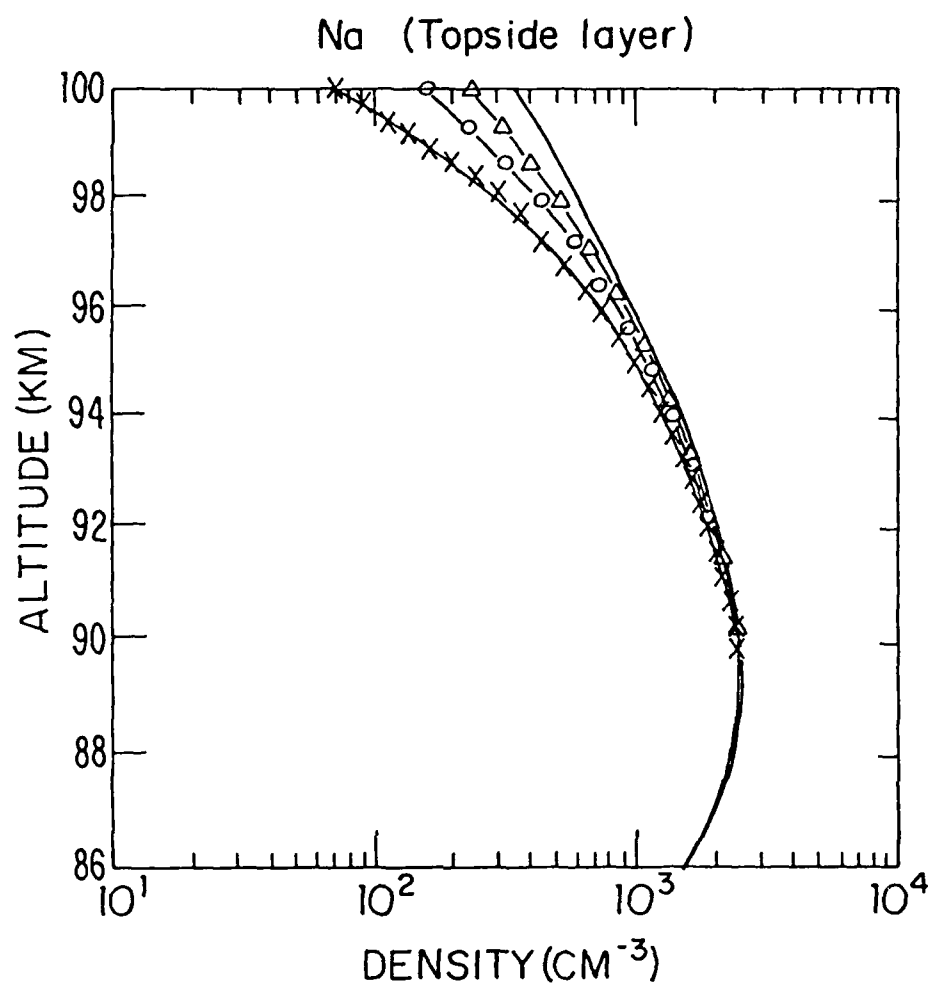


Figure 15. Calculated profiles of the Na layer, assuming vertical ion drift velocities of 0 (—), -4 (-Δ-Δ-), -10 (-o-o-), and -20 (-x-x-) cm/s.

PART IV

Seasonal Variation of the Chemistry and Transport of Sodium Species in the Mesosphere

ABSTRACT

Seasonal variations have been observed in the total column abundance of Na and the D-line emission rate. Previous studies by Garcia and Solomon (1985) have successfully explained seasonal variations of O and O₃ in terms of changes in the vertical diffusion coefficient K_{zz} induced by corresponding variations in the breaking of gravity waves in the mesosphere. We have incorporated transport effects into our model and investigated the sensitivity of our results to seasonal changes in K_{zz} and background atmospheric density and temperature. Seasonal changes in the background atmosphere induce a winter maximum in the Na column density a factor of 1.4 higher than the summer minimum in qualitative agreement with observations. Seasonal changes in K_{zz} induce a seasonal variation of factors of 3-4 in the Na column abundance and the D-line emission, peaking at the equinoxes. This result is in agreement with low-latitude D-line observations, but in disagreement with high-latitude D-line observations at all latitudes. We cannot thus reconcile the Na observations with the seasonal changes in K_{zz} within the context of the present photochemical model. The calculated diurnal variation of the Na column density is also sensitive to seasonal changes in background trace species, particularly O and H₂O.

Table of Contents

	<u>Page</u>
ABSTRACT	84
1. INTRODUCTION	85
2. TRANSPORT CALCULATION	86
2. SEASONAL VARIATIONS	91
4. CONCLUSIONS	96

1. INTRODUCTION

The calculations presented in Part I concentrated on the diurnal variation of background and sodium species in the mesosphere. As indicated in the discussion of the available sodium data (Part I, Section 2), seasonal patterns have been detected in both the Na column density and the nighttime sodium D-line emission. The observed Na column density exhibits a maximum in winter at all latitudes with the winter-summer ratio increasing with latitude (Simonich et al., 1979; Gibson and Sanford, 1971). Spectral analysis of the northern hemisphere data on D-line emission indicates a dominant semiannual component with peaks at the equinoxes at low latitudes while the high-latitude data contains a stronger annual component peaking in winter (Fukuyama, 1977).

Seasonal variability has been observed or deduced for other trace gases in the mesosphere. Most important, the O₃ concentrations deduced from the IR observations by the Solar Mesosphere Explorer (SME) exhibit a maximum during early fall in the region near 80 km (Thomas et al., 1984; Garcia and Solomon, 1986). A similar maximum is observed in the green line emission of atomic oxygen, originating near 100 km (Garcia and Solomon, 1985).

Assessment of the mechanisms proposed to explain the seasonal variability of O and O₃ may shed some light on the processes controlling sodium species. We note that modeling of the seasonal behavior of atmospheric species may require inclusion of meridional transport and thus demands utilization of a two-dimensional model. However, recent calculations by Garcia and Solomon (1985) have explained the observed midlatitude seasonal variations in O and O₃ in terms of corresponding changes in the vertical diffusion coefficient K_{zz} . These authors have introduced a parameterization of K_{zz} based on the breaking of gravity waves in the mesosphere. The seasonal variability of K_{zz} is induced by seasonal changes in the stratospheric zonal wind. Although their calculations utilize a two-dimensional model, the variability in O and O₃ is controlled primarily by vertical diffusion. These results suggest an initial analysis of the seasonal behavior of the sodium species utilizing a 1-D model and considering seasonal changes in the eddy coefficient, background atmosphere, and rates of chemical reactions.

We present in this part results of our calculations of the seasonal variation of background and sodium trace species in the mesosphere and lower thermosphere. This problem requires inclusion of a self-consistent calculation of

"slow" species (i.e., species affected by transport) in our code. The calculated seasonal behavior of the mesosphere has also implications for the diurnal variation of the Na column abundance discussed in Part I, since the diurnal behavior of sodium species is sensitive not only to the adopted chemical scheme but also to the abundance of trace gases such as O and H₂O.

The code utilized to calculate both "fast" and "slow" species is described in Section 2. Section 3 presents results of the calculated seasonal variation for background trace gases (3(a)) and sodium species (3(b)). Section 4 addresses again the diurnal variation of the sodium column density taking into account the variability of the background atmosphere. Conclusions are presented in Section 5.

2. TRANSPORT CALCULATION

Our previous calculations, presented in Part I, have fixed the concentrations of long-lived species to the values of Allen et al. (1984). The effects of eddy diffusion were incorporated in our diurnal model by means of a diffusion term consistent with the assumed profiles for slow species. Details of this procedure were given in Part I and Rodriguez et al. (1984). This approach is satisfactory for studying the diurnal behavior of short-lived species for fixed conditions. However, it precludes the ability to self-consistently calculate concentrations for arbitrary vertical eddy diffusion coefficient (K_{zz}) and solar zenith angle. The need for such calculations is particularly important in studying the effect of changes in K_{zz} on the column abundance of sodium.

We extended our one-dimensional mesospheric model to include the effects of eddy and molecular diffusion. The species calculated by the model are: odd-oxygen species, O_x -- O, O(¹D), O₃; odd-hydrogen species, HO_x -- H, OH, HO₂, H₂O₂; sodium species, NaX -- Na, NaO, NaO₂, NaOH, and H₂O, H₂, and O₂. The nitrogen species are not included in this calculation, since their effect on O_x , HO_x , and NaX is minor. The photochemical lifetimes of the odd-oxygen and hydrogen species are less than one day at altitudes below 85 km. However, these lifetimes increase rapidly above 85 km and the concentrations of O_x and HO_x are then primarily determined by transport processes. The principal sources of HO_x and O_x are photolysis of H₂O and O₂, respectively. A large fraction of the HO_x produced by H₂O photolysis above 75 km recombines to form

H₂ (Liu and Donahue, 1974). We thus have to calculate all the above species in a formulation including eddy and molecular transport.

The model solves the time-averaged continuity equation for the flux ϕ_i of the i^{th} species

$$\frac{d\langle\phi_i\rangle}{dz} = \langle P_i \rangle - \langle L_i \rangle, \quad (1)$$

where P_i and L_i represent the production and loss processes for the i^{th} species. The brackets $\langle \rangle$ denote an average over a full diurnal cycle. Equation (1) translates into an equation for the densities n_i by using the expression for the vertical flux (Hunten, 1975)

$$\langle\phi_i\rangle = -Kn \frac{d\langle f_i \rangle}{dz} - D_i \left[\frac{1}{n} \frac{d\langle n_i \rangle}{dz} + \frac{m_i g}{kT} + \frac{(1 + \alpha_i)}{T} \frac{dT}{dz} \right]. \quad (2)$$

In the above, K and D_i denote the eddy and molecular diffusion coefficients, respectively; n , the background atmospheric density; m_i , the molecular mass of species i ; and α_i , the thermal diffusion coefficient. Equations (1) and (2) can be combined into a single second-order differential equation for the species concentration n_i with unique solutions for given boundary conditions at the bottom and top altitudes (60 and 120 km).

The solution of equations (1) and (2) requires specifying the production and loss mechanisms, the boundary conditions, and the eddy and molecular diffusion coefficients. Each of these will be discussed in Sections 2(a) through 2(c). The actual computational procedure for the solution is presented in Section 2(d).

(a) Production and Loss Mechanisms

The production and loss mechanisms for the long-lived species are obtained from the chemical scheme presented in our diurnal model (Part I) and summarized in Table 1. In the lower mesosphere, HO_x is produced mainly by



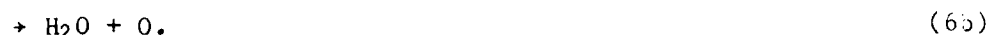
and removed by



The production of HO_x above 70 km occurs primarily through photolysis of water



An additional sink of HO_x in this region is the reaction

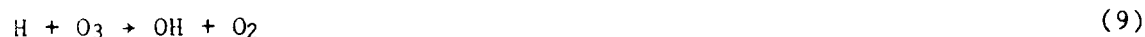


Reactions (5) and (6a) eventually convert all water into HO_x (mostly H) and H_2 . Molecular hydrogen is the dominant hydrogen-bearing species below 120 km.

Odd oxygen is produced by photolysis of O_2 :



the main sinks for O_x are the reactions



Above 90 km, three-body recombination of O becomes important:



Reactions (7) - (11) also constitute the main sinks and sources of O_2 .

We assume that the sodium species NaX are produced by meteor ablation between 80 and 100 km (Gadsden, 1968; Hunten et al., 1980). These species diffuse down to the troposphere where they are removed by washout with a time constant of 10 days (Liu and Reid, 1979). We have adopted the production profile of Hunten et al. (1980), shown in Figure 1.

(b) Boundary Conditions

Equations (1) and (2) are solved between 60 and 120 km. We adopt a fixed mixing ratio boundary condition for all species at 60 km. The mixing ratios of H_2O (7 ppmv), H_2 (0.5 ppmv), and O_2 (21%) at 60 km are adopted from

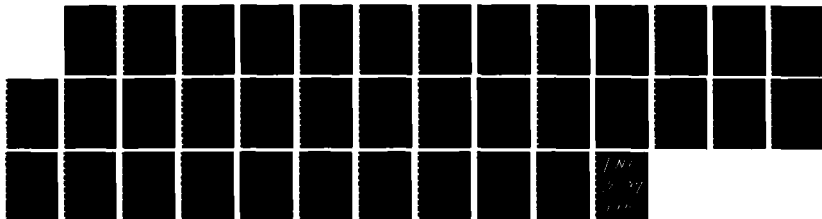
AD-A175 234

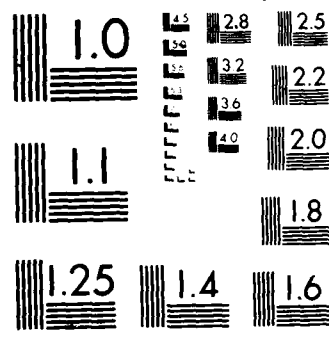
A RESEARCH PROGRAM FOR THE NEUTRAL/ION CHEMISTRY OF
METALS IN THE STRATOS. (U) ATMOSPHERIC AND
ENVIRONMENTAL RESEARCH INC CAMBRIDGE MA M K KO ET AL.
30 JUL 86 AFGL-TR-86-0169 F19628-83-C-0123 F/G 4/1

2/2

UNCLASSIFIED

NL





PHOTOCOPY RESOLUTION TEST CHART

previous stratospheric calculations. At this altitude, both O_x and HO_x have photochemical lifetimes of less than one day. The diurnal average of their mixing ratio is then independent of transport and can be obtained from our diurnal calculation.

We adopt flux boundary conditions at the upper boundary. Fluxes are assumed to be zero for all slow species except as indicated below. For the oxygen species,

$$2\phi_{O_2}(120 \text{ km}) = -\phi_{O_x}(120 \text{ km}) = \int_{120 \text{ km}}^{\infty} 2J_7 [O_2] dz, \quad (12)$$

where J_7 is the photolysis rate in reaction (7). Equation (2) neglects recombination of O above 120 km. The integral in equation (13) can be approximated by

$$\int_{120 \text{ km}}^{\infty} J_7 [O_2] dz \approx J_7(120 \text{ km}) n_{O_2}(120 \text{ km}) H_{O_2}(120 \text{ km}), \quad (13)$$

where H_{O_2} is the scale height of O_2 (approximately 6.5 km).

Atomic hydrogen escapes from Earth at a rate of $2-3 \times 10^8 \text{ cm}^{-2} \text{ s}^{-1}$ (Hunten and Donahue, 1976). We therefore have, at 120 km,

$$\phi_{HO_x} + 2\phi_{H_2O} + 2\phi_{H_2} = 2-3 \times 10^8 \text{ cm}^{-2} \text{ s}^{-1}. \quad (14a)$$

Previous models by Liu and Donahue (1974) show that most of the elemental hydrogen flux at 120 km is in the form of H_2 . We thus adopt the boundary condition

$$\phi_{HO_x}(120 \text{ km}) = \phi_{H_2O}(120 \text{ km}) = 0 \quad (14b)$$

$$\phi_{H_2}(120 \text{ km}) = 1-1.5 \times 10^8 \text{ cm}^{-2} \text{ s}^{-1}.$$

(c) Molecular and Eddy Diffusion Coefficients

Turbulent mixing in the vertical direction is parameterized by an eddy diffusion coefficient K_{zz} (Hunten, 1975). Several authors have proposed different values of K_{zz} to explain the observed altitude distribution of mesospheric species (Hunten, 1975; Allen et al., 1981; Garcia and Solomon, 1985). While values such as those of Allen et al. (1981) are adjusted to fit specific

observations, the parameterization of Garcia and Solomon (1986) relates turbulent mixing to physical processes in the mesosphere (i.e., gravity-wave breaking). We are thus particularly interested in the variations induced by the seasonally-dependent K_{zz} proposed by Garcia and Solomon (1985). Profiles for these eddy diffusion coefficients are shown in Figure 2.

The effects of molecular diffusion become important above 100 km. Molecular diffusion coefficients are given by (Banks and Kockarts, 1973)

$$D_i = \frac{b_i}{n} \quad (15a)$$

where

$$b_i = A_i T^{s_i}, \quad (15b)$$

and n and T are the background atmospheric density and temperature. Table 2 presents our adopted values for the parameters A_i and s_i for each species. Adopted values for the thermal diffusion coefficient α_i are -0.27, -0.39, and -0.31 for O_x , HO_x , and H_2 , and zero otherwise (Allen et al., 1981).

Total densities and temperature of the background atmosphere exhibit considerable seasonal variability between 80 and 100 km (see, i.e., Cole and Kantor, 1978). We have adopted the seasonally-dependent model atmosphere of Cole and Kantor (1978) ($z < 90$ km) and CIRA, 1972) ($z > 90$ km) in the calculations described below, unless otherwise specified. The seasonally-dependent background temperature and density adopted in our calculations are shown in Figures 3 and 4.

(d) Computational Procedures

The basic structure of the coupled diurnal-diffusion code is illustrated by the flow chart in Figure 5. An initial guess for the altitude profile of slow species is given as input. Our previous diurnal code is then used to solve for the diurnal variation of fast species consistent with the fixed slow species density at each altitude. The calculated diurnal species are then used to calculate the time-averaged $\langle P_i \rangle$ and $\langle L_i \rangle$ for equations (1) and (2). Solutions of these equations give us a new estimate for the slow species which is used again as input to the diurnal code. The process is iterated until the difference in the densities calculated in two successive iterations is less than some specified value.

With the assumed values for K_{zz} and D_1 , resident times due to eddy and molecular diffusion are of the order of days, except at night between 80 and 85 km (Allen et al., 1984). In this region, the effect of transport is introduced by means of a constant term P^* in the diurnal continuity equation (Part I and Rodriguez et al., 1984).

3. SEASONAL VARIATIONS

The coupled diurnal transport model described in the previous section was used to calculate seasonally-dependent densities of the background trace gases and sodium species. Calculations were performed for spring, summer, fall, and winter conditions at 45° latitude using the respective K_{zz} profiles and background atmospheres. Results are presented for fall and winter to illustrate the effect of maximum and minimum values of K_{zz} .

Our results for background trace species are presented in Section 3(a). Section 3(b) discusses our calculations for the seasonal variation of the sodium column abundance and D-line emission.

(a) Background Trace Species

Results of our calculations for H_2O , O (noon), and H (noon) are presented in Figures 4 through 6 for fall and winter conditions. These fall and winter trace species were calculated by allowing for changes in the photolysis rates, background atmosphere (n, T), and eddy diffusion coefficients. We also include for comparison the values used in the calculations described in Parts I and III, corresponding to the profiles calculated by Allen et al. (1984) which used an adjusted K_{zz} to simulate the observed concentrations.

Water is photodissociated primarily by Lyman-alpha radiation above 75 km. The abundance of water in the upper mesosphere is then determined by the efficiency of the vertical transport from the lower atmosphere. The eddy diffusion coefficients derived by Garcia and Solomon (1985) are considerably lower in fall than in winter. As a result, water is transported less efficiently to the upper mesosphere in the fall, leading to considerably lower H_2O abundances. This seasonal behavior is illustrated in Figure 6.

The H densities shown in Figure 7 also exhibit lower values in the fall, particularly above 85 km. In this region, most of the HO_x species are in the form of atomic hydrogen. Since the source of HO_x is photolysis of H_2O , the

the lower water concentration in the fall leads to lower HO_x densities. Higher photolysis rates for H_2O in fall tend to partially compensate for the lower H_2O concentration resulting in HO_x density differences of less than 50 percent. The variation below 85 km reflects the effect of changes in solar zenith angle resulting in larger production rate and higher concentration of hydrogen in the fall.

Figure 8 shows calculated O densities which exhibit larger values in fall than in winter above 85 km. This behavior is a consequence of: 1) the lower concentrations of HO_x species which constitute a sink of O_x through the reactions of OH and H with O_3 , and 2) the slower transport of atomic oxygen, produced by photolysis of O_2 above 90 km, out of this region. Calculated densities of O_3 at midnight are shown in Figure 9 for fall and winter. The O_3 profile exhibits the minimum near 80 km typical of both observations and calculations (see Allen et al., 1984). The seasonal changes in O, H, and O_3 illustrated in Figures 5 through 9 are consistent with the midlatitude 2-D results of Garcia and Solomon (1985).

(b) Seasonal Variation of Sodium Abundance and D-line Emission

Observations of the mesospheric sodium layer have established the existence of a maximum in the Na column density during winter. This maximum is a factor of two larger than the summer minimum at low latitudes (Simonich et al., 1979) and up to three to four times larger at high latitudes (Gibson and Sandford, 1971). Three different processes could contribute to the observed seasonal variation of the sodium column density: changes in the vertical transport, changes in photochemical control (Swider, 1985), and changes in downward fluxes of Na^+ from above 95 km. The relative contributions of each of the above to the seasonal variation have been assessed with our one-dimensional model.

We can best understand the direct effect of vertical transport by considering the behavior of a species with a source restricted to the upper atmosphere ($z > z_1$) and a sink restricted to the lower atmosphere ($z < z_2$) with $z_1 > z_2$. The mixing ratio f at an altitude $z > z_2$ is then given by

$$f(z) = f_0 + \int_{z_2}^z \frac{\phi(z')}{K_{zz}(z')n(z')} dz', \quad (16)$$

where f_0 is the mixing ratio at z_2 , $K_{zz}(z)$ is the vertical eddy diffusion

coefficient, n is the background atmospheric density, and $\phi(z)$ is the downward flux ($\text{cm}^{-2} \text{s}^{-1}$) equal to the integrated production $\int_z^\infty P dz$ in the upper atmosphere. Equation (16) can be applied to the family of sodium species $\text{NaX} = \text{Na} + \text{NaO} + \text{NaO}_2 + \text{NaOH}$, which is produced by meteor ablation between 80 and 100 km (Gadsden, 1968; Hunten, 1981) and lost in the stratosphere or troposphere by attachment to aerosol particles, polymer formation, or washout (Hunten, 1981; Lamb and Benson, 1986; Liu and Reid, 1979). We can also disregard f_0 in (16) for $z_2 < 30$ km when compared to the integral term for altitudes below the Na peak at 90 km. We can then see that the abundance of NaX (and thus of Na) in the sodium layer (80 to 100 km) will be inversely proportional to the adopted eddy diffusion coefficient. The largest contributions to the integral in (16) come from altitudes near the region of meteor ablation, thus it is most sensitive to K_{zz} between 80 and 100 km. Consideration of the eddy diffusion coefficients in Figure 2 in conjunction with (16) suggests that the mixing ratio of NaX should have maxima at equinoxes with minima at the solstices.

Another important seasonal effect has been pointed out by Swider (1985). The density of Na in the bottomside layer is controlled by the rapid formation of NaO_2 through



The seasonal dependence of the temperature and background density below 90 km combine to minimize the loss of Na through (17) in the winter, thus maximizing the sodium density in this season. We have investigated the above effect by incorporating the seasonally-dependent background atmosphere of Cole and Kantor (1978) into our one-dimensional model.

The column density of Na could also be sensitive to changes in the topside scale height due to seasonal variations of Na^+ . Hanson and Donaldson (1967) suggested a mechanism to explain the small topside scale height, by which upward diffusion of neutral Na should be roughly balanced by the downward ion drift flux $W[\text{Na}^+]$, where W is the ion drift velocity. We can then expect that changes in either W or $[\text{Na}^+]$ will change the upward flux of Na, and thus the topside scale height and total column density. Details of this effect were discussed in Part III. We have assumed a constant vertical

drift velocity of -20 cm/s as in Part III and investigated the sensitivity of our results to different diurnally-averaged Na^+ resulting from changing length of day.

The sensitivity of the calculated Na column abundance to each of the above parameters is illustrated by the results in Table 3. The one-dimensional model was run for conditions typical of 45°N spring, summer, fall, and winter. In the first set of runs (Case 1), the eddy diffusion coefficient was held constant at the summer values in Figure 2, while the temperature and background density were varied according to Cole and Kantor (1978) and CIRA (1972). The second set of runs (Case 2) held the background atmosphere constant while varying K_{zz} according to Figure 2. The third set (Case 3) changed both the eddy diffusion coefficient and the background atmosphere. For each set, we also investigated the effect of excluding and including the vertical ion drift.

The results in Table 3 indicate that a fall-winter maximum is obtained if we vary the background atmosphere (Case 1). The winter-summer contrast (~ 1.4) is, however, closer to the low-latitude value of ~ 2.0 of Simonich et al., 1979 (23° S) than to the high latitude value of 3 to 4 observed by Gibson and Sanford (1971) at 51° N. We can expect the seasonal effect in Case 1 to increase with latitude, in response to a larger seasonal variation of the background atmosphere, and larger contrast in the length of day between summer and winter.

The results in Cases 2 and 3 indicate that the response to seasonal variations of K_{zz} is much larger than the corresponding response to variations in the background atmosphere. The column density of Na changes by about a factor of 3 between minimum and maximum. We note, however, that the results exhibit two maxima at the equinoxes, whereas observations indicate a single maximum during winter.

Our results indicate that the observed winter maximum in Na column density can be obtained from changes in the background temperature and density (Swider, 1985). Although inclusion of ions changes the absolute magnitude of the column density, it does not seem to affect the seasonal contrast. The magnitude of the variation is, however, smaller than observed. The proposed behavior of K_{zz} by Garcia and Solomon (1985) thus seems inconsistent with the observed seasonal variation of Na, at least within the context of a 1-D model. Further work is needed to reconcile the O_3 , O , and Na behavior.

In contrast to the lidar measurements, the Na D-line emission observations do not give direct measurement of the column abundance. The D-line emission is given by:

$$I_o(R) = \int k_2 [NaO][O] \approx \int k_1 [Na][O_3], \quad (18)$$

where k_1 and k_2 are the reaction rate constants for the reactions $Na + O_3 \rightarrow NaO + O$ and $NaO + O \rightarrow Na + O_2$, respectively (Swider, 1986). It should be noted that the magnitude of the intensity of the sodium D line depends on the convolution of the sodium and ozone altitude profiles. Since O_3 decreases rapidly with height above 80-85 km, the D-line emission is most sensitive to the Na concentration in the bottomside layer.

The seasonal behavior of the observed intensity of the sodium night-glow is shown in Fig. 10. Emission rates in this figure are normalized to 50 R. This emission exhibits maxima at the equinoxes and minima at the solstices (Kirchoff et al., 1981) at a latitude of 23°S. For high-latitudes, however, the D-line nightglow exhibits a maximum in winter, with lesser peaks at the equinoxes (Fukuyama, 1977). This behavior of the sodium D line cannot be explained solely by seasonal changes in the J rates as these changes would tend to produce a maximum in summer. However, the low-latitude behavior is consistent with the expected response of Na to the effect of eddy transport where the larger values of K_{zz} during solstices provides more efficient removal of Na by transport into the stratosphere.

Our calculated emission rates for each season are also shown in Figure 10. The absolute magnitude of the emission rate is proportional to the total NaX production and the branching for Na(2P) production by (18); since these quantities are uncertain, we concentrate on the seasonal changes rather than the absolute magnitude (histogram). The seasonal behavior shown in Fig. 10 is in good agreement with observation at 23°S. The calculated absolute magnitude of the seasonal change is larger than observed. Our calculations do not reproduce, however, the winter peak observed at high latitudes (Fukuyama, 1977).

We note that our calculated equinox maximum in the D-line emission is a result of maxima in both NaX and O_3 . A smaller equinox maximum would still be obtained if we only included the O_3 density behavior, as pointed out by Swider

(1986). This can explain the D-line observations at low latitudes. On the other hand, the winter maximum at high latitudes is probably related directly to the maximum in the Na abundance.

4. CONCLUSIONS

The results presented above have utilized a 1-D model and relied on a particular parameterization of K_{zz} to obtain most seasonal effects. Two-dimensional effects, however, could be important. The values of K_{zz} deduced by Garcia and Solomon (1985) assume a particular spectrum for breaking gravity waves, for which there is little observational data at present. The above uncertainties in our calculation imply that we should concentrate on qualitative rather than quantitative features of the seasonal variation of different species in the evaluation of the model results.

Our model calculates seasonal profiles for O_x , HO_x , and H_2O , which are consistent with the results of Garcia and Solomon (1985) and with available observational data. The seasonal parameterization of K_{zz} accounts for the first-order features of the seasonal behavior of O_x , HO_x , and H_2O in the mesosphere.

The K_{zz} parameterization is less successful in describing the observed seasonal behavior of the Na column abundance. Although a large seasonal variation is obtained, the calculated maxima occur at the equinoxes, while observations indicate a peak in winter. The seasonal behavior of Na is better explained by the variations in background temperature and density (Swider, 1985) if we disregard changes in K_{zz} . The inconsistency between the model required to explain the seasonal behavior of O_x and that for Na is not resolved at present. Further work on this issue would provide important insights on mesospheric processes.

Similar conclusions hold for the results on the Na D-line emission. The agreement between our calculations and the low-latitude observations of Kirchoff et al. (1981) may be misleading. The same qualitative agreement could be obtained by involving seasonal changes in O_3 . Swider (1986) indicated that most of the D-line emission is emitted within 2 to 3 km below the Na peak at 90 km, where the seasonal variation of Na is expected to be small, particularly at low latitudes. The behavior of the D-line emission thus decouples from that of the Na abundance. At the same time, the high-

latitude seasonal variability exhibits a winter maximum (Fukuyama, 1977). This may be due to a stronger seasonal variation of Na near the peak at these latitudes, in which case the behavior of the D-line emission and the Na abundance are coupled.

An extensive data base exists for Na density and emission rates. Since these observations are ground-based, they can be carried out over extensive periods of time at a wide range of locations.. The sodium observations could thus provide an important complement to the species most often utilized at present in validating mesospheric models (i.e., O_3 , O , OH). The question raised in this section then points toward important areas of future research.

The sensitivity of the seasonal variation of Na to changes in K_{zz} is larger than that of O_3 and O . It is thus puzzling that the present transport parameterization does not yield the observed sodium seasonal behavior. A more realistic study requires utilization of a 2-D model for the mesosphere. Although beyond the scope of the present research, such study can provide additional light on mesospheric transport mechanisms of importance not only for sodium species but also for H_2O , O_x , and HO_x . The parameterization of K_{zz} should be examined more closely to determine possible modifications which could explain all the available observations. Finally, chemical mechanisms for Na species not included in this study should also be considered (see, for example, Hunten, 1981).

Expansion of reanalysis of the Na data base could also shed light on the issues raised above. The chemical mechanism proposed by Swider (1985) implies little seasonal variation of Na near the peak, whereas changes in K_{zz} would induce changes in Na at all altitudes. Further examination of data for possible detection of seasonal changes in Na peak altitude and magnitude is necessary. Data on the diurnal variation of the Na column abundance should also be analyzed for possible seasonal trends. The extent of the correlation between Na D-line emission and Na column density at different altitudes should also be determined.

Table 1
Production and Loss Mechanisms for Diffusive Species

Species	Production	Loss
HO_x	$\text{H}_2\text{O} + \text{O}(^1\text{D}) \rightarrow 2\text{OH}$	$\text{H} + \text{HO}_2 \rightarrow \text{H}_2 + \text{O}_2$
	$\text{H}_2\text{O} + h\nu \rightarrow \text{H} + \text{OH}$	$\text{H} + \text{HO}_2 \rightarrow \text{H}_2\text{O} + \text{O}$
	$\text{OH} + \text{HO}_2 \rightarrow \text{H}_2\text{O} + \text{O}_2$	
	$\text{OH} + \text{OH} \rightarrow \text{H}_2\text{O} + \text{O}$	
O_x	$\text{O}_2 + h\nu \rightarrow \text{O} + \text{O}$	$\text{O} + \text{OH} \rightarrow \text{O}_2 + \text{H}$
	$\text{H} + \text{O}_3 \rightarrow \text{OH} + \text{O}_2$	
	$\text{O} + \text{HO}_2 \rightarrow \text{OH} + \text{O}_2$	
	$\text{O} + \text{O} + \text{M} \rightarrow \text{O}_2 + \text{M}$	
H_2O	$\text{OH} + \text{HO}_2 \rightarrow \text{H}_2\text{O} + \text{O}_2$	$\text{H}_2\text{O} + \text{O}(^1\text{D}) \rightarrow 2\text{OH}$
	$\text{OH} + \text{OH} \rightarrow \text{H}_2\text{O} + \text{O}$	$\text{H}_2\text{O} + h\nu \rightarrow \text{H} + \text{OH}$
H_2	$\text{H} + \text{HO}_2 \rightarrow \text{H}_2 + \text{O}_2$	
O_2	$\text{O} + \text{OH} \rightarrow \text{O}_2 + \text{H}$	$\text{O}_2 + h\nu \rightarrow 2\text{O}$
	$\text{H} + \text{O}_3 \rightarrow \text{OH} + \text{O}_2$	
	$\text{O} + \text{HO}_2 \rightarrow \text{OH} + \text{O}_2$	
	$\text{O} + \text{O} + \text{M} \rightarrow \text{O}_2 + \text{M}$	
NaX	Meteor ablation	Washout in troposphere

Table 2
Molecular Diffusion Coefficients

$$D = \frac{b}{n} = \frac{AT^s}{n} \text{ cm}^2 \text{ s}^{-1}$$

	A	s	Reference
H ₂	2.6 x 10 ¹⁷	0.750	Mason and Marrero (1970)
HO _x (H)	4.8 x 10 ¹⁷	0.7	Banks and Kockarts (1973)
H ₂ O	1.37 x 10 ¹⁶	1.07	Mason and Marrero (1970)
O ₂	6.84 x 10 ¹⁶	0.77	Estimated ^a
O _x (O)	9.68 x 10 ¹⁶	0.77	Mason and Marrero (1970)

^aEstimated from the O diffusion coefficient assuming an inverse dependence on the square root of the molecular mass (Mason and Marrero, 1970).

Table 3
Calculated Column Densities (cm^{-2}) of Na at 45°N

	No Na^+	With Na^+ ($W = -20 \text{ cm/s}$)
Case 1: Constant K_{zz} , seasonal T, n		
Spring	3.7×10^9	2.8×10^9
Summer	3.1×10^9	2.3×10^9
Fall	4.3×10^9	3.3×10^9
Winter	4.0×10^9	3.2×10^9
Case 2: Seasonal K_{zz} , constant T, n		
Spring	10.7×10^9	8.1×10^9
Summer	3.9×10^9	3.0×10^9
Fall	9.8×10^9	7.4×10^9
Winter	2.7×10^9	2.1×10^9
Case 3: Seasonal K_{zz} , T, n		
Spring	10.3×10^9	7.6×10^9
Summer	3.1×10^9	2.3×10^9
Fall	11.8×10^9	8.9×10^9
Winter	3.5×10^9	2.8×10^9

References

- Allen, M., J. I. Lunine, Y. L. Yung (1984) The vertical distribution of ozone in the mesosphere and lower thermosphere. J. Geophys. Res., 89, 4841.
- Allen, Mark, Y.L. Yung, and J.W. Waters (1981) Vertical transport and photochemistry in the terrestrial mesosphere and lower thermosphere (50-120 km). J. Geophys. Res., 86, 3617.
- Banks, P. M., and G. Kockarts (1973) Aeronomy, Vol. B. Academic Press, New York and London (pp. 38-43).
- Clemesha, B. R., D. M. Simonich, P. O. Batista, and V. W. J. H. Kirchoff (1982) The diurnal variation of atmospheric sodium. J. Geophys. Res., 87, 181.
- Cole, A. E., and A. J. Kanton (1978) Air Force Reference Atmospheres. AFGL-TR-78-0051, Air Force Geophysics Laboratory, Hanscom AFB, MA, ADA058505.
- Fukayama, K. (1977) Airglow variations and dynamics in the lower thermosphere and upper mesosphere, II, Seasonal and long-term variations. J. Atmos. Terr. Phys., 39, 1.
- Gadsden, M. (1968) Sodium in the upper atmosphere: Meteoritic origin. J. Atmos. Terr. Phys., 30, 151.
- Garcia, R. R., and S. Solomon (1985) The effect of breaking gravity waves on the dynamics and chemical composition of the mesosphere and lower thermosphere. J. Geophys. Res., 90, 3850.
- Gibson, A. J., and M. C. W. Sandford (1971) The seasonal variation of the night-time sodium layer. J. Atmos. Terr. Phys., 33, 1675.
- Gibson, A. J., and M. C. W. Sandford (1972) Daytime laser radar measurements of the atmospheric sodium layer. Nature., 239, 509.
- Hanson, W. B., and J. S. Donaldson (1967) Sodium distribution in the upper atmosphere. J. Geophys. Res., 72, 5513.
- Hunten, D. M. (1975) Vertical transports in atmospheres. In Atmospheres of Earth and Planets. B. M. McCormac (ed.), Dordrecht, Holland, pp. 59-72.
- Hunten, D. M. (1981) A meteor-ablation model of the sodium and potassium layers. Geophys. Res. Lett., 8, 369.
- Hunten, D. M., and T. M. Donahue (1976) Hydrogen loss from the terrestrial planets. Annu. Rev. Earth Planet. Sci., 4, 256.
- Hunten, D. M., R. P. Turco, O. B. Toon (1980) Smoke and dust particles of meteoritic origin in the meso- and stratosphere. J. Atmos. Sci., 37, 1342.
- Kirchoff, V. W. J. H., B. R. Clemesha, and D. M. Simonich (1981) Average nocturnal and seasonal variations of sodium nightglow at 23°S, 46°W. Planet. Space Sci., 29, 765.

- Lamb, J. J., and S. W. Benson (1986) Some kinetic and thermochemical aspects of sodium in the stratosphere. J. Geophys. Res. (in press).
- Liu, S. C., and T. M. Donahue (1974) Realistic model of hydrogen constituents in the lower atmosphere and escape flux from the upper atmosphere. J. Atmos. Sci., 31, 2238
- Liu, S. C., and G. C. Reid (1979) Sodium and other minor constituents of meteoric origin in the atmosphere. Geophys. Res. Lett., 6, 283.
- Mason, E. A., and T. R. Marrero (1970) The diffusion of atoms and molecules. At. Mol. Phys., 6, 155.
- Rodriguez, J. M., M. K. W. Ko, and N. D. Sze (1984) The diurnal variation of the neutral sodium species in the upper atmosphere: A model study. Report #AFGL-TR-84-0204, Air Force Geophysics Lab., Bedford, MA, ADA154988.
- Simonich, D. M., B. R. Clemesha, and V. W. J. H. Kirchoff (1979) The Mesospheric Sodium Layer at 23°S: Nocturnal and Seasonal Variations. J. Geophys. Res. 84, 1543.
- Swider, W. (1986) Sodium nightglow: Chemically independent of sodium content. J. Geophys. Res., 91, 6742.
- Swider, W. (1985) Enhanced seasonal variations for chemical rates with inverse temperature dependencies: Application to seasonal abundance of mesospheric sodium. Geophys. Res. Lett., 12, 589-591.
- Thomas, R. J., C. A. Barth, and S. Solomon (1984a) Seasonal variations of ozone in the upper mesosphere and gravity waves. Geophys. Res. Lett., 11, 673.

Figure Captions

- Figure 1. Adopted production of Na atoms by meteor ablation. The shape of the profile is taken from Hunten et al. (1980) and scaled to yield an NaX density of $3 \times 10^3 \text{ cm}^{-3}$ at 90 km for the summer K_{zz} in Figure 2.
- Figure 2. Vertical eddy diffusion coefficient K_{zz} adopted in our calculations for spring (---), summer (—), fall (---), and winter (···) conditions. These profiles are taken from Garcia and Solomon's (1985) parameterization of mixing induced by gravity-wave breaking at 45° latitude. The profile deduced by Allen et al. (1981) is also shown for comparison.
- Figure 3. Background neutral densities adopted in our calculations for spring (---), summer (—), fall (···), and winter (---) conditions below 90 km from Cole and Kantor (1978).
- Figure 4. Same as Figure 3 but for the background temperature.
- Figure 5. Flow chart for coupled diurnal-diffusion program. The box marked with an asterisk (*) corresponds to our previous diurnal code. The term P_i^* represents the effects of transport in the diurnal calculation, as explained in Rodriguez et al. (1984).
- Figure 6. Mixing ratio of H_2O for different seasonal conditions used in calculations. The seasonally-dependent eddy diffusion coefficients of Garcia and Solomon (1985) have been used to calculate the H_2O mixing ratio for fall (—) and winter (---) conditions. The profile calculated by Allen et al. (1984) (-o-), used in our Part I calculations, is also shown for comparison.
- Figure 7. Same as Figure 4 but for the density of H at noon.
- Figure 8. Same as Figure 4 but for the density of O at noon.
- Figure 9. Density of O_3 at midnight, calculated for fall (—) and winter (---) conditions using the K_{zz} parameterization of Garcia and Solomon (1985).
- Figure 10. Calculated seasonal variation of the sodium D line nightglow at 45°N (histogram) compared to the observed seasonal variation at 23°S (—) (Kirchoff et al., 1981) and 41°N (---) (Fukuyama, 1977). Calculated and observed emissions have been normalized to 50R. The northern hemisphere data of Fukuyama (1977) (---) has been shifted by six months for comparison with the southern seasons.

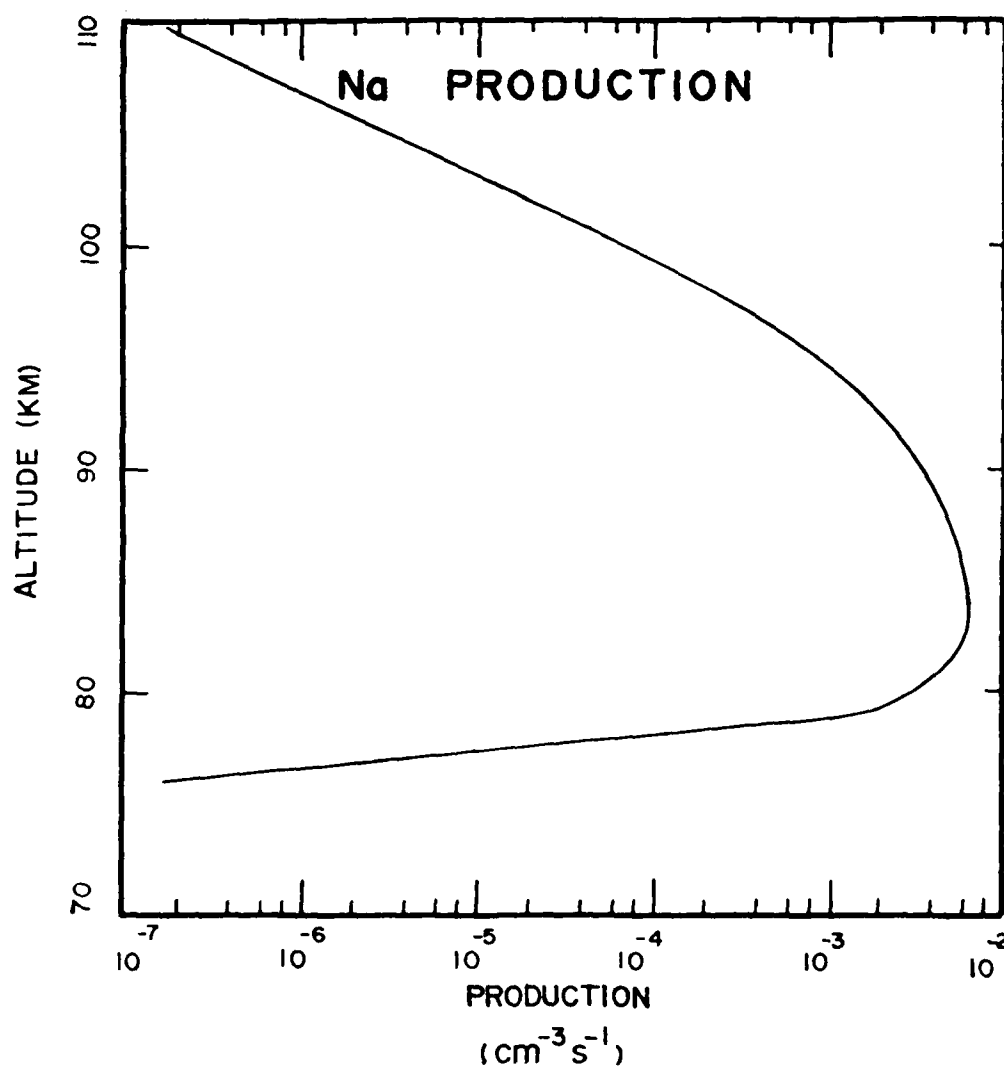


Figure 1. Adopted production of Na atoms by meteor ablation. The shape of the profile is taken from Hunten et al. (1980) and scaled to yield an NaX density of $3 \times 10^3 \text{ cm}^{-3}$ at 90 km for the summer K_{zz} in Figure 2.

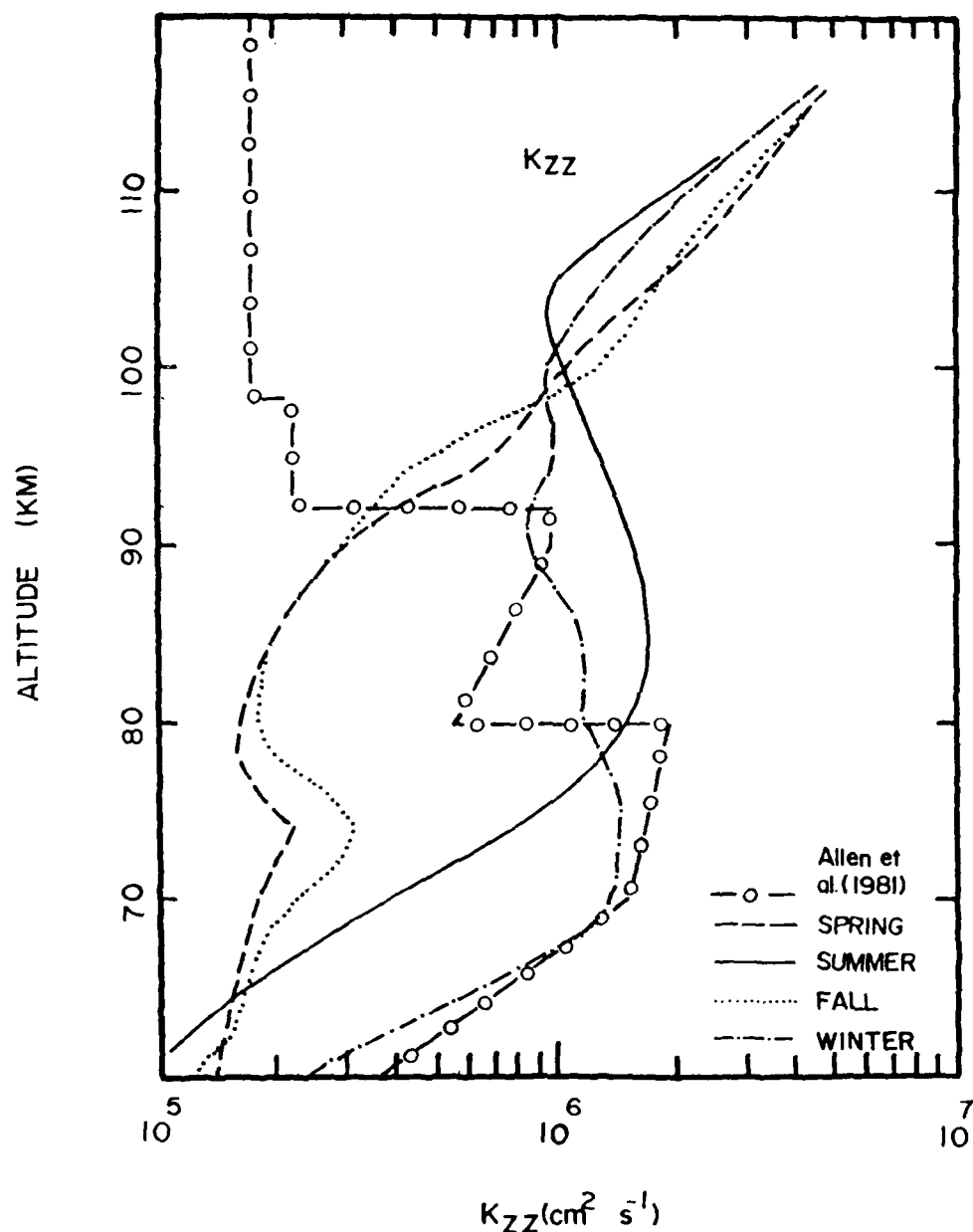


Figure 2. Vertical eddy diffusion coefficient K_{zz} adopted in our calculations for spring (---), summer (—), fall (···), and winter (-·-) conditions. These profiles are taken from Garcia and Solomon's (1985) parameterization of mixing induced by gravity-wave breaking at 45° latitude. The profile deduced by Allen et al. (1981) is also shown for comparison.

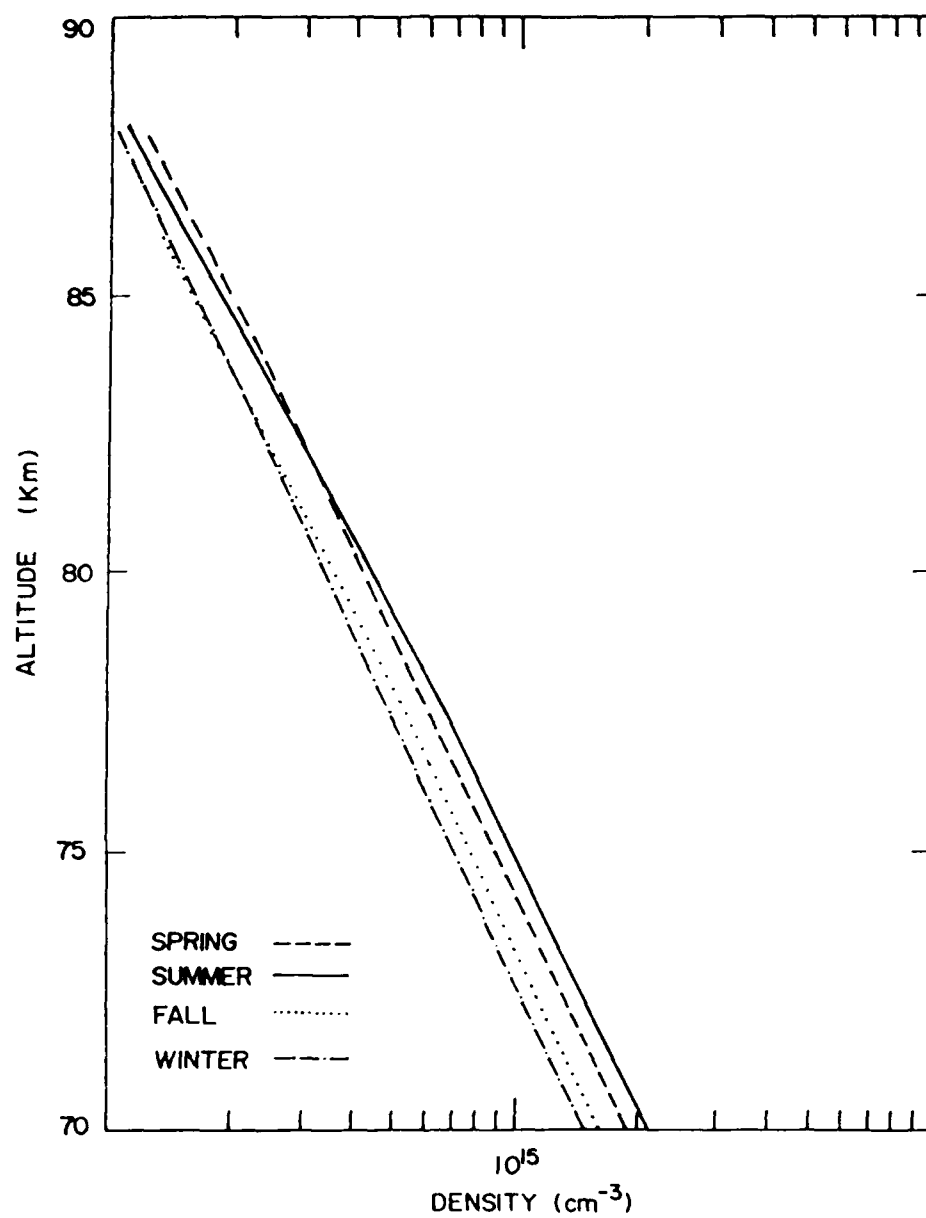


Figure 3. Background neutral densities adopted in our calculations for spring (---), summer (—), fall (···), and winter (-·-) conditions below 90 km from Cole and Kantor (1978).

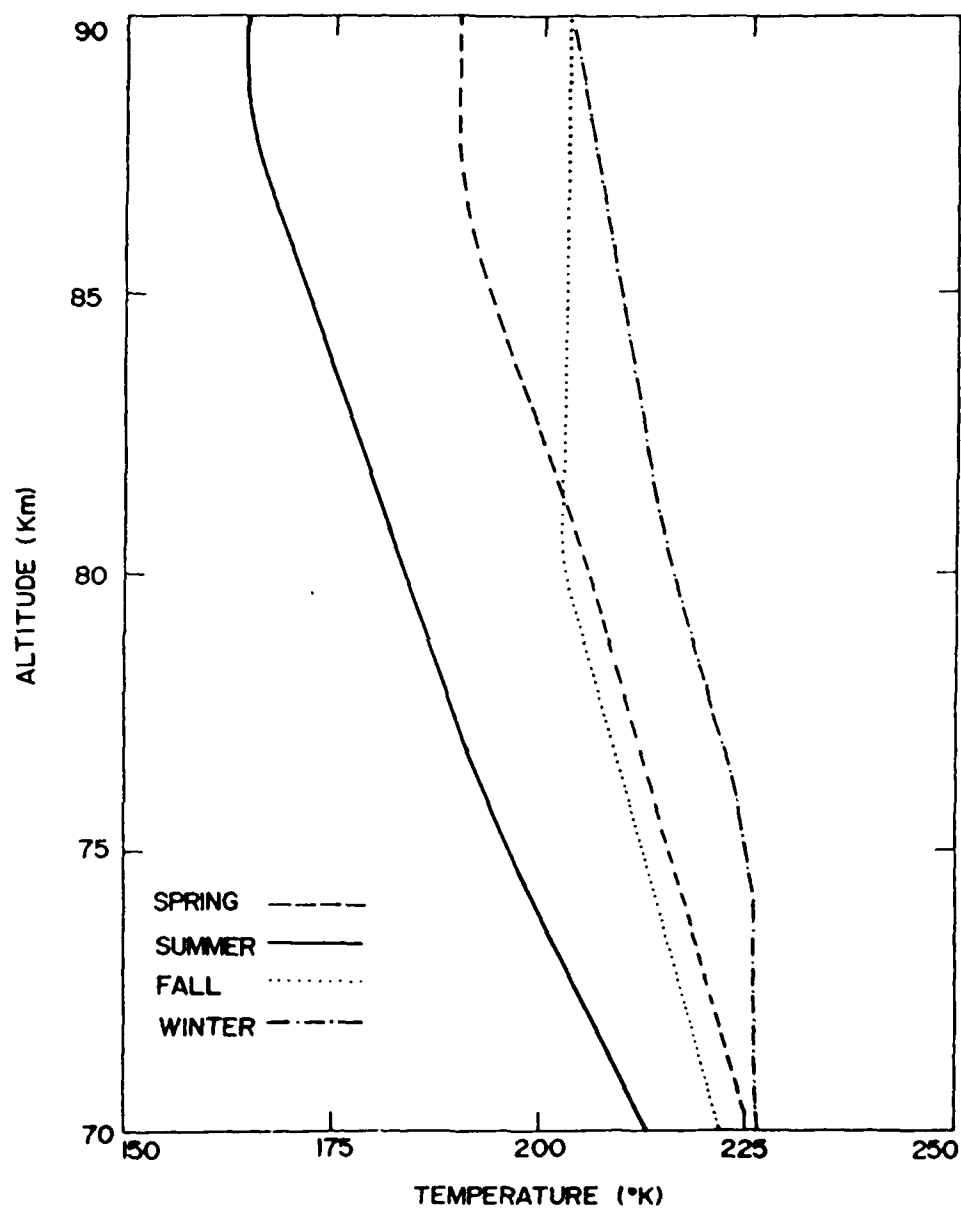


Figure 4. Same as Figure 3 but for the background temperature.

Neutral Chemistry

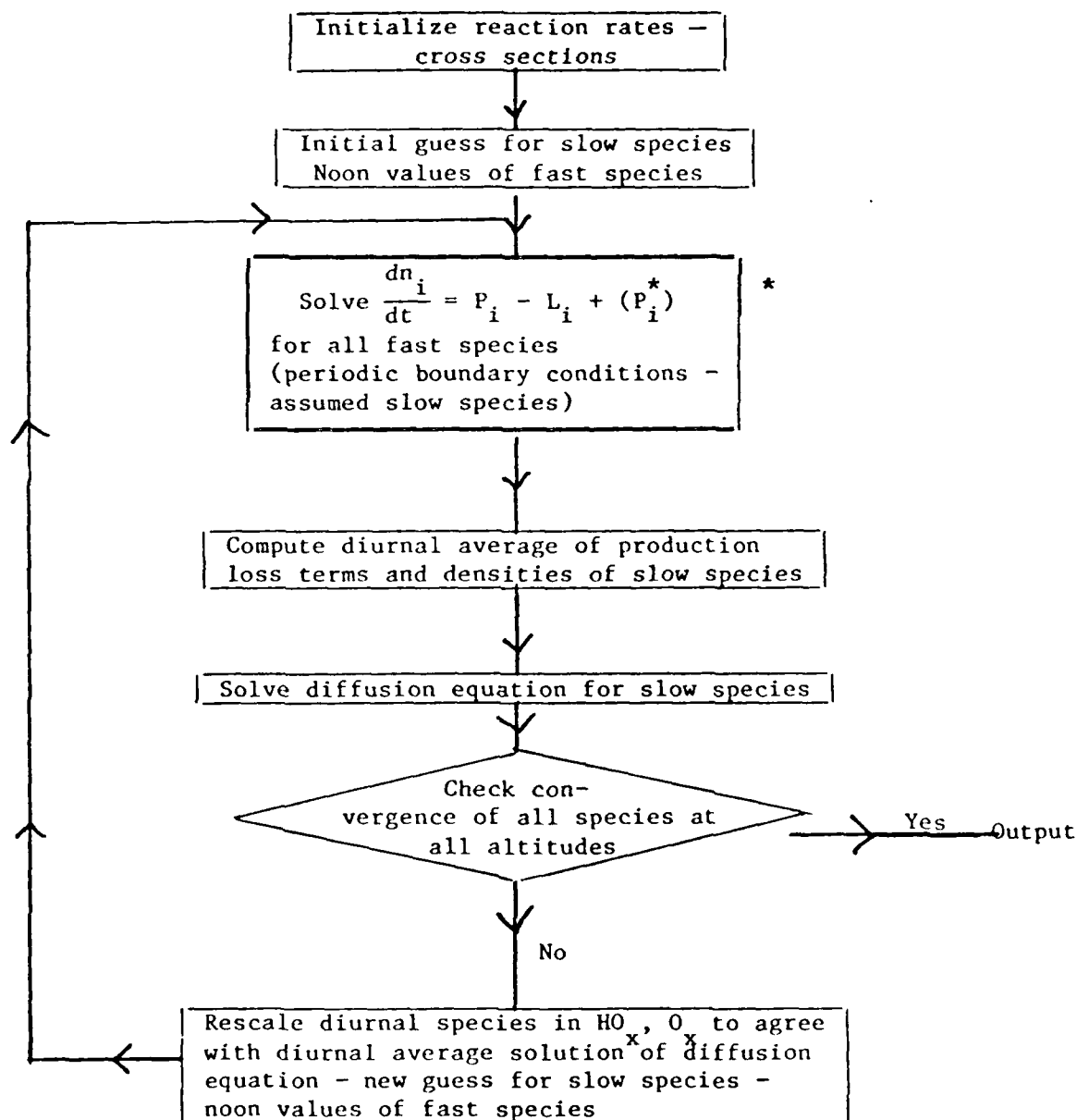


Figure 5. Flow chart for coupled diurnal-diffusion program. The box marked with an asterisk (*) corresponds to our previous diurnal code. The term P_i^* represents the effects of transport in the diurnal calculation, as explained in Rodríguez et al. (1984).

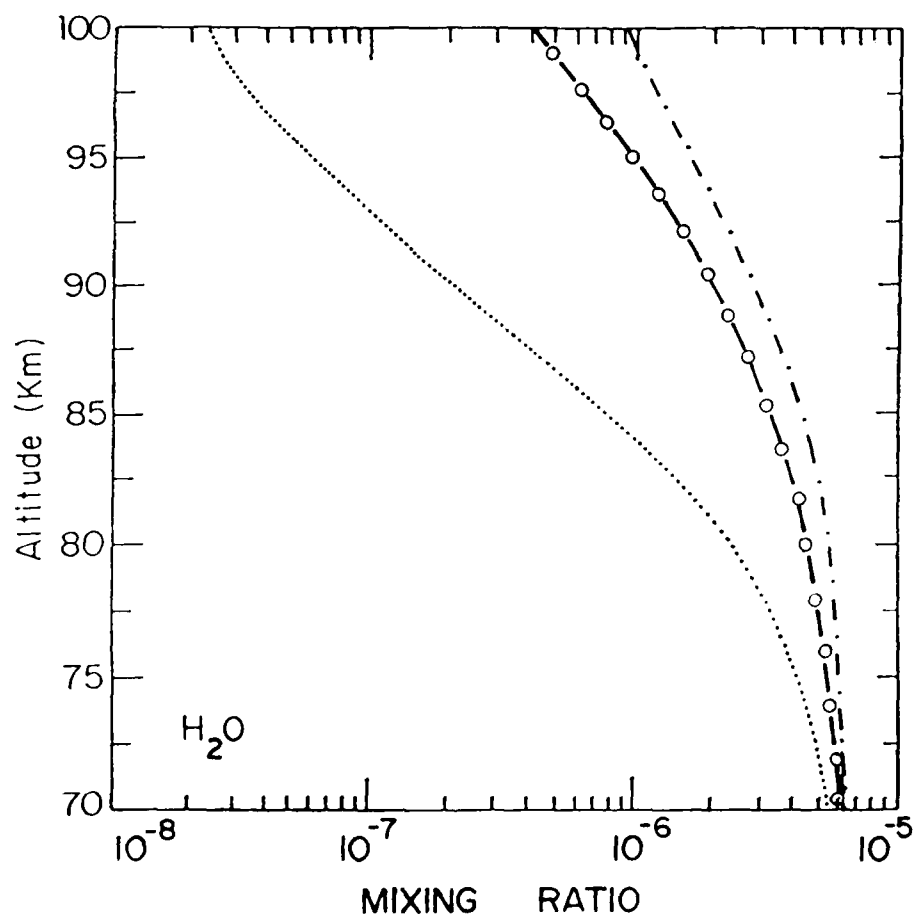


Figure 6. Mixing ratio of H_2O for different seasonal conditions used in calculations. The seasonally-dependent eddy diffusion coefficients of Garcia and Solomon (1985) have been used to calculate the H_2O mixing ratio for fall (...) and winter (-.-) conditions. The profile calculated by Allen et al. (1984) (-o-), used in our Part I calculations, is also shown for comparison.

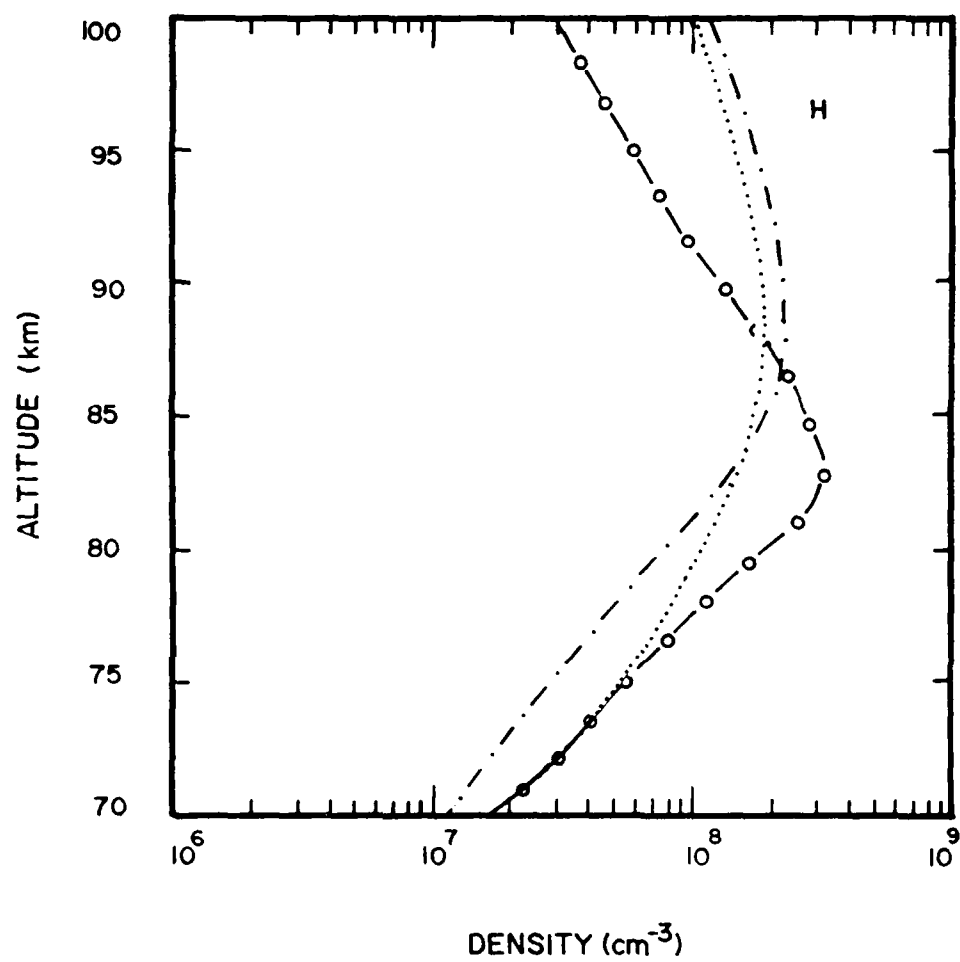


Figure 7. Same as Figure 4 but for the density of H at noon.

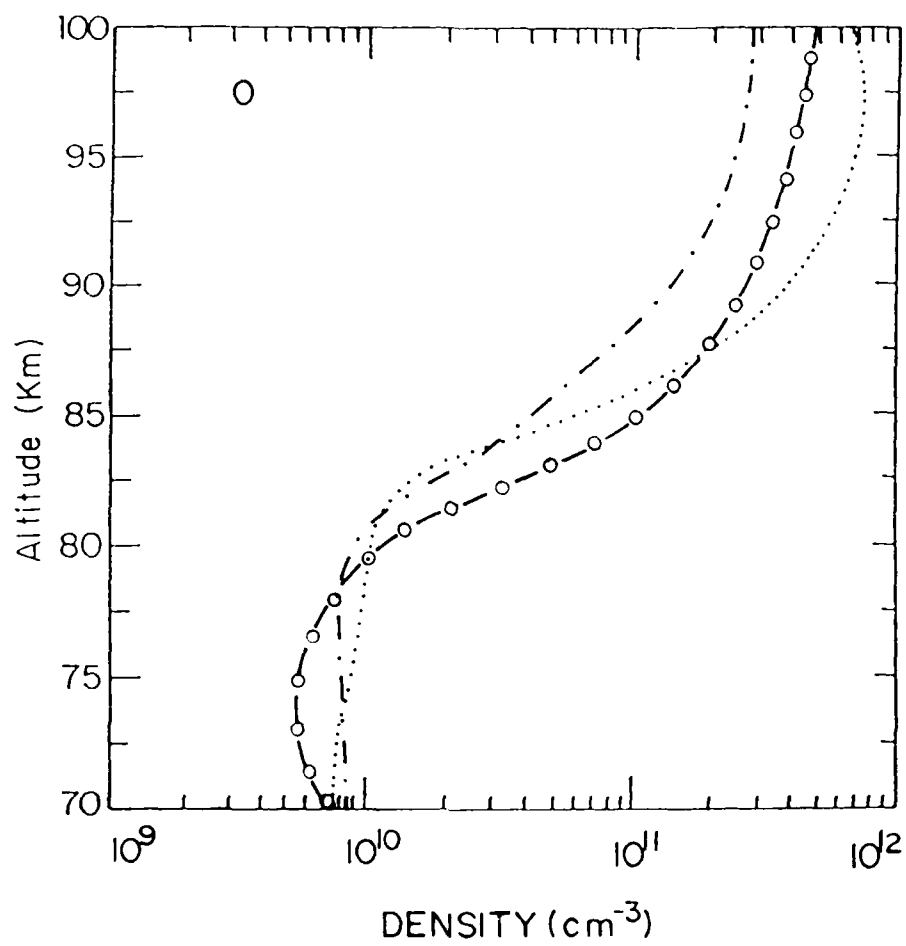


Figure 8. Same as Figure 4 but for the density of 0 at noon.

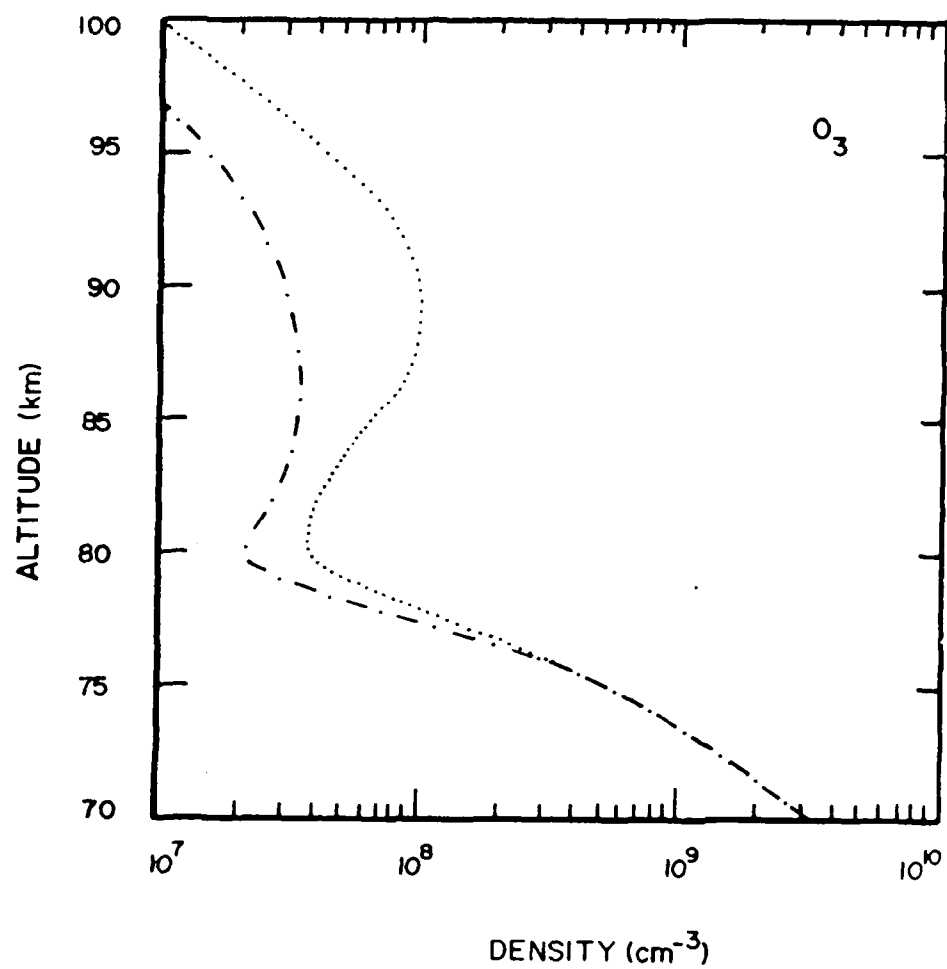


Figure 9. Density of O₃ at midnight, calculated for fall (···) and winter (---) conditions using the K_{zz} parameterization of Garcia and Solomon (1985).

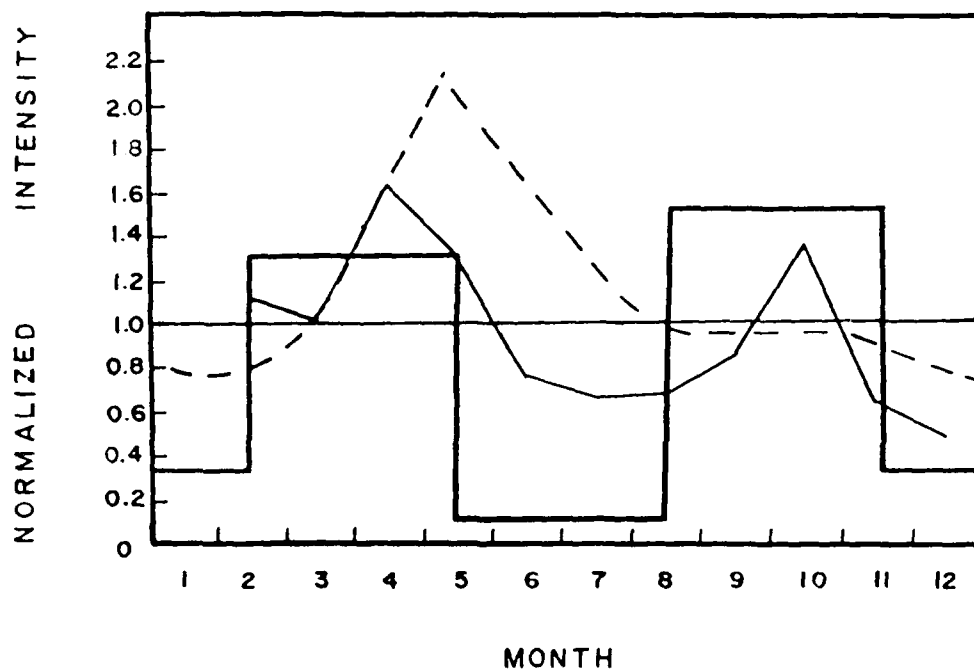


Figure 10. Calculated seasonal variation of the sodium D line nightglow at 45°N (histogram) compared to the observed seasonal variation at 23°S (—) (Kirchoff et al., 1981) and 41°N (---) (Fukuyama, 1977). Calculated and observed emissions have been normalized to 50R. The northern hemisphere data of Fukuyama (1977) (---) has been shifted by six months for comparison with the southern seasons.

PART V

Extension of Model Results to Other Models

ABSTRACT

The diurnal variation and altitude profiles for Li and K have been calculated using our photochemical model. Lack of kinetic data precludes detailed analysis of the behavior of the above species. Our results are consistent with the few available observations, if we adopt chemical schemes similar to those for Na and assume sources equal to 10^{-1} and 10^{-3} times that of Na.

Table of Contents

	<u>Page</u>
ABSTRACT	114
1. INTRODUCTION	115
2. REVIEW OF OBSERVATIONS AND KINETIC DATA	115
3. RESULTS AND DISCUSSIONS	116

1. INTRODUCTION

Detailed analysis of the alkali metals are difficult because of the lack of observation and laboratory kinetic data. However, based on the available observation and thermal data, it is reasonable to assume that the source for the alkali metals is also from meteor ablation and that the photochemical sections should be similar. Thus, a zeroth order description of the alkali metals such as potassium (K) and Lithium (Li) should be obtained by simply scaling the sodium results by the respectively meteoric abundances. We will discuss some of the model findings in this section for K and Li.

2. REVIEW OF OBSERVATIONS AND KINETIC DATA

The observational data on potassium and lithium are also less abundant than for sodium. Twilight observations (Sullivan and Hunten, 1964; Gault and Rundle, 1968) and more recent nighttime lidar measurements (Megie et al., 1978; Jegou et al., 1980) have established the existence of K and Li layers with abundances a factor of 10 and 10^3 smaller than that of Na, respectively. Simultaneous observations of the Na and K layers indicate that the peak of the K layer may be 1-2 km below that of the Na layer. The Li data also indicate a peak near that of Na (Jegou et al., 1980), although considerable variability is observed throughout the night.

The seasonal variations of Li have been observed to be similar to that of Na by measurements twilight resonance emissions (Gault and Rundle, 1968) and Lidar technique (Jegou et al., 1980). The observed column attained a maximum in the fall and winter which is about a factor of five larger than the summer values. It is difficult to obtain seasonal behaviors of K because of the large day-to-day variations (Gault and Rundle, 1968).

Kinetic data for these species are essentially nonexistent. The only available measurements are those of Silver et al. (1984) for the reaction



and of Kramer et al. (1982) for the Li reaction analogous to (1). The measured rates ($5.4 \times 10^{-30} (300/T)^{0.56} \text{ cm}^6 \text{ s}^{-1}$ for potassium, $3.1 \times 10^{-30} \text{ cm}^6 \text{ s}^{-1}$ for lithium) indicate fast three-body recombinations similar to Na.

On the basis of the similarity in the observed behavior of the column abundances, the chemistry of K and Li seem therefore similar to that of Na. We have thus adopted a chemical scheme similar to that of Na. This scheme is presented in Table 1. The similarity of Li, K, and Na observations suggest that the reaction



may occur at rates similar to the analogous Na reaction. Thermochemical data for KO, LiO and KO₂, LiO₂ (Murad, 1979; Pedley and Marshall, 1983; Figger et al., 1983) indicate that reactions (2) are exothermic. We thus adopt values for (2) ranging from 10^{-14} to $10^{-10} \text{ cm}^3 \text{ s}^{-1}$.

3. RESULTS AND DISCUSSIONS

Calculated profiles for K at midnight are illustrated in Figure 1. These profiles have been calculated assuming a source of potassium whose magnitude is one-tenth that of sodium. The Na source is scaled to yield peak densities of $3 \times 10^3 \text{ cm}^3 \text{ s}^{-1}$ for "fall" conditions as calculated in Part IV. The "standard" chemistry model adopts a value of $10^{-13} \text{ cm}^3 \text{ s}^{-1}$ for (2) similar to our preferred value for Na. The dashed-dot line and dashed line denotes extreme cases with (2) equal to 10^{-14} and $10^{-10} \text{ cm}^3 \text{ s}^{-1}$. The Na profile calculated with similar chemical scheme is also illustrated for comparison, with the densities scaled down by a factor of 10. We also show a potassium profile obtained by averaging our diurnal densities over the whole night (thin solid line). The circles correspond to the data of Megie et al. (1978).

The Na and K profiles for the standard cases are very similar. Agreement between our calculated profiles and the data is poor in the bottomside layer. This discrepancy is probably due to the long integration times (~ 12 hours) used to obtain the experimental profiles. Dynamical processes at night are observed to produce vertical oscillations in the Na layer (Batista et al., 1985). These oscillations may then yield average concentrations at a given altitude much higher than their instantaneous values.

The lack of diurnal data on potassium precludes deducing any further constraints on the unknown reaction rates, particularly that of (2). A similar

situation occurs for Li. The vertical profiles calculated at midnight is shown in Figure 2, again using the standard chemical model, a source equal to 10^{-3} that of Na, and "fall" conditions. Variations in the profile (not shown) similar to that of K are also obtained if we consider extreme values for the rate of (2). The shape of the Li layer is also similar to that of Na and in general agreement with data.

Figures 3 and 4 show our calculated diurnal variation for K (Figure 3) and Li (Figure 4) using the standard chemistry. These variations, calculated at 82, 86, and 90 km, are similar to that of Na.

Given the similarity in the altitude profiles, it follows that the calculated seasonal behavior of the column abundances for K and Li are similar to that of the sodium. With the present status of the observational and kinetic data, the above treatment appears to be an adequate approach. Although measurements are available for Fe^+ , Mg^+ , Ca^+ from rocket-borne spectrometers, the lack of seasonal and diurnal observations preclude further analysis. Further clarification awaits more kinetic and observational data.

Table 1: Reaction Scheme and Rate Constants for Neutral K, Li

Reaction	Rate (K) ^a	Rate (Li)
1. $M + O_3 \rightarrow MO + O_2$ ^b	$\sim 10^{-10}$	$\sim 10^{-10}$
2. $MO + O \rightarrow M + O_2$	$\sim 10^{-11}$	$\sim 10^{-11}$
3. $M + O_2 + N_2 \rightarrow MO_2 + N_2$	$5.4 \times 10^{-30} (T/300)^{-0.56}$ ^c	3.1×10^{-30} ^d
4. $MO_2 + O \rightarrow MO + O_2$	$10^{-10} - 10^{-13}$	$10^{-10} - 10^{-13}$
5. $MO_2 + h\nu \rightarrow M + O_2$	$\sim 10^{-3}$	$\sim 10^{-3}$
6. $MO_2 + H \rightarrow MOH + O$	$\sim 10^{-12}$	$\sim 10^{-12}$
7. $MO + H_2O \rightarrow MOH + OH$	$\sim 10^{-10}$	$\sim 10^{-10}$
8. $MOH + h\nu \rightarrow M + OH$	$\sim 10^{-3}$	$\sim 10^{-3}$
9. $MOH + H \rightarrow M + H_2O$	$\sim 10^{-12}$	$\sim 10^{-12}$

^aUnits are $\text{cm}^3 \text{s}^{-1}$, except $\text{cm}^6 \text{s}^{-1}$ for (3) and s^{-1} for (6) and (8).

^bM = K, Li.

^cMeasurement by Kramer et al. (1982) at 393° K.

^dMeasured by Silver et al. (1984).

References

- Batista, P. P., B. R. Clemesha, D. M. Simonich, and V. W. J. H. Kirchhoff (1985) Tidal oscillations in the atmospheric sodium layer. J. Geophys. Res., 90, 3881-3888.
- Figger, H., W. Schrepp, and Xu-Hui Zhu (1983) Chemiluminescent reaction between alkali dimers and oxygen molecules. J. Chem. Phys., 79(3), 1320.
- Gault, W. A., and H. N. Rundle (1969) Twilight observations of upper atmospheric sodium, potassium, and lithium. Can. J. Phys., 47, 85.
- Jegou, J. P., M. L. Chanin, J. E. Blamont, and C. Megin (1980) Lidar measurements of atmospheric lithium, Geophys. Res. Lett., 7, 995.
- Kramer, S. D., B. E. Lehmann, G. S. Hurst, M. G. Payne, and J. P. Young (1982) The reaction of Li with O₂ in the presence of He and Ar. J. Chem. Phys., 76, 3614.
- Liu, S. C., and G. C. Reid (1979) Sodium and other minor constituents of meteoric origin in the atmosphere. Geophys. Res. Lett., 6, 283.
- Megie, G., F. Bos, J. E. Blamont, and M. L. Chanin (1978) Simultaneous nighttime lidar measurements of atmospheric sodium and potassium, Planet. Space Sci., 26, 27.
- Murad, E. (1978) Problems in the chemistry of metallic species in the D and E regions. J. Geophys. Res., 83, 5525.
- Pedley, J. B., and E. M. Marshall (1983) Thermochemical data for gaseous monoxides. J. Phys. Chem., 12, 967.
- Silver, J. A., M. S. Zahniser, A. C. Stanton, and C. E. Kolb (1984) Temperature-dependent termolecular reaction rate constants for potassium and sodium peroxide formation. Presented at the 20th International Symposium on Combustion, the Combustion Institute, Pittsburgh, PA.
- Sullivan, H. M., and D. M. Hunten (1964) Lithium, sodium, and potassium in the twilight airglow. Can. J. Phys., 42, 937.

Figure Captions

- Figure 1. Calculated altitude profiles of nighttime potassium and sodium. The value of k ($\text{K}\text{O}_2 + \text{O}$) was set to 10^{-13} (—), 10^{-14} (-.-.-), and 10^{-10} (---) $\text{cm}^3 \text{ sec}^{-1}$. The Na profile (···) is calculated using the chemical scheme of Table 1 and reduced by a factor of 10 for comparison. All the above profiles have been calculated at midnight. The open dot line (-o-) represents the K profile with k ($\text{Na}\text{O}_2 + \text{O}$) = $10^{-13} \text{ cm}^3 \text{ sec}^{-1}$ averaged over the whole night. We use the calculated "fall" background atmosphere. The magnitude of the sodium source is scaled to yield a peak noontime density of $3 \times 10^3 \text{ cm}^{-3}$. The potassium source is assumed to be 10^{-1} times the sodium source. Circles correspond to the data of Megie et al. (1978).
- Figure 2. Calculated altitude profiles of lithium (—) and sodium (---) at midnight. The value of k ($\text{Li}\text{O}_2 + \text{O}$) is $10^{-13} \text{ cm}^3 \text{ sec}^{-1}$. The sodium profile is calculated using the chemical scheme of Table 1 and reduced by a factor of 1000 for comparison. We use the "fall" background atmosphere. The sodium source is as described in Figure 1. The lithium source is assumed to be 10^{-3} times the sodium source.
- Figure 3. Diurnal variation of potassium species at (a) 82 km, (b) 86 km, and (c) 90 km. Source magnitude and background atmosphere are as in Figure 1. The value of k ($\text{K}\text{O}_2 + \text{O}$) is $10^{-13} \text{ cm}^3 \text{ sec}^{-1}$.
- Figure 4. Same as Figure 3, but for lithium species.

NUMBER DENSITY, MIDNIGHT

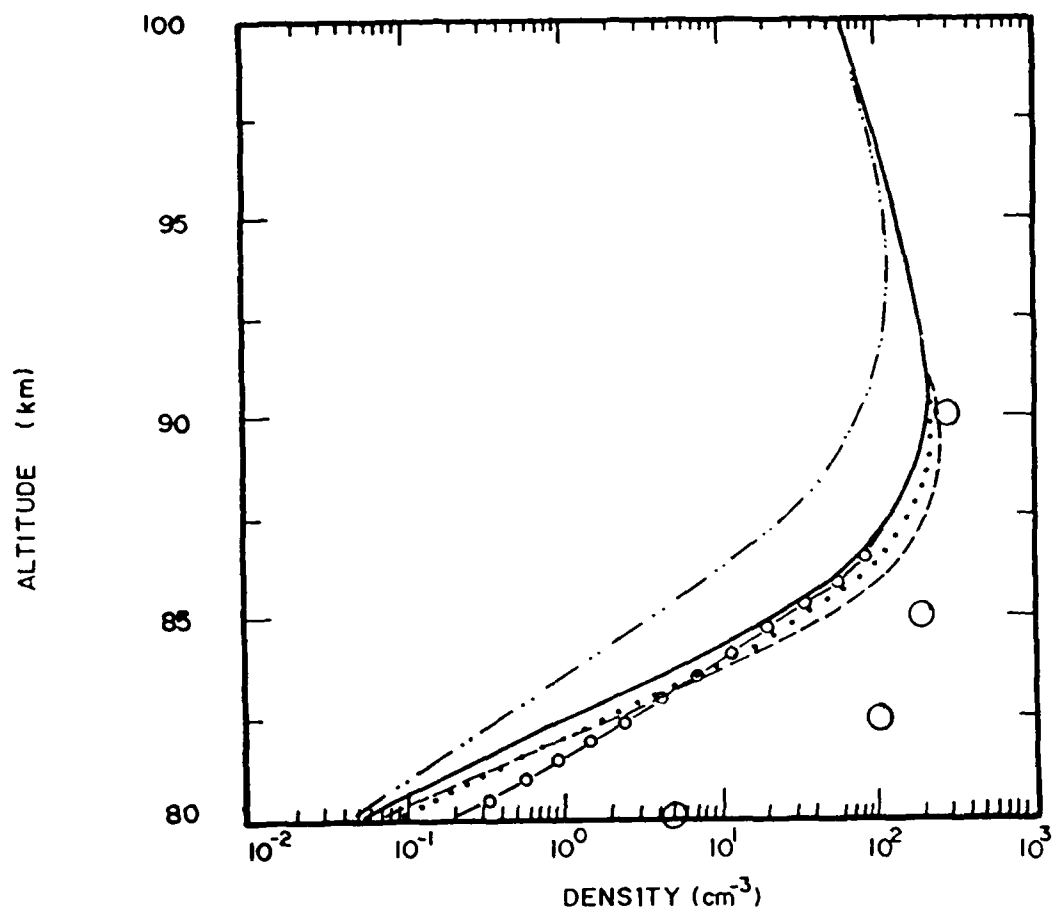


Figure 1. Calculated altitude profiles of nighttime potassium and sodium. The value of k ($\text{K}\text{O}_2 + \text{O}$) was set to 10^{-13} (—), 10^{-14} (-.-.), and 10^{-10} (---) $\text{cm}^3 \text{ sec}^{-1}$. The Na profile (···) is calculated using the chemical scheme of Table 1 and reduced by a factor of 10 for comparison. All the above profiles have been calculated at midnight. The open dot line (-o-) represents the K profile with k ($\text{Na}\text{O}_2 + \text{O}$) = $10^{-13} \text{ cm}^3 \text{ sec}^{-1}$ averaged over the whole night. We use the calculated "fall" background atmosphere. The magnitude of the sodium source is scaled to yield a peak noontime density of $3 \times 10^3 \text{ cm}^{-3}$. The potassium source is assumed to be 10^{-1} times the sodium source. Circles correspond to the data of Megie et al. (1978).

NUMBER DENSITY, MIDNIGHT

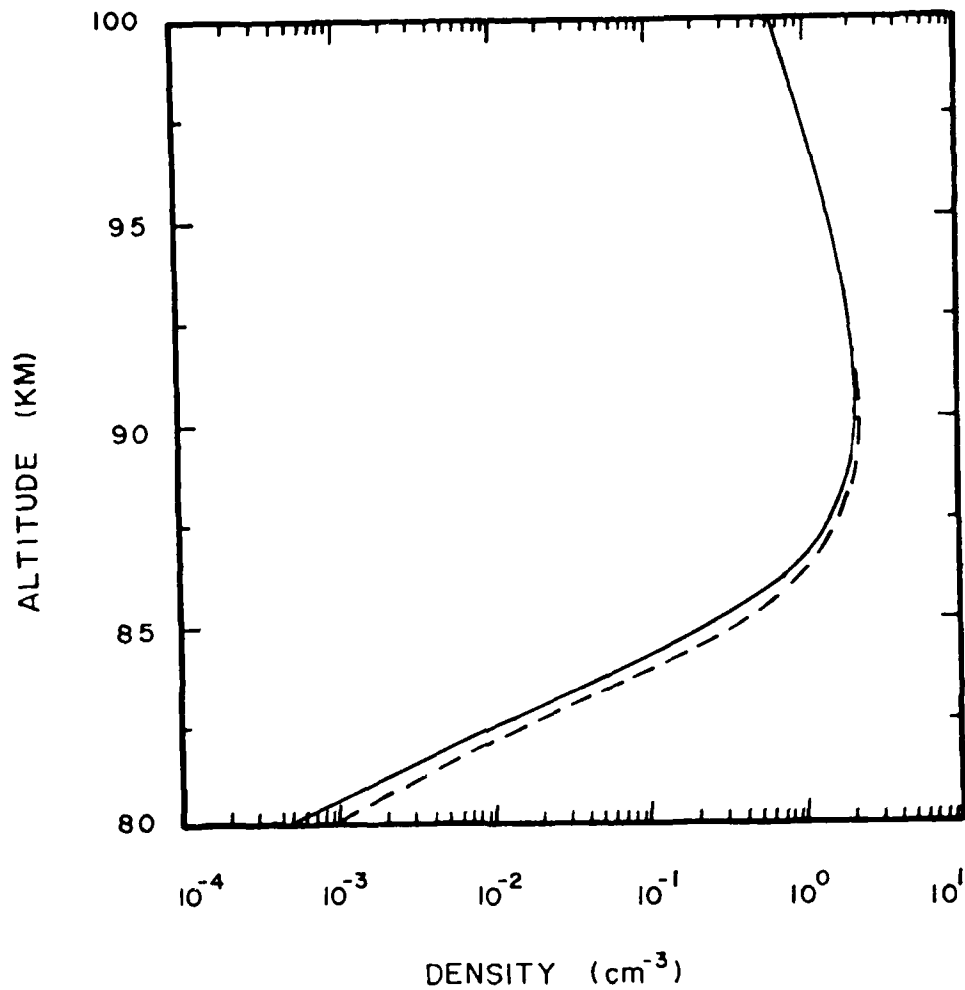


Figure 2. Calculated altitude profiles of lithium (—) and sodium (---) at midnight. The value of k ($\text{LiO}_2 + \text{O}$) is $10^{-13} \text{ cm}^3 \text{ sec}^{-1}$. The sodium profile is calculated using the chemical scheme of Table 1 and reduced by a factor of 1000 for comparison. We use the "fall" background atmosphere. The sodium source is as described in Figure 1. The lithium source is assumed to be 10^{-3} times the sodium source.

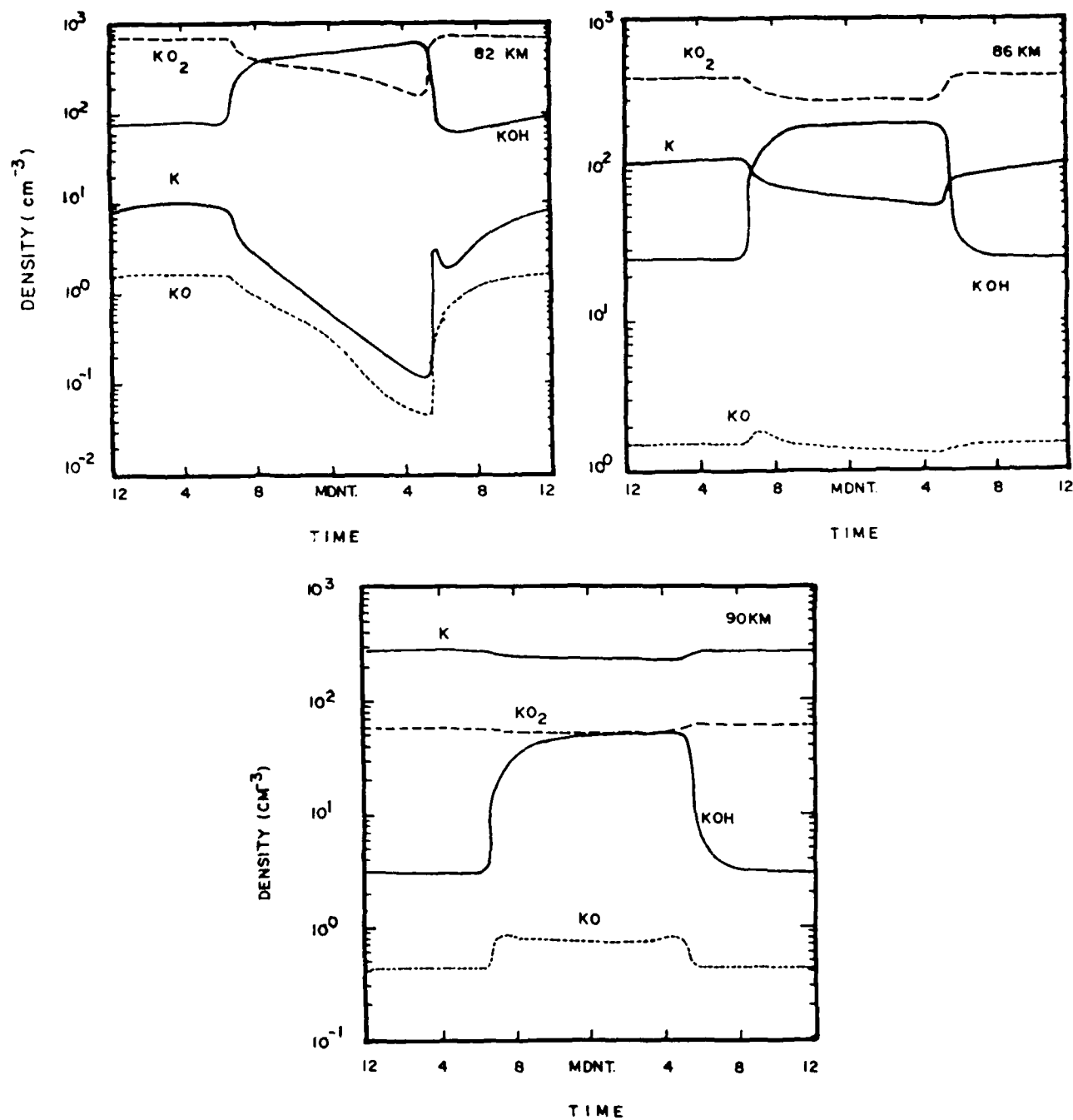


Figure 3. Diurnal variation of potassium species at (a) 82 km, (b) 86 km, and (c) 90 km. Source magnitude and background atmosphere are as in Figure 1. The value of K ($KO_2 + O$) is $10^{-13} \text{ cm}^3 \text{ sec}^{-1}$.

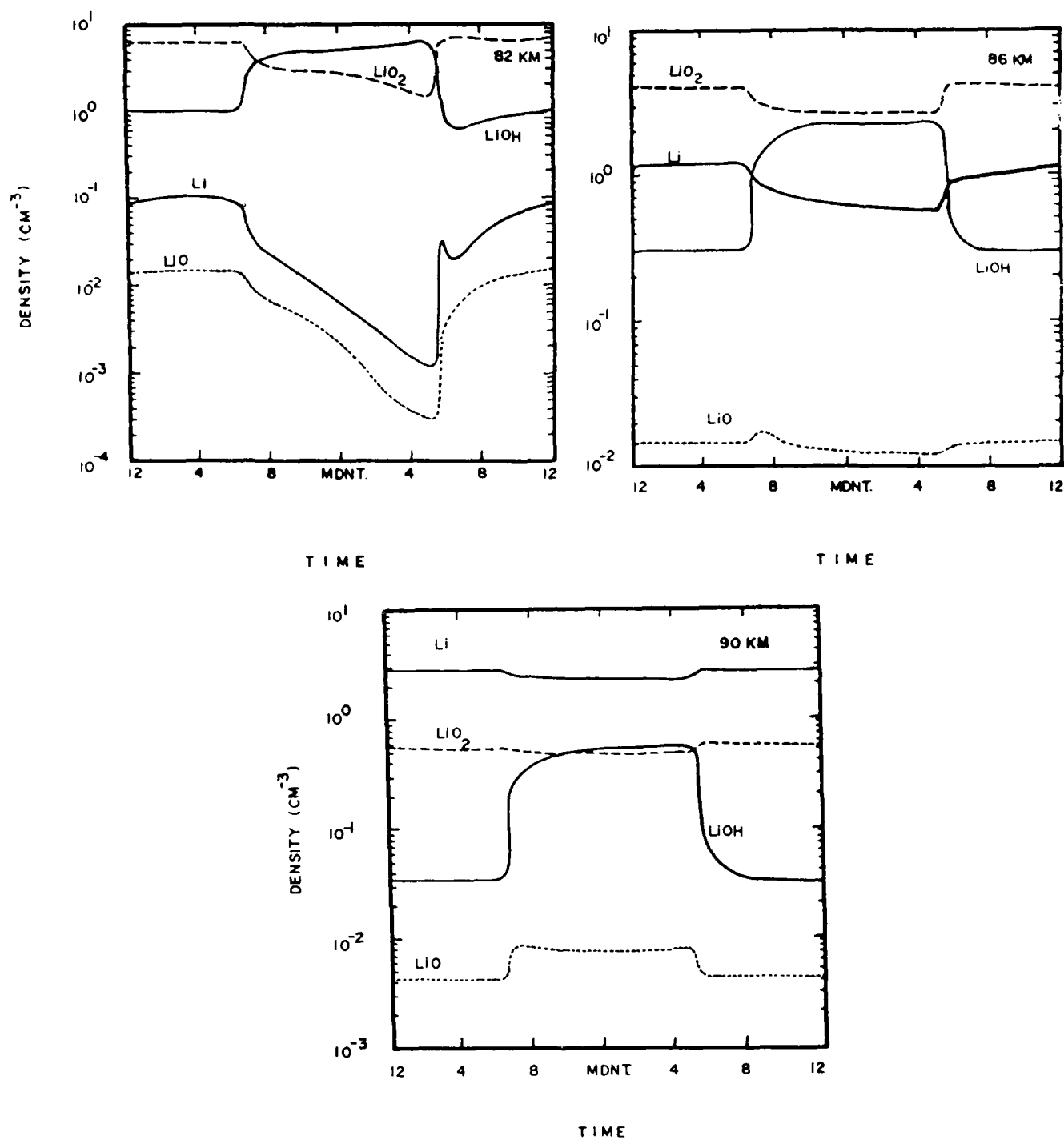


Figure 4. Same as Figure 3, but for lithium species.

END

2-87

DTIC